STOCHASTIC SIMULATIONS WITH APPLICATIONS IN MATERIAL SCIENCES

Deák Robert
Ph.D. thesis

In joint Ph.D. supervision between:

Department of Physics
Babeş–Bolyai University, Cluj-Napoca, Romania
Scientific advisor: Dr. Néda Zoltán, D.Sc., professor, external member of HAS

and

Department of Materials Physics
Eötvös Loránd University, Budapest, Hungary
Scientific advisor: Dr. Groma István, D.Sc., professor

Graduate School of Physics
Doctoral Program for Material Science and Solid State Physics
Head of School: Dr. Palla László, D.Sc., professor
Head of Program: Dr. Lendvai János, D.Sc., professor

Cluj–Napoca, Romania

2013

Contents

If, in some cataclysm, all of scientific knowledge were to be destroyed, and only one sentence passed on to the next generations of creatures, what statement would contain the most information in the fewest words? I believe it is the atomic hypothesis (or the atomic fact, if you wish to call it that) that:

All things are made of atoms - little particles that move around in perpetual motion, attracting each other when they are a little distance apart, but repelling upon being squeezed into one another.

In that one sentence, you will see, there is an enormous amount of information about the world, if just a little imagination and thinking are applied.

Richard P. Feynman

Acknowledgements

First I would like to thank my scientific advisors, **Dr. Néda Zoltán** and **Dr. Groma István** their guidance, patience, and support during my Ph.D. studies. Their bright ideas and love of science inspired me.

I would like to express my honor and thanks to **Prof. Dr. Barna B. Péter**, **Dr. Lábár János**, **Dr. Radnóczi György**, and **Dr. Lázár Zsolt** for the helpful and creative conversations in reaching the aims and optimizing the tasks. I am also thankful for all my colleagues and friends who encouraged me in these last years.

Finally, I would like to thank my broader family and especially **Mimi**, my wife, for all their love, support and encouragement to start, to proceed with, and to finish my studies.

I dedicate this work to my lovely son, **Olivér**, who many times asked me to take a break to play with him, to keep my brain fresh and not to get lost in the details.

Introduction

Physical vapor deposition (PVD) is a highly versatile process in the creation of thin films and coatings. Vapor deposition generally refers to the growth of materials by the condensation of their vapors. Nowadays, vapors can be created with several technics, like thermal evaporation, electron beam evaporation, pulsed laser deposition, filtered and unfiltered cathodic arc deposition, ion plating, pulsed laser deposition, or one of the many variants of sputtering (planar magnetron, ion beam sputtering, diode, triode, etc.) presented in details in Ref. [1]. Other deposition technics are the Chemical Vapor Deposition (CVD) [1], the Molecular Beam Epitaxy (MBE) [2, 3], and the hybrid methods that are combinations of the different technics [1].

The variety of vapor deposition technics also show the multiplicity of applications of thin films. They are used in the industry of integrated circuits, displays, hard disk drives, magnetic memories, large area detectors; in reducing the friction coefficient of surfaces; to improve wear resistance of gas turbine engines; to grow nanoscale particles with practical interest, and many other applications (for reviews see [1, 4, 5, 6, 7, 8, 9, 10, 11, 12, 13]).

Because of the increasing interest in thin films, this area of Material Science is widely studied. In the last two decades several experimental and theoretical studies were carried out in order to understand the various surface phenomena like surface diffusion of atoms and atomic clusters, island nucleation and growth, island coalescence and Ostwald ripening, simultaneous deposition of different types of atoms, morphology of two-dimensional islands formed by the deposited atoms, etc.

The process where crystals are grown on crystalline surfaces by the deposition of atoms in vacuum is called epitaxial growth. Typically, the deposition rate is small and the crystal is grown, loosely speaking, one layer at a time. In the specific case of deposition from vapor it is well-known that individual atomic events can strongly influence and even dominate the final micro or nanostructure of epitaxial thin films. Over the years, experimental technics like Scanning Tunneling Microscopy (STM), in-situ Transmission Electron Microscopy (TEM), Field Ion Microscopy (FIM), and Reflection High-Energy Electron Diffraction (RHEED)

have mostly been carried out on clean, low-index metal surfaces at low temperatures, to study the individual atomic events of surface phenomena. In spite of modern visualization tools in the experiments, the researchers are still not able to identify the atomic processes responsible for surface diffusion. Because of the very fast nature of atomic diffusion it is hard to explain and give a detailed picture of the observed and studied processes. To overcome the experimental difficulties, several theoretical and computational technics were developed, like Molecular Dynamics (MD), first-principle (or ab-initio) calculations, Monte Carlo (MC) methods, static calculations, effective medium theory calculations, and many hybrid methods, combining the different technics. As the different vapor deposition technics have their own strengths for creating thin films with specific properties, also the theoretical and computational technics have their own strengths and weaknesses in calculating or simulating specific properties or phenomena with different accuracy or speed. For example, it is known that MC methods are much weaker approximations to reality than the nowadays fashionable ab-initio MD simulations, but on the other hand, with MC methods we are able to simulate much larger systems for much longer dynamical time, as long as with ab-initio MD the simulated time and system size is much more reduced.

Using these theoretical and computational methods one could better understand the atomic processes and also shade light on the effects of the experimentally controllable parameters, and therefore one can engineer structures with the desired practical properties.

The present thesis is structured in the following way. The first chapter reviews the main three categories of computational technics: the deterministic models, the stochastic models and the hybrid models. The second chapter is devoted to present the developed original kinetic Monte Carlo (kMC) methods and their motivating studies. The third chapter discusses the applicability of the developed methods and presents and discusses the obtained results. After the final conclusions, a comprehensive bibliography for this subject is given.

Chapter 1

Simulation Methods in the Physics of Thin Films

In this chapter the simulation methods used for simulating thin film related phenomena are presented.

There are three main types of models and methods (according to our classification) that are used to connect the experiments to atomic-level parameters. The first category stands for the deterministic models. This family of models contains the Burton-Cabrera-Frank type fully continuum models [14]; the theory of rate equations (REs) and rate-diffusion equations [15], and the more recently developed level set (LS) method [16]. With Molecular Dynamics (MD) simulations [17] the individual atomic motions are followed in real time, but a much better approximation to reality is given by the nowadays fashionable ab-initio or first principles Molecular Dynamics simulations (ab-initio MD) [18]. These models are deterministic too, so using the same initial configuration of the system, after a given number of simulation steps the results will be identical.

The second model category incorporates the stochastic models, the so-called kinetic Monte Carlo (kMC) methods [19, 20, 21, 22]. These incorporate statistical fluctuations and is widely used for epitaxial growth simulations. These models are also called solid-on-solid models, or lattice kinetic Monte Carlo models, because the atoms can be deposited on the surface only on well-defined geometrical sites, depending on the structure of the substrate. It is well-known that kMC simulations are much weaker approximations to reality than ab-initio MD simulations or even the classical MD simulations. By considering kMC simulations, several processes are taken into account only in a phenomenological manner, without microscopically realistic dynamics. The interaction potentials governing the dynamics of the atoms are either heuristic or determined for example from the ab-initio Density Functional

Theory (DFT) calculations [23]. However, MC simulations offer a great advantage (for a review see ref. [24]): they are fast and thus one can study larger systems and longer time-scales. Due to this advantage it is also more adaptable for moderate computational resources than MD methods. Quite a reasonable number of atoms can be studied on cheep PC type computers. In stochastic models, starting several simulations from the same initial configuration, after the same simulation steps the results are not identical, just similar - in a statistical sense.

The third main type of models is the hybrid Monte Carlo models (hybrid MC), or in other words the off-lattice kMC models. In case of heteroepitaxial crystal growth, when one type of atomic species grows on a substrate of another material, because of the different lattice constant of the different materials, a lattice misfit will appear. This gives rise to elastic effects which can destabilize a flat interface, resulting in the formation of mounds. One example is when Germanium is grown on a Silicon substrate, the mismatch varies from 0% to 4%. The mismatch can be tuned by using different materials. As the lattice misfit and the strength of the spontaneous stress increases, the growth mode changes from Frank-van der Merwe (FM) to Stranski-Krastanov (SK), and finally to Volmer-Weber (VW) mode [for a review see ref. [25, 26]]. This type of problem can be simulated with MD or ab-initio MD methods, but not with lattice kMC methods. The off-lattice kMC method keeps the advantage of both kMC and MD methods by performing the dynamics of the system with kMC algorithm and calculating the positions of the atoms from an energy minimization procedure. The method is an optimal reconciliation between the realistic nature of the MD simulations and the higher speed of the kMC approach.

In this chapter an overview will be given only on the classical MD and ab-initio MD methods from the enumerated list of deterministic type of models; lattice kMC method for the stochastic type of models and off-lattice kMC method as a hybrid MC model. For each model (method) we will also give some applications illustrating some results obtained with them in simulating specific nanostructure growth on surfaces. We discuss only three methods here because these are the basic ones for atomistic simulations in Material Science and many times our simulation results are compared with their results.

At the end of this chapter we will give some comparisons of the described methods regarding the general features of the simulated system sizes, the simulated time-scales and effective computational time.

1.1 Deterministic models

1.1.1 The classical Molecular Dynamics method

We call Molecular Dynamics (MD) a computer simulation technique where the time evolution of a set of interacting particles is followed by integrating their equations of motion.

In MD we follow the laws of classical or quantum mechanics, therefore in contrast with MC methods, MD is a deterministic technique. Given an initial set of positions and velocities (or wave-functions), the time evolution is in principle completely determined.

The atoms will move, bumping into each other, together or alone, or even evaporating from the system if they were constrained on a free surface. For N classical particles the computer calculates a trajectory in a $6N$-dimensional phase space ($3N$ positions and $3N$ momenta) during the simulation. Molecular Dynamics can also be regarded as a statistical method. Like MC, it is a way to generate a set of configurations distributed according to some statistical distribution function or statistical ensemble. Calculation of a physical quantity by simulation is simply obtained as an arithmetic average of the various instantaneous values assumed by the quantity during the MD run, according to a time average in statistical physics. In this sense, statistical physics is the link between the microscopic behavior and the thermodynamics of the system. MD simulations generate the microscopic configurations, and with statistical physics we are able to get out the thermodynamic quantities from these. Even if the simulation runs are always of finite length and the phase space is thus not fully sampled, MD can be used to measure thermodynamical properties, and therefore evaluate the phase diagram of a specific material. Beyond this "traditional" use, MD is also used to study non-equilibrium processes and as an efficient tool for optimization of structures overcoming local energy minima.

Applications MD simulations have a widespread use in the materials science community. It has been used to simulate the melting of Silicon, crystal growth, crack propagation, ion bombardment, multi-layer deposition - to name just a few areas. A full MD atomistic simulation of vapor-phase crystal growth is actually extremely difficult. There are two limiting factors: (i) the large number of vapor atoms that must be added to the substrate to grow a new layer, and (ii) the length of time that must pass between introduction of new vapor atoms. This latter factor is the primary difficulty in MD, due to the enormous disparity in time scales between experimental and simulated time scales (perhaps 8-10 orders of magnitude). This makes such simulations potentially misleading.

Nowadays there are several packages written on various computer architectures to run

MD simulations, like AMBER [27], NAMD [28], DL_POLY [29] or MARVIN [30]. One can use these packages even without a deep knowledge of the basics of MD by setting up the initial configuration of the system and setting the specific parameters for the MD run. These packages contain a lot of useful tools to create the initial configuration or analyze the results, and they are distributed for reasonable prices or are even free for academical use.

In classical MD simulations (or kMC simulations as will see later) one can use several forms for the interaction potential between the particles, from two-body potential like Lennard-Jones potential to more sophisticated many-body potentials like Embedded Atom Methods and many others. Later on, the mentioned two interatomic potential will be discussed in details, because in our kMC models these potentials are used. Using simulation packages like the above listed ones, there are several useful force-fields, like the GROMACS, AMBER, CHARMM, CFF, PCFF [27, 28, 29, 30, 31], and others which are distributed in dedicated packages. Every one of them is useful for specific MD simulations of non-organic, organic, or mixed systems. Using Lagrangian schemes one can compute the internal stress, and using thermostat algorithms it is possible to control the temperature. It is important to recognize that in MD it is necessary to use very small time-steps to perform realistic simulations.

We now turn our attention to the basics of the MD simulations.

Basic idea of Molecular Dynamics

The classical MD simulations numerically integrate Newton's equations of motion for the particles building up the system:

$$m\frac{d^2\vec{r}_i}{dt^2} = \vec{F}_i(\vec{r}_1, \vec{r}_2, ..., \vec{r}_N),\ i = 1, 2, ..., N, \tag{1.1}$$

Here $\vec{r}_i$ are the position vectors and $\vec{F}_i$ are the forces acting upon the N atoms in the system. Quite often the forces are derived from a potential function, $U(\vec{r}_1, \vec{r}_2, ..., \vec{r}_N)$, representing the potential energy of the system for the specific geometric arrangement of the particles and thus the force is:

$$\vec{F}_i(\vec{r}_1, \vec{r}_2, ..., \vec{r}_N) = -\nabla_{r_i} U(\vec{r}_1, \vec{r}_2, ..., \vec{r}_N), \tag{1.2}$$

This form implies the conservation of the total energy $E = E_{kin} + U$, where E_{kin} is the instantaneous kinetic energy.

In the simplest case of the absence of external forces, the potential can be represented as the sum of pairwise interactions:

$$U = \sum_{i=1}^{N} \sum_{j>i}^{N} u(r_{ij}). \tag{1.3}$$

Interatomic potentials

MD and kMC simulations provide powerful tools in the study of microscopic level atom by atom assembly process in vapor deposition. This is not accessible in experiments except in only a few experimental techniques such as STM [32, 33, 34] and FIM [35, 36, 37, 38]. As a result, physical properties for individual surface dynamics of the atoms are extremely difficult to obtain under real observations. Very little experimental data exist for example on the barrier height of an atomic jump. The ab-initio methods solving the many-electron Schrödinger equation would be desirable [39], but they are computationally too expensive. Even with approximations to this scheme, such as Local-Density Approximation (LDA) [40] or Generalized Gradient Approximation (GGA) [41], and with recent impressive advances in computers and algorithms, these traditional band-structure calculations are impractical for systems with very low symmetry, such as grain boundaries [42].

An alternative approach is through the analysis of interatomic force laws which are often empirically derived by fitting coefficients in physical expressions to experimental quantities.

The computational effort to solve the set of equations of motion (1.1) grows proportionally with N^2 and is mainly associated with the evaluation of forces. Therefore, for tractable computations the forces should be expressed analytically. To further reduce the computational effort, the potential can be cut off at some distance (for $r_{ij} > r_{cut}$) beyond which the potential becomes numerically negligible.

The Lennard-Jones potential One of the most famous potentials for systems with Van der Waals interaction is the well-known Lennard-Jones potential (or $12-6$ potential), which is a typical pairwise, two-body potential. It was proposed in 1924 by John Lennard-Jones [43]. The Lennard-Jones potential (LJ) is given by the expression

$$U_{LJ}(r) = 4\epsilon \left[\left(\frac{\sigma}{r}\right)^{12} - \left(\frac{\sigma}{r}\right)^{6} \right], \tag{1.4}$$

where ϵ is the depth of the potential well, σ is the (finite) distance at which the inter-particle potential is zero and r is the distance between the particles. The parameters ϵ and σ are chosen to fit the physical properties of the material.

This potential has an attractive tail at large r, it reaches a minimum around 1.122σ (this is r_0, the equilibrium distance) and is strongly repulsive at shorter distance, passing through

0 at $r = \sigma$ and increasing steeply as r is further decreased. The term $1/r^{12}$, dominating at short distance, models the repulsion between atoms when they are brought very close to each other. Its physical origin is related to the Pauli principle: when the electronic clouds surrounding the atoms start to overlap, the energy of the system increases abruptly. The exponent 12 was chosen exclusively on a practical basis and the form (1.4) is particularly easy to compute. In fact - on physical grounds - an exponential behavior would be more appropriate.

The term $1/r^6$, dominating at large distances, constitute the attractive part. This is the term which gives cohesion to the system. The $1/r^6$ attraction is originated from Van der Waals dispersion forces. This is due to dipole-dipole interaction originating from fluctuating dipoles. These are rather weak interactions, which however dominate the bonding character of closed-shell systems.

Nowadays, the LJ $12 - 6$ potential constitutes an extremely important model system. There is a vast body of papers which investigate the behavior of atoms interacting via LJ on a variety of different geometries: solids, liquids, surfaces, clusters, two-dimensional systems, etc. The simulation works done on LJ systems helped us to understand basic aspects in many areas of condensed matter physics, even if it is unable to reproduce or calculate some properties of the system, like the lattice structure of metals. Many-body potentials, like Tersoff potential [44], the different versions of Embedded Atom Method (EAM) [45, 46, 47], and many others are able to reproduce bulk and surface properties of metallic and semiconductor systems at a higher computational cost than LJ.

Many body potentials Since the mid '80s researchers started to figure out how to get closer to reality by incorporating many-atoms effect in potentials. As a consequence of the Pauli principle, the bonds become weaker when the local environment becomes more crowded. So, the cohesive energy in function of coordination should not decrease linearly as in two-body systems, but should decrease faster when coordination is low, and more slowly as coordination increases.

The repulsive part is treated by a pair-interaction approach. Several forms for the attractive part can be obtained with the tight-binding formalism [48]. Following this formalism for metals, the glue model [49], the embedded atom method [42, 45], and Finnis-Sinclair potentials [50] was constructed .

Semiconductors are even more challenging than metals. In simulations one can use the Stillinger-Weber potential [51] or the Tersoff potential [44]. In the following we will discuss in more details only the generalized EAM method because in some of our studies [52, 53]

the interatomic potentials are calculated with this method.

The generalized Embedded Atom Method In general, EAM methods are appropriate for metallic systems, to study effects of impurities, surface related phenomena and properties of defects. The key assumption of the EAM method is that all atoms are conside- red as being embedded in the surrounding of the other atoms.

The generalized EAM method developed by Wadley at al. [46, 54] was used with success in MD simulations to determine bulk properties of multilayer films [54] and in simulations for structural deformation and mechanical strength of defective Cu nanowire, which contain about $22 - 38\%$ surface atoms [55].

In the gEAM approach the potential energy for an atom i is the sum of two terms:

$$U_i = \sum_{j \neq i} \phi\left(r_{ij}\right) + F\left(\rho_i\right) \tag{1.5}$$

The first term contains the pair-interaction potentials between the i.-th and all the other atoms

$$\begin{aligned} \phi\left(r_{ij}\right) &= \frac{A \cdot exp\left[-\alpha\left(\frac{r_{ij}}{r_e} - 1\right)\right]}{1 + \left(\frac{r_{ij}}{r_e} - \kappa\right)^{20}} - \\ &- \frac{B \cdot exp\left[-\beta\left(\frac{r_{ij}}{r_e} - 1\right)\right]}{1 + \left(\frac{r_{ij}}{r_e} - \lambda\right)^{20}}, \end{aligned} \tag{1.6}$$

where r_{ij} is the distance between atom i and j, r_e is the equilibrium distance between the nearest neighboring atoms. $A, B, \alpha, \beta, \kappa$ and λ are the adjustable parameters of the potential.

The second term of equation (1.5) is the many-body term resulting from the interaction energy which is needed to embed the i.-th atom in the local-electron density, ρ_i, provided by the other atoms. To ensure a well-working embedding energy function over a wide range of electron density, three cases are separated, $\rho_i < \rho_n$, $\rho_n \leq \rho_i < \rho_0$ and $\rho_0 \leq \rho_i$, where $\rho_n = 0.85\rho_e$, $\rho_0 = 1.15\rho_e$, and ρ_e is the equilibrium electron density:

$$F(\rho_i) = \begin{cases} \sum_{x=0}^{3} F_{nx} \left(\frac{\rho_i}{\rho_n} - 1 \right)^x, if\ \rho_i < \rho_n, \rho_n = 0.85\rho_e \\ \sum_{x=0}^{3} F_x \left(\frac{\rho_i}{\rho_n} - 1 \right)^x, if\ \rho_n \leq \rho_i < \rho_0, \rho_0 = 1.15\rho_e \\ F_e \left[1 - ln \left(\frac{\rho_i}{\rho_e} \right)^\eta \right] \cdot \left(\frac{\rho_i}{\rho_e} \right)^\eta, if\ \rho_0 \leq \rho_i. \end{cases} \tag{1.7}$$

ρ_i can be calculated using

$$\rho_i = \sum_{j \neq i} f_j(r_{ij}), \tag{1.8}$$

where $f_j(r_{ij})$ is the electron density of atom j, and can be written as

$$f_j(r_{ij}) = \frac{f_e \cdot exp\left[-\beta \left(\frac{r_{ij}}{r_e} - 1 \right) \right]}{1 + \left(\frac{r_{ij}}{r_e} - \lambda \right)^{20}}, \tag{1.9}$$

where f_e is the equilibrium electron density.

All the adjustable parameters can be determined from the material properties like cohesive energy, bulk modulus, lattice constant, elastic constant, vacancy formation energy, and sublimation energy. In the ref. [54] there is a list of parameters for more then 15 metals. The described method uses a single format for all materials and it can be used even for alloys of the listed compounds, as described in ref. [54], therefore in this sense this potential is normalized. Another difficulty of the atomistic models is that long range potentials are computationally inefficient and they must have a cut-off after a certain distance. The cut-off range is an important aspect of the gEAM method, this being an intrinsic part of the two-body potential.

Boundary conditions

One possibility for fixing the boundary of the studied system is to apply free boundary conditions. In this case the system simply terminates and the atoms near the boundary would have less neighbors than atoms inside. But if we really want to simulate large systems, this situation is not realistic. A solution is to use Periodic Boundary Conditions (PBC).

When using BPC, particles are enclosed in a box and this box is replicated by rigid translation in all three cartesian directions. When simulating thin film growth on surfaces, only two of the directions have to be periodic, the direction perpendicular to the surface has

free boundary condition.

Time integration algorithm

The "engine" of a MD simulation is its time integration algorithm. In order to follow the trajectory of interacting particles it is required to integrate the equations of motion of particles of the system.

In all the available algorithms, the time is discretized and the time-step is denoted with δt. By knowing the positions and the velocities of the particles, the algorithms give the new positions and velocities of the particles at time δt later. Because all the different schemes are approximations, different amount of errors are associated with them.

The two most popular integration methods for MD calculations are the Verlet algorithms [56, 57] and the predictor-corrector algorithms [58]. The former one is a low-order method which is easy to implement, the latter one is of higher accuracy even when using larger time-steps.

The Verlet integration methods

The Verlet algorithm The basic idea in the Verlet algorithms consists of writing two third-order Taylor expansions for the positions $r(t)$, one forward and one backward in time. For a one-dimensional case:

$$\begin{aligned} r\left(t+\delta t\right) &= r\left(t\right) + v\left(t\right)\delta t + \tfrac{1}{2}a\left(t\right)\delta t^2 + \tfrac{1}{6}b\left(t\right)\delta t^3 + O\left(\delta t^4\right), \\ r\left(t-\delta t\right) &= r\left(t\right) - v\left(t\right)\delta t + \tfrac{1}{2}a\left(t\right)\delta t^2 - \tfrac{1}{6}b\left(t\right)\delta t^3 + O\left(\delta t^4\right). \end{aligned} \tag{1.10}$$

Here v is the velocity, a the acceleration, and b the third derivative of r with respect to t. Adding the two expressions will give the basic form of the Verlet algorithm:

$$r\left(t+\delta t\right) = 2r\left(t\right) - r\left(t-\delta t\right) + a\left(t\right)\delta t^2 + O\left(\delta t^4\right). \tag{1.11}$$

In this algorithm the velocities are not directly generated, although their knowledge is sometimes necessary. Moreover, they are required to compute the kinetic energy, whose evaluation is necessary to test the conservation of the total energy. This is one of the most important tests to verify that an MD simulation of a conservative system is proceeding correctly.

To overcome this difficulty, some variants of the Verlet algorithm have been developed. The Leap-Frog algorithm [59] is one of such variants where the velocities are handled somewhat better.

The Leap-Frog algorithm In this algorithm the velocities are first calculated at time $t + 1/2\delta t$; these are used to calculate the new positions, $r(t + \delta t)$:

$$\begin{aligned} v\left(t + \tfrac{1}{2}\delta t\right) &= v\left(t - \tfrac{1}{2}\delta t\right) + a\left(t\right)\delta t, \\ r\left(t + \delta t\right) &= r\left(t\right) + v\left(t + \tfrac{\delta t}{2}\right). \end{aligned} \tag{1.12}$$

In this way, the velocities leap over the positions, then the positions leap over the velocities. The advantage of this algorithm is that the velocities are explicitly calculated; however, the disadvantage is that they are not calculated at the same time as the positions. The velocities at time t can be approximated by the relationship:

$$v\left(t\right) = \frac{1}{2}\left[v\left(t - \frac{1}{2}\delta t\right) + v\left(t + \frac{1}{2}\delta t\right)\right], \tag{1.13}$$

The Velocity Verlet algorithm An even better implementation of the same basic algorithm is the Velocity Verlet scheme. Here the positions, velocities, and accelerations at time $t + \delta t$ are obtained from the same quantities at time t in the following way:

$$\begin{aligned} r\left(t + \delta t\right) &= r\left(t\right) + v\left(t\right)\delta t + \tfrac{1}{2}a\left(t\right)\delta t^2, \\ v\left(t + \tfrac{\delta t}{2}\right) &= v\left(t\right) + \tfrac{1}{2}a\left(t\right)\delta t, \\ a\left(t + \delta t\right) &= -\tfrac{1}{m}\nabla U\left(r\left(t + \delta t\right)\right) \\ v\left(t + \delta t\right) &= v\left(t + \tfrac{\delta t}{2}\right) + \tfrac{1}{2}a\left(t + \delta t\right)\delta t \end{aligned} \tag{1.14}$$

The Predictor-Corrector algorithms As mentioned above, the Predictor-Corrector algorithms constitute another commonly used class of methods to integrate the equation of motion, and consist of three steps:

1. Predictor.

   Predicts the system configuration (position, velocity, acceleration, or even higher derivatives of position) at the end of the next time-step using Taylor expansion.

$$\begin{aligned} r^p\left(t + \delta t\right) &= r\left(t\right) + v\left(t\right)\cdot\delta t + \tfrac{1}{2}a\left(t\right)\cdot\left(\delta t\right)^2 + \tfrac{1}{6}b\left(t\right)\cdot\left(\delta t\right)^3 + ..., \\ v^p\left(t + \delta t\right) &= v\left(t\right) + a\left(t\right)\cdot\delta t + \tfrac{1}{2}b\left(t\right)\cdot\left(\delta t\right)^2 + ..., \\ a^p\left(t + \delta t\right) &= a\left(t\right) + b\left(t\right)\cdot\delta t + ..., \\ b^p\left(t + \delta t\right) &= b\left(t\right) + ..., \\ &..., \end{aligned} \tag{1.15}$$

2. Force evaluation.

Evaluates forces at the next time-step using the predicted system state. The difference between the predicted (signed with p) and newly calculated (not signed) acceleration is the error.

$$\delta a\left(t+\delta t\right)=a\left(t+\delta t\right)-a^{p}\left(t+\delta t\right) \tag{1.16}$$

3. Corrector.

   Uses the calculated error to correct all next step values (signed with c).

$$\begin{aligned} r^{c}\left(t+\delta t\right) &= r^{p}\left(t+\delta t\right)+c_{0}\delta a\left(t+\delta t\right), \\ v^{c}\left(t+\delta t\right) &= v^{p}\left(t+\delta t\right)+c_{1}\delta a\left(t+\delta t\right), \\ a^{c}\left(t+\delta t\right) &= a^{p}\left(t+\delta t\right)+c_{2}\delta a\left(t+\delta t\right), \\ b^{c}\left(t+\delta t\right) &= b^{p}\left(t+\delta t\right)+c_{3}\delta a\left(t+\delta t\right), \\ &.... \end{aligned} \tag{1.17}$$

Regarding the number (let's say q) of position derivatives used, the methods are q-order predictors and a number of q coefficients (c_0, c_1, c_2 ... c_q) must be used. With these coefficients one can optimize the stability of the solution. The coefficients are dependent as a function on both the equation and the order of the Taylor series expansion. For example using a third-order Nordsieck Predictor-Corrector algorithm [60], the values of coefficients are $c_0 = 1/6$, $c_1 = 5/6$, $c_2 = 1$, and $c_3 = 1/3$.

1.1.2 The ab-initio Molecular Dynamics methods

Classical MD uses "predefined potentials" which are either based on empirical data or on electronic structure calculations. Many times this is a convenient way to analyze atomic systems, however, the analogy of the built system (MD model) to real materials depends on how well the interatomic potential for the studied material was determined (approximated). Looking from the fundamental aspect in case of several constituents there are many parameters that have to be determined (as one can see for the discussed gEAM potential too) and even during the simulation the electronic structure can change qualitatively. To overcome this weakness of the MD simulations a family of technics were elaborated, which are called ab-initio molecular dynamics methods. There are other names currently in use for these methods, such as Car-Parrinello, Hellmann-Feynmann, first principles, quantum chemical, on-the-fly, direct, potential-free, quantum, etc. Molecular Dynamics.

Applications The basic idea of every ab-initio MD method is to calculate the forces from electronic structure calculations as the molecular dynamics trajectory is generated. In these cases the question is not how to approximate the potential, but which particular approximation to use for solving the Schrödinger equation. Following this process of solving fundamental equations of the system, one can understand the need and widespread use of the ab-initio MD methods from Material Science to Biochemistry.

The first application ofthe Car-Parrinello molecular dynamics [61] dealt with Silicon, one of the basic materials in semiconductor industry. It is impossible to enumerate all the applications of the ab-initio methods because it has a wide usage in physics, biology, and chemistry of solids, polymers, materials of different components, surfaces, interfaces, liquids and solutions, amorphous and crystallized systems, chemical reactions and transformations, and many more. Just to emphasize applications of ab-initio MD in the field of Physics of Thin Films, the studies focusing on CO adsorbates on $Si(001)$ surface [62], homoepitaxial crystal growth on $Si(001)$ [63], oxidation of CO on Pt(111) [64, 65], calculation of step end kink formation energies on $Cu(111)$ [66], the height of the step edge barriers on Pt(111) [67, 68], and the calculation of self-diffusion hopping energies for Al, Rh, Ir, Ni, Pd, Pt, Cu, Ag and Au [69] can be mentioned.

Ab-initio Molecular Dynamic approaches

In order to explicitly take into account the electrons in ab-initio MD, one has to solve the time-dependent Schrodinger equation:

$$i\hbar\frac{\partial\Phi\left(\{r_i\},\left\{\vec{R}_I\right\};t\right)}{\partial t}=\hat{H}\Phi\left(\{\vec{r}_i\},\left\{\vec{R}_I\right\};t\right). \tag{1.18}$$

Denoting with M_I, Z_I and $\vec{R}_I$ the mass, the charge and the coordinates of the nuclei, and with $\vec{r}_i$ and m_e the coordinates and the electronic mass, in the coordinate representation the Hamiltonian is:

$$\begin{aligned}\hat{H}&=-\textstyle\sum_I\frac{\hbar^2}{2M_I}\nabla_I^2-\sum_I\frac{\hbar^2}{2m_e}\nabla_i^2+\sum_{i<j}\frac{e^2}{|\vec{r}_i-\vec{r}_j|}-\sum_{I,i}\frac{e^2Z_I}{\left|\vec{R}_I-\vec{r}_j\right|}+\sum_{I<J}\frac{e^2Z_IZ_J}{\left|\vec{R}_I-\vec{R}_J\right|}\\&=-\textstyle\sum_I\frac{\hbar^2}{2M_I}\nabla_I^2-\sum_I\frac{\hbar^2}{2m_e}\nabla_i^2+U_{n-e}\left(\{\vec{r}_i\},\left\{\vec{R}_I\right\}\right)\\&=-\textstyle\sum_I\frac{\hbar^2}{2M_I}\nabla_I^2+\hat{H}_e\left(\{\vec{r}_i\},\left\{\vec{R}_I\right\}\right).\end{aligned} \tag{1.19}$$

To make Molecular Dynamics we have to separate the electronic and nuclear contribution on the wavefunction. Following the Time-Dependent Self-Consistent Field (TDSCF)

approach, the simplest way is to assume:

$$\Phi\left(\{\vec{r}_i\},\left\{\vec{R}_I\right\};t\right)\approx\psi\left(\{\vec{r}_i\};t\right)\chi\left(\left\{\vec{R}_I\right\};t\right)\exp\left[\frac{i}{\hbar}\int_{t_0}^{t}dt'\tilde{E}_e(t')\right]. \tag{1.20}$$

A convenient phase factor is also introduced:

$$\tilde{E}_e=\int d\vec{r}d\vec{R}\psi^*\left(\{\vec{r}_i\};t\right)\chi^*\left(\left\{\vec{R}_I\right\};t\right)\hat{H}_e\psi\left(\{\vec{r}_i\};t\right)\chi\left(\left\{\vec{R}_I\right\};t\right). \tag{1.21}$$

By using separation (1.20) for the starting equation (1.18) keeping the $\frac{dH}{dt}=0$, after projecting on $<\Psi|$ and $<\chi|$, we get:

$$\begin{array}{l} i\hbar\frac{\partial\psi}{\partial t}=-\sum_i\frac{\hbar^2}{2m_e}\nabla_i^2\psi+\left\{\int d\vec{R}\chi^*\left(\left\{\vec{R}_I\right\};t\right)U_{n-e}\left(\{\vec{r}_i\},\left\{\vec{R}_I\right\}\right)\chi\left(\left\{\vec{R}_I\right\};t\right)\right\}\psi, \\ i\hbar\frac{\partial\chi}{\partial t}=-\sum_i\frac{\hbar^2}{2M_I}\nabla_I^2\chi+\left\{\int d\vec{r}\psi^*\left(\{\vec{r}_i\};t\right)U\hat{H}_e\left(\{\vec{r}_i\},\left\{\vec{R}_I\right\}\right)\psi\left(\{\vec{r}_i\};t\right)\right\}\chi \end{array} \tag{1.22}$$

These coupled equations are the basis of the TDSCF method. The next step is to rewrite the nucleic wavefunction in order to approximate the nuclei as classical point particles, by writing:

$$\chi\left(\left\{\vec{R}_I\right\};t\right)=A\left(\left\{\vec{R}_I\right\};t\right)\exp\left[iS\left(\left\{\vec{R}_I\right\};t\right)/\hbar\right], \tag{1.23}$$

where A and S are considered to be real functions. After separating the real and imaginary parts, for the nucleic part of the TDSC equation (1.22) we get:

$$\begin{array}{l} \frac{\partial S}{\partial t}+\sum_I\frac{1}{2M_I}\left(\nabla_I S\right)^2+\int d\vec{r}\psi^*\hat{H}_e\psi=\hbar^2\sum_I\frac{1}{2M_I}\frac{\nabla_I^2 A}{A}, \\ \frac{\partial A}{\partial t}+\sum_I\frac{1}{M_I}\left(\nabla_I A\right)\left(\nabla_I S\right)+\sum_I\frac{1}{2M_I}A\left(\nabla_I^2 S\right)=0. \end{array} \tag{1.24}$$

In classical limits where $\hbar=0$, the first equation in (1.24) becomes

$$\frac{\partial S}{\partial t}+\sum_I\frac{1}{2M_I}\left(\nabla_I S\right)^2+\int dr\psi^*\hat{H}_e\psi=0, \tag{1.25}$$

or in analogy with the Hamilton-Jacobi formulation, denoting the momentum nuclei I with $\vec{P}_I$ is:

$$\frac{\partial S}{\partial t}+\sum_I\frac{1}{2M_I}\left(\vec{P}_I\right)^2+U_e=0. \tag{1.26}$$

Using the transformation $\vec{P}_I = \nabla_I S$, the Newtonian equation of motion will be:

$$\begin{aligned} M_I \ddot{\vec{R}}_I(t) &= -\nabla_I \int d\vec{r} \psi^* \hat{H}_e \psi = \\ &= -\nabla_I U_e^E \left(\left\{ \vec{R}_I(t) \right\} \right). \end{aligned} \tag{1.27}$$

Thus, the nuclei move in an effective potential of electrons which is a function of the nuclear positions only, at the given time t.

The Ehrenfest approach Because the nuclear wavefunction occurs in the TDSCF equation part for electrons, in the classical limits ($\hbar = 0$) the position operator writes as:

$$\int d\vec{R} \psi^* \left(\left\{ \vec{R}_I \right\}; t \right) \vec{R}_I \chi \left(\left\{ \vec{R}_I \right\}; t \right) \overset{h \to 0}{\to} \vec{R}_I(t). \tag{1.28}$$

Therefore the time-dependent wave equation for the electrons is:

$$\begin{aligned} & i\hbar \tfrac{\partial \psi}{\partial t} = -\textstyle\sum_i \tfrac{\hbar^2}{2m_e} \nabla_i^2 \psi + \\ & + U_{n-e} \left(\{\vec{r}_i\}, \left\{ \vec{R}_I(t) \right\} \right) \psi \hat{H}_e \left(\{\vec{r}_i\}, \left\{ \vec{R}_I(t) \right\} \right) \psi \left(\{\vec{r}_i\}, \left\{ \vec{R}_I(t) \right\}; t \right) = \\ & = \hat{H}_e \left(\{\vec{r}_i\}, \left\{ \vec{R}_I(t) \right\} \right) \psi \left(\{\vec{r}_i\}, \left\{ \vec{R}_I(t) \right\}; t \right) \end{aligned} \tag{1.29}$$

The approach of solving equation (1.27) using the approximation presented in (1.28) is called Ehrenfest Molecular Dynamics. Ehrenfest was the first one to address the question of how to derive form Schrödinger equation the classical, Newtonian laws of dynamics [70].

Summarizing the Ehrenfest approach one can state that:

1. the wavefunction is explicitly propagated
2. the wavefunction is coupled to the nuclei
3. except for $t = 0$ no electronic minimizations are used
4. the transitions between the electronic states are explicitly described
5. the time-step ($\triangle t$) is very small because it is imposed by the dynamics of the electrons.

The Born-Oppenheimer approach Another approach, where the wavefunction is not propagated, is the Born-Oppenheimer (BO) approach. Here the time-independent Schrödinger equation is solved for each nucleus and the time-dependence of the electronic structure is a consequence of nuclear motions. The molecular dynamics for electronic ground states is:

$$
\begin{aligned}
M_I \ddot{\vec{R}}_I(t) &= -\nabla_I \min_{\Psi_0} \left\{ \langle \Psi_0 | \hat{H}_e | \Psi_0 \rangle \right\} \\
E_0 \Psi_0 &= \hat{H}_e \Psi_0
\end{aligned}
\tag{1.30}
$$

The first difference from the Ehrenfest approach is in the way of solving the equation of motion for nuclei. The minimum of $< H_e >$ must be reached at each MD step. Another difference is the time-step ($\triangle t$). Here the time-step is imposed by the nuclei, therefore it is relatively large. Its usage started to become popular two decades ago, when sufficient computational power becomes available to calculate more efficiently the electronic structures. Independent electron methods, such as Hartree-Fock (HF) or the Kohn-Sham density functional theory, are simplifications of this approach, but we will not go into these details.

The Car-Parrinello approach The Car-Parrinello (CP) approach which benefits from all advantages of earlier approaches was proposed by Car and Parrinello in 1985 [61]. In this approach there is no electronic minimization as in the Ehrenfest approach and the time-step is large as in the BO approach. The used tool is the adiabatic separation between the fast electrons and the slow nuclei by describing the molecular orbitals as classical variables, decoupled from the nuclei. Car and Parrinello postulated the following extended Lagrangian formulation

$$
L_{CP} = \sum_I \frac{1}{2} M_I \dot{\vec{R}}_I^2 + \sum_i \frac{1}{2} \mu_i \langle v_i \mid v_i \rangle - \langle \Psi_0 | \hat{H}_e | \Psi_0 \rangle + constraints, \tag{1.31}
$$

where the first two terms represent the kinetic energy, the third one the potential energy, and the constraints are the orthogonality conditions. μ_i is the fictitious mass of the electrons. The equations of motion are obtained similarly as in classical mechanics:

$$
\begin{aligned}
M_I \ddot{\vec{R}}_I(t) &= -\tfrac{\partial}{\partial \vec{R}_I} \langle \Psi_0 | \hat{H}_e | \Psi_0 \rangle + \tfrac{\partial}{\partial \vec{R}_I} \{constraints\}, \\
\mu_I \ddot{\vec{v}}_I(t) &= -\tfrac{\partial}{\partial \vec{v}_I} \langle \Psi_0 | \hat{H}_e | \Psi_0 \rangle + \tfrac{\partial}{\partial \vec{v}_i^*} \{constraints\}.
\end{aligned}
\tag{1.32}
$$

Here the constraints must be mixed functions of the nuclear positions and the set of orbitals.

Even if the time-step is approximately 5 to 10 times smaller than in the BO approach, the CP method is preferred, because in the BO the energy conservation is not taken into account accurately. The Ehrenfest and CP approaches have the advantage compared to the BO method that no diagonalization of the Hamiltonian is necessary to obtain the wavefunction, except the first step. The biggest disadvantage of the Ehrenfest approach relative to the CP

approach remains the very small time-step.

As mentioned for the BO approach, there are several electronic structure methods usable for calculating the ab-initio forces. The strength or weakness of an ab-initio scheme does not depend only on the chosen approach but also on the chosen electronic structure. Over the years, many electronic structure methods were created and used with molecular dynamics, such as Density Functional Theories (DFT) [71, 61, 72, 73], the Hartree-Fock methods [74, 75, 76], the Generalized Valence Bond (GVB) as a post Hartree-Fock method [77, 78], the Complete Active Space Self Consistent Field (CASSCF) [79], the semiempirical methods [80, 81] - to just mention some of them.

Similarly to the MD simulations, there is a software package for running ab-initio simulations, namely the Vienna Ab-initio Simulation Package (VASP) [82]. Using this package one can choose the desired electronic structure. For example Chiho Kim and his co-workers [83] used the VASP with Ultrasoft Pseudopotential (USPP) [84] for DFT calculations in the Local Density Approximation (LDA) [40] to investigate the early stage of the nano-scale thin film growth of Al and Co on Co (111) surfaces. Another example for use of VASP is the work of P. Feibelman [85], who calculated the step- and kink-formation energies on $Cu(111)$. He also used the USPP database but with the Generalized Gradient Approximation (GGA) [41] for the density functional theory.

1.2 Stochastic models

In general, the stochastic (non-deterministic) simulation methods (also named Monte Carlo (MC) methods) are those simulation technics where the use of random number generation plays a crucial role in the algorithm. There are many types of MC methods widely used for problems of statistical physics, condensed matter physics, material science, surface science, econo-physics, biophysics, physical chemistry, and many more fields outside physics too.

MC methods are also used to calculate integral equations and to calculate ensemble averages in statistical physics. In Material Science in case of MC simulations the time evolution of a model is not deterministic according to the Newton's equation of motion, like in MD simulations, but it is stochastic, depending on a sequence of random numbers. This way, two simulations of the same system will not give identical results after the same number of simulation steps, the results being just similar, giving the possibility to analyze the system in a statistical manner.

An alternative method to MD for atomistic simulations in Material Science at low temperatures is the so called kinetic Monte Carlo (kMC) methods [19]. In the following just this type of MC method will be presented in details, due to the fact that we developed this method for simulating thin films related phenomena.

1.2.1 The kinetic Monte Carlo method

In general, kinetic (or resident time, or BKL-type) Monte Carlo (kMC) methods are appropriate for simulating those dynamical phenomena where several processes with widely different time-scales are simultaneously present. In the case of epitaxial thin-film growth this is the case, since:

1. atoms can be deposited on a crystalline surface with a given rate,
2. atoms can diffuse on the surface (this diffusion being governed by different rates depending on the binding energy of the specific atom), and
3. decohesion of adatoms from the surface are also possible,
4. in case of co-deposition of different types of atoms, neighboring atoms of different kinds can exchange their positions following complicated microscopic mechanisms. This exchange is also characterized by a specific rate.

All these processes are schematically presented in Fig. 1.1.

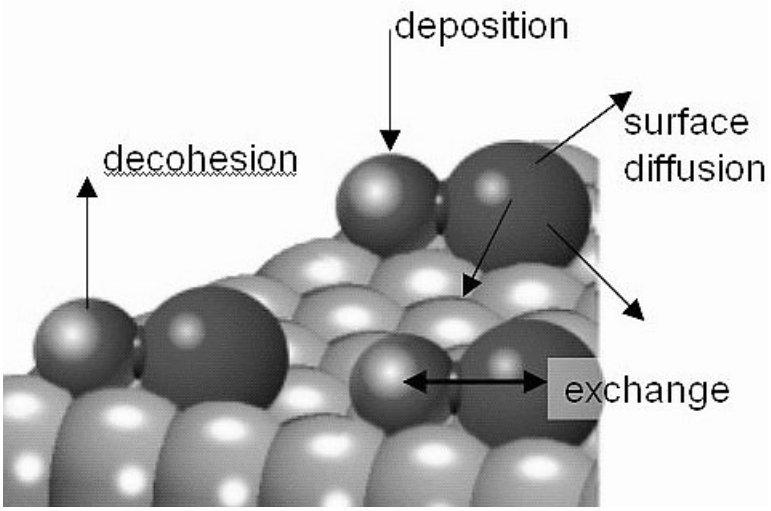

Figure 1.1: *Processes with widely different rates that govern the dynamics of atoms during epitaxial growth.*

The main idea of kMC methods is that in each simulation step one process is probabilistically selected (probability proportional with the rate of the process) and carried out. Many (in reality) deterministic effects are replaced with a single stochastic force. Therefore, the dynamics of the system is assumed to be the effect of an ensemble of stochastic forces and the different processes are characterized by different rates. The time is updated non-uniformly, depending on the rates of all possible processes at that given moment.

Generally, the **deposition rate** is fixed and calculated from the deposition speed (deposition flux) given as the number of new monolayers deposited in unit time (ML/s). The **diffusion rate** ($r_{X\to Y}$) of an atom is governed by the thermodynamic temperature (T) of the system and the potential barrier ($\Delta E_{X\to Y}$) that an atom has to overcome between the initial (X) and the final (Y) position

$$r_{X\to Y} = f_0 \exp(-\frac{\Delta E_{X\to Y}}{kT}), \tag{1.33}$$

where k is the Boltzmann factor and f_0 is the attempt rate, which is roughly the vibration frequency of atoms in the crystal ($f_0 \approx 10^{12}$ Hz). Since the value of the barrier is not straightforward to estimate (even if the pair-potential between the atoms is known), several simplifying methods are used [5]. The simplest approach is to consider the potential barrier dependent only on the binding energy of the atom in the initial X state [86, 87, 88, 89] or by applying the transition state theory [90]. A better, but computationally more costly approach is to consider a realistic pair-potential between the atoms [91] and estimate the potential in several points between the initial and final state. The already discussed EAM approach

[45, 46, 54] offers another possibility for estimating the potential energies in the hopping process. In this case the difference between the maximum and initial value will yield the potential barrier. Nowadays, with the advances in ab-initio methods, DFT calculations can also be successfully applied to estimate the value of the potential energy [20, 23, 92]. All these methods were discussed or mentioned in earlier sections.

The **decohesion rate** is obtained either by fixing a phenomenological potential barrier, E_{dec} for this process or by calculating the more realistic potential barrier from first principles, as the binding energy of the chosen atom at the given site.

Exchange between neighboring and different types of atoms are microscopically realized through complex vacancy mechanisms. In kMC simulations, however, usually an oversimplified geometry is considered where many degrees of freedom for diffusion are not taken into account, so exchange possibilities are mostly blocked. The **exchange rate** is then usually postulated in form (1.33) by assigning a hypothetical E_{ex} potential barrier for this process.

Applications kMC simulations are usually performed in a two-dimensional geometry [21, 22, 24, 89], the atoms being allowed to occupy the sites of a pre-defined lattice. By this approach one reproduces an idealized situation where a new layer is growing on a perfect crystalline substrate. These types of kMC methods, using pre-defined lattice sites, are called lattice kMC methods. The simplest possibility is to consider square lattice and the sites on the growing layer positioned exactly on the top of the atoms forming the substrate [21, 22, 24, 89]. In such manner sometimes non-realistic three-dimensional cubic structures are simulated. However, approaches on more complex geometries are also possible. One can use lattices with different symmetries and different stacking sequences for positioning the atoms in the growing layer [20, 23, 92]. Simulations can be made more realistic by considering a second layer on top of the simulated one so that interchanges between these two layers become possible. This allows the formation of additional defects and vacancies.

With these types of models many different types of systems were studied: surface diffusion of atoms and atom clusters [21, 93, 94, 52], vacancy diffusion in alloy [95], island nucleation, crystal growth and segregation of impurities [96, 97], Ostwald ripening [98, 99], shape of 2D islands [100, 101, 53]. An even more interesting field is the deposition of several types of atoms, for example the deposition of type A and B atoms on a planar crystal surface formed by atoms A. In this case [24, 89] has been observed a segregation of the 'impurity' (B) atoms that decorate the islands formed by the type A atoms.

The kinetic Monte Carlo algorithm

To present the kMC algorithm, consider a system with a set of transitions W_i from a state x_a into other possible states x_b.

$$W_i\left(x_a \rightarrow x_b\right) \tag{1.34}$$

For each W_i there is a transition probability per unit time, i.e. rate of transition (r_i). Here i loops over all possible transitions. The rates are typically given by $k \cdot e^{-c\Delta E}$.

The kMC algorithm steps are the following [19]:

- 0^o Set the time $t = 0$
- 1^o Form a list of all the rates, r_i and of all possible transitions, W_i, in the system.
- 2^o Calculate the cumulative function $R_i = \sum_{j=0}^{i} r_j$ for $i = 1, ..., N$, where N is the total number of transitions. Denote $R = R_N$.
- 3^o Get a uniform random number $u \in [0, 1]$.
- 4^o Find the event to carry out by finding the i for which $R_{i-1} < uR \leq R_i$.
- 5^o Carry out event i.
- 6^o Find all W_i and recalculate all r_i which may have changed due to the transition.
- 7^o Get a new uniform random number $u \in [0, 1]$.
- 8^o Update the time with $t = t + \triangle t$, where $\triangle t = -\frac{log(u)}{R}$.
- 9^o Continue from step 1.

In the following we will give a very simple example to demonstrate the basic approach of kMC, after that we will discuss the origin of the event frequency and the equation of time used in the algorithm.

The basic approach in a simple example Let us assume that we have a system with 3 possible final states at a given time:

$$A_1, A_2 \text{ and } A_3$$

According to this, we have three transition rates at this moment. Let us suppose that they are:

$$r_1 = 0.1,\, r_2 = 0.3 \text{ and } r_3 = 1.2,$$

which would give the cumulative rate-function R_i as:

$$R_1 = 0.1,\, R_2 = 0.4 \text{ and } R_3 = 1.6$$

Visualizing this, we can now plot the r_i as regions and the $R_i = \sum_{j=0}^{i} r_j$ as points on a line as follows:

Figure 1.2: *Transition rates, r_i, arranged in a row. Under the line we indicate the cumulative transition rates.*

If we now generate a random number u between 0 and 1 and multiply it by $R = 1.6$, this number (uR) will correspond to one point on this line. It is clear from figure 1.2 that the probability of obtaining transition for example to state 2 is:

$$0.1 < uR < 0.4$$

Namely, it is proportional to the distance between R_1 and R_2, accordingly proportional to r_2/R. So, in kMC we will get the different events with a probability which corresponds to their rates.

The attempt frequency Let us now consider the formation of any kind of defect in a solid. In many cases these are activated processes - they start when the internal energy exceeds some barrier.

Typically, the jump over the barrier occurs by thermal activation. In this case, considering the system in contact with a heat-bath, the probability of exceeding the barrier most often simply follows a Boltzmann distribution:

$$P \sim e^{-\frac{E_b}{k_b T}} \tag{1.35}$$

The activated events do not necessarily need to be jumps, but could be other processes as well, which behave according to this equation. By introducing a proportionality constant, we can write the event frequency as:

$$EventRate\,(T) = w = w_0 e^{-\frac{E_b}{k_B T}} \tag{1.36}$$

Where w_0 can be interpreted as "attempt frequency" telling us how often an attempt is made to exceed the barrier. In solids it is easy to understand the attempt frequency: it is simply the vibration frequency of the atom. It can often even be predicted with good accuracy when the atom vibration (elastic and sound) properties of the lattice are well known. Typically it is of order of 10^{12} Hz. As a very good approximation, w_0 is independent of T, at least in solids, basically because the elastic constants are weakly dependent of T.

The time update We assume that the probability of a jump occurring is independent of the previous history of the system. As a consequence, the process is a Poisson process.

To derive the functional form of the explicit time dependence, consider a single object with a uniform transition probability r. Let f denote the probability for not occurring the transition up to time t. The change of $f(t)$ over a short time interval dt is proportional to r, dt and f:

$$df(t) = -rf(t)dt. \tag{1.37}$$

By using the boundary condition $f(0) = 1$, the solution of (1.37) is:

$$f(t) = e^{-rt}. \tag{1.38}$$

A useful feature of Poisson processes is that a large number N of processes, with rates r_i, will behave as another Poisson process with the same properties as the single process. Hence, for these combined processes one can write the probability density as:

$$F(t) = e^{-Rt}. \tag{1.39}$$

Where R is the cumulative rate:

$$R = \sum_{i=1}^{N} r_i. \tag{1.40}$$

$F(t)$ now gives directly the transition probability density for the whole system.

From [19] we know how to generate random numbers following in any distribution. In order to get the desired exponential distribution we update the time as

$$t = -\frac{\ln u}{R}, \tag{1.41}$$

where u is a uniform random number between 0 and 1.

1.3 Hybrid models

The area of Hybrid models, in general sense, is a very broad topic. Restricting our discussion to the field of thin film growth simulations, there are still many ways to create hybrid models. Hybrid models use a combination of MD with kMC methods. For example, in the model described in Ref. [102] the main idea is that the algorithm is based upon an extra possibility of collective motion to the standard MC single-atom moves. With MC the evolution of the system is definitely faster than with the standard MD; moreover, because of the collective moves, it is possible to overcome high potential barriers that otherwise would trap the system in metastable states.

Another problem in thin film growth is the computation of strain that arises because of the different lattice spacings of the substrate and the deposited material. This is called mismatch, leading to the appearance of misfit dislocations that ultimately leads to different growth dynamics. In case of high mismatch the Volmer-Weber growth appears, where three dimensional islands form on the flat substrate. For small mismatch values a layer-by-layer or Frank-Van der Meer growth is observed. For intermediate mismatch the Stranski-Krastanov growth is observed, which starts with layer by layer growth but continues with the Volmer-Weber growth. Refs. [25, 103] can give overviews of these modes.

In order to simulate these strained heteroepitaxial growths, one must overcome the limitations of the fixed lattices. One way to perform off-lattice simulations is the choice of MD. The MD methods have their advantages to simulate off-lattice depositions, but can only be applied to much smaller systems compared to MC methods.

Another way to perform off-lattice simulations are given by the so-called off-lattice Monte Carlo methods. There are several methods, suggested by Faux et al. [104], Plotz et al. [105], Schindler [106], Russo et al. [107], F. Much et al. [108, 109], or Chi-Hang Lam et al. [110], able to simulate misfit dislocations and hetero-epitaxial growth.

In the following we will present only one model, proposed by F. Much [108]. F. Much and his co-workers were able to simulate heteroepitaxial growth for rather thick adsorbate layers and over a wide range of mismatch.

1.3.1 A typical off-lattice kinetic Monte Carlo method

For simplicity F. Much and coworkers [108] considered growth in only 1+1 dimensions, however, the method can be extended to (2+1)-dimensional growth as well. The method described in the following is the first one in which the critical layer thickness for the appearance of dislocations was observed in kinetic Monte Carlo simulations.

The used potential is the Lennard-Jones potential discussed earlier (in Section 1.1.1), which is easy to handle and saves computer time compared to more realistic empirical potentials like the EAM (also discussed earlier in the same Section with the L-J potential). The used potential is simple, however, the authors focused on the observation of effects which should not depend on the particular choice of potential.

Because of the isotropy of the Lennard-Jones potential, the particles are arranged in a triangular lattice. In order to save further computer time calculating the interaction potential (U_{ij}), a cut-off of 3 lattice constant is introduced ($r_c = 3r_0$, where r_0 is the equilibrium distance of the L-J potential). The interaction strength at this distance is less than 1% of the value at the equilibrium distance and therefore interactions smaller than this value can be neglected.

The substrate particles are taken to be the same, denoted simply by S. In this case, the interaction of two substrate particles is given by $U_{ij}(\sigma_S)$. Two adsorbate particles, let say A (other than S), interact via $U_{ij}(\sigma_A)$, whereas we assume that a substrate and an adsorbate particle interact via:

$$U_{ij}(\sigma_{SA}) = U_{ij}(\sigma_{AS}) = 0.5(U_{ij}(\sigma_S) + U_{ij}(\sigma_A)). \tag{1.42}$$

The process is not simulated on a fixed lattice and the particles are separated by a continuous distance r_{ij}. There are two possible events in this model: deposition and diffusion of adsorbate particles. As calculated by Schindler [106], in the Lennard-Jones systems the activation barriers for exchange diffusion are up to three times higher than those for hopping diffusion. Because the simulations take place at relatively low temperatures, hopping diffusion can be considered as the preferred diffusion mode, and for the sake of simplicity the exchange diffusion is completely neglected.

The deposition is characterized like in classical kMC with the deposition flux (F) and the deposition rate, $R_d = LF$, where the L is the system size. The rate for a diffusion is given by the Arrhenius law, presented also in Eq. 1.36.

The hopping energy barrier for the i-th particle, $E_{a,i}$ is given by

$$E_{a,i} = E_{t,i} - E_{b,i}, \tag{1.43}$$

where $E_{t,i}$ denotes the energy of the particle at the transition state or saddle point and $E_{b,i}$ the energy at the initial binding state. The search of saddle point for calculation of $E_{t,i}$ can be replaced by a simple maximum search in $1 + 1$ dimensions in this case.

The main differences - and in the same time the advantages - of this model relative to the other kMC methods used for simulation of heteroepitaxial growth are in the relaxation of the

crystal lattice, as it will be discussed in the following.

Relaxation of the crystal

To consider the elastic deformation of the crystal after each microscopic event (diffusion or deposition), the total potential energy of the n-particle system

$$E_{tot} = \sum_{i=1}^{n} \sum_{j=i+1}^{n} U_{ij}, \tag{1.44}$$

is minimized using the conjugate gradient method [111] under variation of the coordinates of all particles (substrate and adsorbate) within a radius of $3 \cdot r_0$ around the particle where the event took place. In order to avoid strains caused by this local relaxation of the crystal, after a distinct number of microscopic events, depending on the misfit ε, minimizations of the total energy E_{tot} (now under variation of all particles coordinates) is performed.

Both mentioned types of relaxations will not lead to a substantial rearrangement of the crystal, but the coordinates and activation energies of the affected particles are slightly changed. The number of events between two global relaxations is chosen in such a way that the change of the activation energy due to the relaxation is less than 0.5 percent.

Results of the model

The authors report in [108] that each simulation run starts with the substrate of 6 atomic layers with a fixed bottom layer. The system size L (number of particles in the substrate's upper layer) is between $L = 100$ and $L = 200$. Within this range they found no important finite-size effects.

However, because of the periodic boundary conditions, for $L = 30$ the critical layer thickness is increased for misfits $\mid \varepsilon \mid \leq 5\%$ in comparison to systems with $L = 100$ or $L = 200$. Results from smaller system sizes are therefore affected by finite-size effects.

Measuring lengths in units of σ_S, σ_A are chosen between 0.85 and 1.11, so one can simulate heteroepitaxial growth for misfits

$$\varepsilon = \frac{\sigma_A - \sigma_S}{\sigma_S}, \tag{1.45}$$

between -15% and $+11\%$.

Heteroepitaxial growth is therefore simulated in order to determine the critical layer thickness (h_c) for the appearance of dislocations as a function of the misfit (ε). To obtain

good averages, between 5 and 10 independent simulation runs are carried out for each value of ε.

In the early stages of the simulations dislocation-free mounds of adsorbate particles are formed on the substrate. With an increasing number of deposited particles these mounds grow and dislocations appear where two mounds merge. The diameter of the initial mounds depends therefore on the misfit: the smaller $\mid \varepsilon \mid$ is, the fewer and larger dislocation-free mounds arise and fewer dislocations are finally observed. The thickness of the adsorbate layer at which dislocations first appear is registered as h_c.

To prove the existence of dislocations, the authors determined the coordination number (n_c) of each particle by performing a Voronoi tessellation [112, 113]. Briefly, the obtained Voronoi polyhedra is a generalization of the Wigner-Seitz cell to a system without a fixed lattice. The number of sides of a Voronoi polyhedron gives the coordination number n_c (e.g. n_c = 6 for a particle in a triangular lattice). Drawing a Burgers circuit [114] around regions of the crystal with $n_c \neq 6$, a non-vanishing Burgers vector then indicates the appearance of a dislocation.

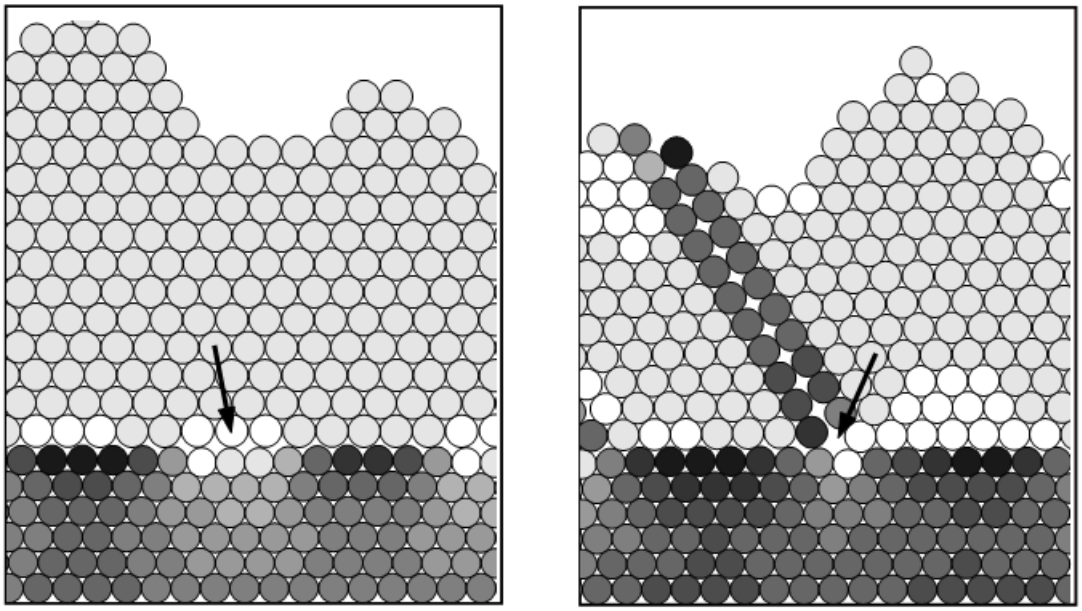

Figure 1.3: *Typical sections of crystals obtained in 1+1D off-lattice kMC simulations [108]. The six bottom layer represents the substrate. The dislocations are marked with arrows. The grey level for a particle indicates the particle's average distance to its nearest neighbors: the lighter particles are under more compression. Left panel: perfect dislocation for* $\varepsilon = +10\%$. *Right panel: partial dislocations for* $\varepsilon = +6\%$. *Figure origin: ref. [108]*

Figure 1.3 shows sections of two crystals obtained in simulations for $\varepsilon = +10\%$ in the left panel and $\varepsilon = +6\%$ in the right panel. The grey level of particles illustrates the particle's

average distance to its nearest neighbors. The lighter the grey level, the more this particle is under compression. On this figure one can observe perfect and partial dislocations as well.

Perfect dislocations (Fig. 1.3 left panel) are those for which the crystal topology far from the substrate/adsorbate interface is the same as in the coherent state and the Burgers vector is therefore an integer multiple of the lattice vector. The formation of partial dislocations (Fig. 1.3 right panel), characterized by a Burgers vector which is a fraction of a lattice vector, causes the deviations from the theoretical results, obtained for $-0.07 \leq \varepsilon \leq -0.03$ and $0.04 \leq \varepsilon \leq 0.08$. This is due to the fact that partial dislocations are spatially more extended than perfect dislocations. The reason why partial dislocations only appear for distinct values of ε is still unknown.

As another result, the simulation results show a power law dependence of the critical thickness as a function of the lattice mismatch: $h_c \sim \varepsilon^{-3/2}$. This law has been identified in various systems before [115] and may be considered as quite universal.

As mentioned earlier, this method can be extended in (2+1) dimensions. T. Volkmann et al. in Ref. [116] presents for example an off-lattice model which allows for a qualitative reproduction of stripe patterns as well as island ramification in agreement with experimental observations for CoAg/Ru(0001) [117]. In this study the quantitative dependencies of stripe width (and also degree of island ramification) as a function of the misfit and the interaction strength between the two adsorbate types is studied.

The off-lattice kMC models also allows the study of many related problems that appear in ternary systems.

1.4 Conclusions

The aim of this chapter was to give an overview of models and methods used in general to simulate thin film deposition and growth on substrates.

Every presented method, ab-initio MD, classical MD, lattice kMC and off-lattice kMC has its own advantage and limitations. The studied systems and our goals will decide which simulation method is the best to use.

If one wants a very detailed description without using empirical potentials, obviously the selected method is the ab-initio MD. But if we want to analyze evolution of a large system for a long time scale, the used method is obviously the kMC method. When one wants to combine for example the fast nature of the kMC and the more realistic description of MD methods, a good choice is a hybrid method, like the previously presented off-lattice kMC method. In such cases, however, computational resources will limit the simulation time-

scale, system size and dimensionality.

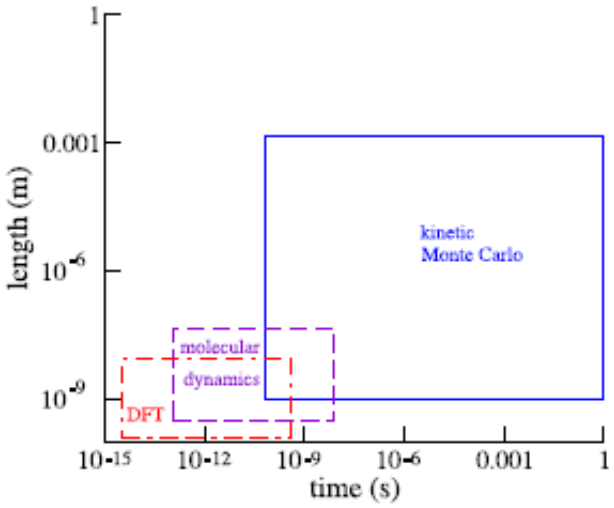

Figure 1.4: *Length and time scales simulated by first-principle calculations, classical Molecular Dynamics simulations and kinetic Monte Carlo simulations. Origin of the picture: ref. [118].*

To be more explicit for the mentioned simulation methods in the following we will give some representative values for important parameters like system size, simulated times, simulation (or CPU) time, and the generally used computer types.

As long as a PC type computer can make a classical MD simulation of 10^{-9} seconds simulated time and 10^6 particles, in a reasonable computational time, the same computer will make ab-inito MD of 10^{-12} seconds simulated time for only 10^3 atoms. With classical MD one can simulate larger systems for longer times compared to the ab-initio MD, but the computational requirements (needed computer strength and computational time) increase very fast if we aim to increase the system size and the simulated time-scale. In comparison to the above values, a kMC simulation of a simulated time of one second for 10^4 atoms takes just a few hours on a normal PC-type computer, which is already enough to simulate even patterned surfaces.

A visual comparison was given by Peter Kratzer in ref [118] for simulated time and length for ab-initio MD, classical MD and kMC methods, which is shown in figure 1.4.

Until the ab-initio MD methods are more realistic and more accurate than kMC methods, the kMC methods as the other extremity of the methods simulate much larger systems for much longer time-scales.

All of these computational approaches can help researchers in predicting and analyzing

atomic level dynamics, and answering questions about structures and their evolutions under different experimental conditions. This way one could also understand the effects of the experimentally controllable parameters and engineer structures with desired practical properties.

Chapter 2

Original contributions to the kinetic Monte Carlo methods

In this chapter two kinetic Monte Carlo methods developed by us and the simulated systems are presented in details. The results and conclusions of these models are discussed in the next chapter, here emphasizing only the details of the models.

With the first method one and two-component submonolayer growth on triangular lattice can be qualitatively studied. The hopping barrier governing surface diffusion of the atoms is estimated using Lennard-Jones type pair interaction potentials. The main advantages of this technique are the speed (it is very fast), the reduced number of free parameters, and the clear diffusion activated mechanism for the segregation of different types of atoms, relative to other methods from the literature used for simulating the same phenomena.

The second method is a more exact method, it uses as interatomic potential the Embedded Atom Method (EAM) (already discussed in Section 1.1.1), and the hopping barrier for the allowed atomic movements are calculated using the Nudged Elastic Band (NEB) [119, 120] method for simulations of surface phenomena using triangular lattice. With this improvement of hopping barrier calculation, the results of this method are in qualitative and quantitative agreement with the ones obtained experimentally and theoretically, for example for statistical studies of diffusion of Pt atom clusters on Pt(111) surface. Also using this techniques we can analyze and explain the formation of 2-dimensional triangular shaped islands on a Pt(111) surface.

2.1 A first contribution to improving the kinetic Monte Carlo methods (kMC method A)

Before presenting the first method, we briefly present the preceding studies which motivate our works.

2.1.1 Introduction

Simultaneous deposition of different types of atoms is widely encountered in experiments and practical applications [4, 7, 9, 10, 11, 12, 13, 20]. It can be used for engineering special coating structures (e.g. nanocomposits by inhibitor additive) [121, 122, 123, 124, 125], or for improving the quality of the epitaxially grown films by using one component as a kind of surfactant [126, 127]. On the other hand, impurities (contaminants), operating generally as inhibitors, are always present during the deposition process and even a tiny amount of them can drastically modify both the bulk structure and the surface growth morphology of the films [85, 128, 129, 130, 131].

Typical topological features related to the inhibitor impurity effects are: (i) irregular shapes of monolayer islands, (ii) bunches of growth steps forming hillocks and dents within the surface of crystals, (iii) truncated and rounded crystal shapes, as well as (iv) deep grain boundary grooves decorated by small crystals in polycrystalline films. Appearance of repeated nucleation and islands on the surface indicates directly that the crystal growth is interrupted by a surface covering layer, i.e. the crystals became encapsulated by the impurity phase [10, 130, 131, 132, 133]. This phenomenon was clearly demonstrated by in-situ transmission electron microscopy experiments in carbon contaminated indium films [10].

The ideal one-component deposition is thus seldom realized and one always encounters the situation where species of several material components participate in the surface atomic processes. Foreign species can control the course of the fundamental phenomena and the pathway of structure evolution. To understand the effect of surfactant or inhibitor impurities on the structure evolution and the complex atomic processes taking place on the growth surface, a common method is to use kMC simulations [19, 20, 21, 22]. This computational approach can help researchers in predicting the pathway of structure evolution and the structures that will form at different experimental conditions. By this way one could also understand the effect of the experimentally controllable parameters and engineer structures with desired practical properties.

2.1.2 Impurity decorated island edges

A problem that was well studied in the literature by kMC simulations is the co-deposition of two types of atoms, let say atoms of type A (as growing material) and B (as impurities) on the planar surface of a perfect 3D single crystal of type A atoms as discussed in ref. [88, 89]. There is a deposition rate for both components (F_A and F_B respectively, with $F_A = F_B$ for simplicity), and the atoms deposited on the substrate are allowed to diffuse there. The conditions necessary to obtain a particular segregation of the A and B atoms where the B (impurities) will surround (decorate) the islands formed by the A adatoms are investigated. In the works of M. Kotrla and co-workers [88, 89] kinetic Monte Carlo simulations were performed on simple square-lattice geometry and a first approximation for the $\Delta E^W_{X\to Y}$ hopping barrier was considered. They concluded the important result that such structures can be obtained only if a direct exchange mechanism between A and B atoms on neighboring sites is postulated.

More precisely, in their simulations they considered that the hopping barrier for an atom of type W ($\Delta E^W_{X\to Y}$) depends only on the initial state of the atom. In their approach this is the sum of a term related to the substrate, E_{sub}, and a contribution related to each lateral nearest neighbor. Contributions depend on the local composition so that we have four pair possibilities: AA, AB, BA and BB. The hopping barrier is then calculated from equation 2.1.

$$\Delta E^W_{X\to Y} = \sum_{Q=A,B} (n_0^{WQ} E_{sub}^{WQ} + n_1^{WQ} E_n^{WQ}), \tag{2.1}$$

where n_0^W is 1 if the substrate atom is of type W and 0 otherwise, n_1^{WQ} is the number of nearest-neighbor $W-$Q pairs, E_n^{WQ} is the corresponding energy contribution of $W-$Q pairs to the barrier (symmetric in W and Q, $E_n^{WQ} = E_n^{QW}$) and E_{sub}^{WQ} is the contribution from a free W atom above a substrate atom Q. In order to perform the kMC simulation for this system one has to postulate the E_{sub}^{WQ} and E_n^{WQ} values and the f_0 attempt frequency. Also, the temperature, T, of the system and the $F_A = F_B$ deposition rates have to be selected. Simulations were performed on a square lattice where the positions of the atoms in the growing layer are on top of the substrate atoms.

These simulations proved that an energetic bias favoring segregation is not sufficient to obtain configurations with impurities (B) mostly positioned at island edges. To achieve this peculiar segregation, a thermally activated exchange mechanism had to be introduced between A and B atoms on neighboring sites. The easiest way to realize this was postulating a phenomenological potential barrier E_{ex} for this process and to use equation 1.36 for calcu-

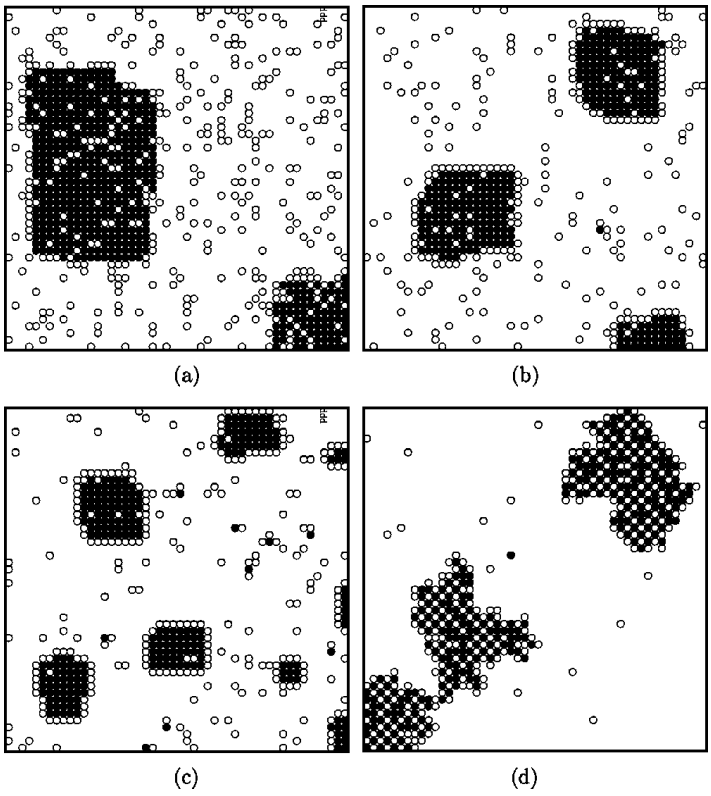

Figure 2.1: *Configurations obtained by simulations for total coverage* $\Theta = 0.2\ ML$ *for fixed: deposition flux* $F_A = F_B = 0.004\ ML/s$ *and* $E_n^{AA} = 0.3\ eV$*; and different: energy barriers* E_n^{AB} *and* E_{ex}*. (a)* $E_n^{AB} = 0.1\ eV$*,* $E_{ex} = 1\ eV$*; (b)* $E_n^{AB} = 0.2\ eV$*,* $E_{ex} = 1\ eV$*; (c)* $E_n^{AB} = 0.4\ eV$*,* $E_{ex} = 1\ eV$*; and (d)* $E_n^{AB} = 0.2\ eV$*,* $E_{ex} = 2\ eV$*. System size is* $50x50$*. Figure origin: ref. [88].*

lating the exchange rate. Results of simulations presented on ref. [88] are visible in figure 2.1 (figure origin: ref. [88]). Keeping the deposition fluxes (F_A and F_B) and the E_n^{AA} energy fixed, we can follow the influence of mixed atom interaction energy (E_n^{AB}) and exchange energy (E_{ex}).

As one can see in figure 2.1 (a), (b) and (c) the island density increases with E_n^{AB}, in the meantime the density of free impurities decreases, as a consequence of the stronger bond between $A - B$ atoms. The edge decoration also depends on E_n^{AB}, the decoration appearing just above a critical value. The influence of exchange energy (E_{ex}) is as follows: for small E_{ex} values impurities float on island edges, as for larger E_{ex} values, where the exchange process is not active, the impurities are incorporated inside the islands.

Our first model and kMC method intends to further improve this simple kMC simulation for this two-component system. Our task is to reduce the number of postulated parameters (e.g., E_{sub}^{WQ} and E_n^{WQ}) and to consider a geometry with better isotropy which will increase

the degrees of freedom for diffusion. As a consequence of this, for a reasonably large parameter set the interchange of A and B atoms will arise automatically and the phenomenological and unrealistic parameter, E_{ex}, is eliminated. In several cases when the energetic bias favors segregation, impurity decorated islands will form.

2.1.3 Details of the method

In the kMC algorithm formulated by us less parameters are postulated, and diffusion of atoms with increased degrees of freedom and improved potential barriers are considered. At the same time, the computational efficiency of the algorithm does not drop in considerable manner, so the advantage of the MC approach is kept.

Starting from the method used by Kotrla and co-workers in [88, 89], we will present the improvements of our method.

Geometrical construction

As first modification, triangular lattice ((111) plane of fcc structure) is used as substrate (filled circles in Figure 2.2). This also leads to a more compact packing of the atoms. It is assumed that atoms are spheres with the same diameter for both A and B components. In such manner there are two triangular sub-lattices (empty circles and crosses in Figure 2.2) on which the adatoms can be deposited forming monolayer lattices of FCC or HCP crystalline phases. Due to geometric restrictions, atoms in the growing layer cannot occupy neighboring sites belonging to different sub-lattices.

Considering a bulk FCC substrate, a stacking fault develops at the interface of the substrate and a growing HCP monolayer island, as visualized in Figure 2.3. This way, phase boundaries will also appear between growing islands of FCC and HCP types. This extra defect mechanism characteristic for this geometry facilitates the diffusion and interchange of atoms between the islands of the two growing phases. In the case of the two-component system only the growth of the FCC phase will be investigated, however, the formation of phase boundaries and their motions for simple homoepitaxy will also be examined.

Diffusion of adatoms on the top of the first FCC type growing monolayer is also taken into account. These adatoms are allowed to jump down on the substrate.

Hopping barrier calculation

Apart of geometry, a second difference relative to the kMC algorithm applied in [88, 89] is the calculation of the hopping barrier for the diffusion. Pair-potentials between the atoms

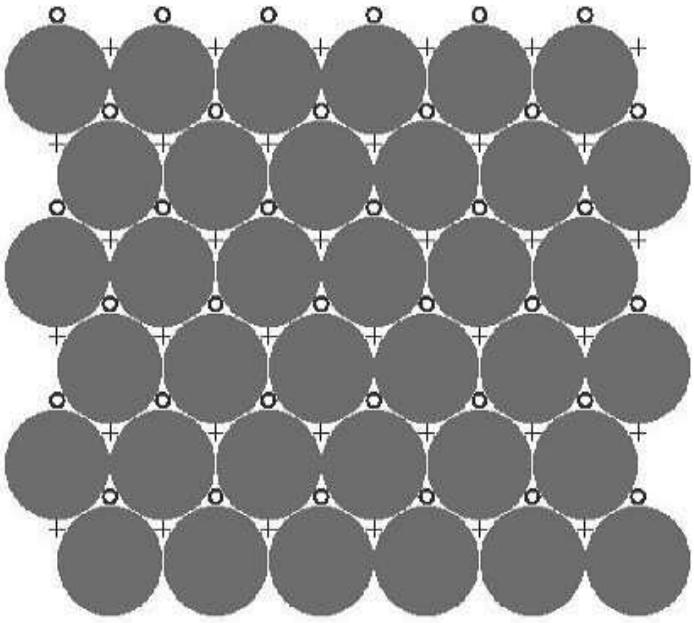

Figure 2.2: *Geometry of the considered lattice. Filled large circles represent the atoms of the substrate, small empty circles and crosses represents the FCC and HCP lattice sites, respectively, that can be occupied by the new layer of atoms.*

are used to compute the binding energies of the atoms. The hopping barrier for the diffusion process is then calculated taking into account the binding energies in the initial and also in the final states.

A Lennard-Jones type pair-potential was considered, although other accepted pair-potentials would lead to qualitatively similar results.

Assuming the lattice constant as length unit, the interaction potential between atoms of type W and Q separated with distance r can be written using one E_{WQ} parameter:

$$U_{WQ} = E_{WQ}(\frac{1}{r^{12}} - \frac{1}{r^6}), \tag{2.2}$$

The parameter E_{WQ} will fix the binding energy at $r = 1$ (units of lattice constant) equilibrium distance. Interactions between atoms are taken into account up to $s = 3$ lattice site distances. It is assumed that the hopping barrier from a site X to a site Y should depend not only on the binding energy in site X, but it should also depend on the change in the binding energy. The following simple form for calculating the hopping barrier of an atom has been proposed [134]:

$$\Delta E^W_{X\to Y} = -\alpha E^X_n + (1-\alpha)(E^Y_n - E^X_n), \tag{2.3}$$

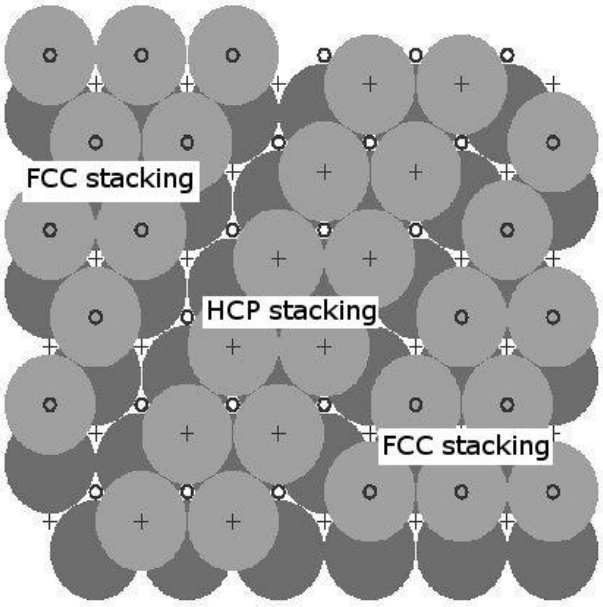

Figure 2.3: *The FCC and HCP phases that can form on a perfect FCC bulk substrate.*

In Eq. 2.3, E_n^X (E_n^Y) is the total interaction energy (binding energy) of the atom at sites X (Y), respectively. α is a parameter between 0 and 1, whose value will be determined later. This is the simplest linear form in which the barrier depends both on the binding energy in the initial position and on the difference between the binding energies of the final and initial sites. Moreover, it yields the good barrier for decohesion ($-E_n^X$) and reasonable values for the self-surface diffusion and edge-diffusion.

In order to get positive barriers for each possible process, α has to be bounded between 0.3 and 0.6.

A simple exercise using Lennard-Jones type potentials on an FCC structure shows that the ratio of the energy barrier for self-surface diffusion and adsorption energy should be around 0.35. It is immediate to realize that this ratio gives exactly the value of α, and a first estimate is thus: $\alpha = 0.35$.

The number of postulated parameters in the simulation code is strongly reduced. One has to fix only the values E_{AA}, E_{AB}, E_{BB}, the $F_A = F_B$ deposition rate, the f_0 attempt frequency, and the T thermodynamic temperature of the system.

In contrast with the method used by Kortla and co-workers [88, 89] this calculation method ensures a faster edge diffusion of the atoms (fast as a freely diffusing atom on the surface) and give possibilities to study edge related phenomenons as well.

Technical details for our simulations

Random number generator The simulation codes were written in C and were run on Linux computers. A so-called "modulo" uniform random number generator written by Tao Pang and published in ref. [135] was used, which has a period of $2^{31} - 1$, independently from the random seed. Also, the use of other uniform random number generators would lead to similar conclusions. Even shorter periods of random number generators would not influence the results, because the computers make errors in calculation of hopping barriers (calculation of exponential functions) and also in summations for calculating the cumulative functions (summing widely different rates), which will put an additional noise over the whole calculation process.

Constructing and updating the event list Another technical question is how to find the selected event to carry out and how to update the list of rates after recalculation of all rates which may have changed due to the transition? These are steps 4 and 6 of the kMC algorithm presented in Section 1.2.1.

The most efficient way to select and update the rates is to arrange the partial sum of individual rates on a binary tree. By this, finding an event and also a rate update is done by k steps, where $k = log_2(2N)$ and N is the number of all possible events in the system. This method uses almost the same amount of memory than if we store the values of the rates in a vector and in another vector the values of the cumulative function. However, for a very big number of possible events it became more efficient.

The usage of the method will be visualized in a simple and fictitious example. Let us suppose the following 7 possible rates in the system: $r_1 = 0.1$, $r_2 = 0.2$, $r_3 = 0.1$, $r_4 = 0.3$, $r_5 = 0.3$, $r_6 = 0.4$, $r_7 = 0.1$.

Because we have 7 possible rates, N will be 8 and the binary tree contains 15 elements $(2N - 1)$. As presented in Figure 2.4, at the bottom (first row) of the tree are the rates. The second row contains the pair sum of values from the first row and so on, finally the cumulative value will be at the top of the tree.

Following this example and the kinetic Monte Carlo algorithm presented in Section 1.2.1, if the value of the generated random number u multiplied by R (in this case $R = 1.5$) is $uR = 1.05$, event 6 will be selected in 3 steps.

For $uR = 1.05$ in the **first step** the value of uR (1.05) is compared to 0.7 (13^{th} box of the tree). Because 1.05 is the bigger one, we go on the right branch of the tree. In the **second step** $1.05 - 0.7 = 0.35$ is compared to 0.7, the 11^{th} box of the tree. In this case 0.35 is the smaller one and we go forward on the left branch. As the last, **third step** 0.35 is compared

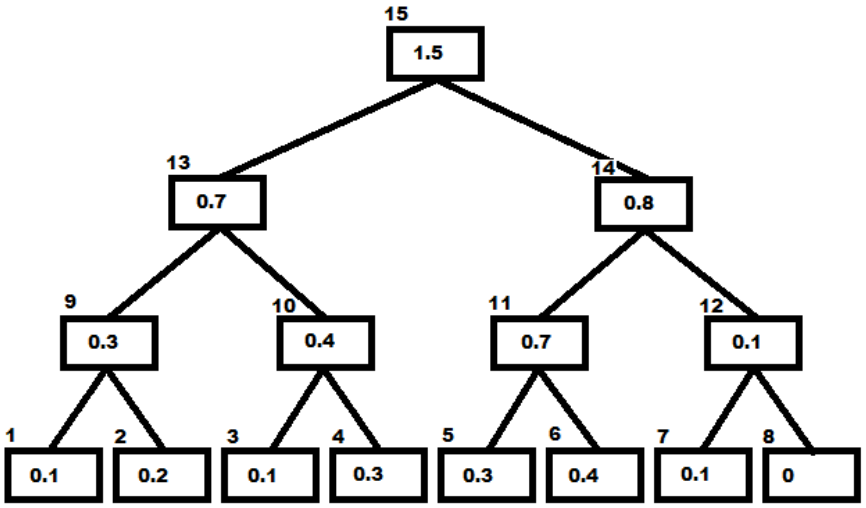

Figure 2.4: *The binary tree of a fictitious system with* 7 *possible rates.*

to the 5^{th} box of the tree and because 0.35 is bigger, we choose event 6 to carry out.

The update of the tree in case of any change in the events rate is possible with 3 steps. For example, the rate of event 4 is changed (4^{th} box of the tree). In this case we must only update the 10^{th}, 13^{nd} and finally the 15^{th} box values, and the new cumulative value of the rates is updated on the 15^{th} box value.

Further speedups The calculation of rates for different possible events of an atom was parallelized in the C code, using OpenMP [136].

Also, pair-potential values for both AA, AB and BB pairs as a function of distances are calculated once, at the beginning of the simulation. These values are stored in a list, therefore in course of the simulation it is more rapid to get the right values for the atoms in the neighborhood of the $s = 3$ lattice constant cutoff distance, than calculate these values over and over using Eq. 2.2. Taking into account both the FCC and HCP lattice sites and the presence of grain boundaries, the number and variety of neighboring atom distances up to cut-off distance is much increased relative to a model taking into account only the jumps on the FCC sites.

2.2 A second contribution to improving the kinetic Monte Carlo methods (kMC method B)

As we will see in the Chapter dedicated to the results, with the first developed method we are able to study several phenomena qualitatively, but this method is not able to give quantitative results for a specific material, because of the rough approximations used in estimating the potential barrier values. In order to study material-related problems, we need a more accurate approximation for the hopping barrier calculations. A basic question in developing such a method is to first reproduce with great accuracy the surface diffusion of the atoms.

2.2.1 Introduction

Understanding the surface diffusion of single adatoms and small adatom clusters is an important step for realistic modeling of various phenomena related to thin film growth: island nucleation, island coalescence, and Ostwald ripening [8]. Over the years experimental techniques like scanning tunneling microscopy (STM) [33, 34] and Field Ion Microscopy (FIM) [35, 36, 37, 38] were used to obtain precious insight into this phenomena. Experimental observations were completed by several theoretical methods like static calculations [137, 138, 139], molecular dynamics (MD) [21, 140], and Monte Carlo methods (MC) [94, 141].

Beside studying simple diffusion, nowadays several experimental and theoretical studies were carried out in order to understand the morphology of two-dimensional (2D) islands formed by atoms deposited on crystalline surfaces [5, 66, 85, 92, 130, 142, 143, 144, 145, 146, 147]. Apart from the obvious interest from the view of basic solid-state physics, such island morphologies might also be important for engineering various nanostructures with practical interest: nanodots, photonic crystals, or patterned surfaces [6].

Learning from the advantages and weaknesses of the previous methods, a new simulation method was developed. In this method we care more about hopping barrier calculations. We focus on the Pt system and experimentally well-investigated phenomena for this system, as diffusion of Pt atoms and clusters on Pt(111) surface, and formation and stability of 2D triangular islands. This particular system was explicitly chosen because Pt is one of the most studied materials in thin film growth, several experimental results and ab-initio calculations are available, allowing verification of the simulation results in special cases.

As motivating studies in developing this second kMC method we mention the formation and inversion of triangular islands on FCC (111) surfaces. We will shortly review now the works that motivated our studies.

2.2.2 Formation and inversion of triangular shaped Pt island on Pt(111) surfaces

On the (111) surfaces of FCC metals the formed compact islands are bounded by two types of topologically non-equivalent steps (edges). These are the (100) microfacet (type A) and the (111) microfacet (type B), as illustrated in Fig. 2.5.

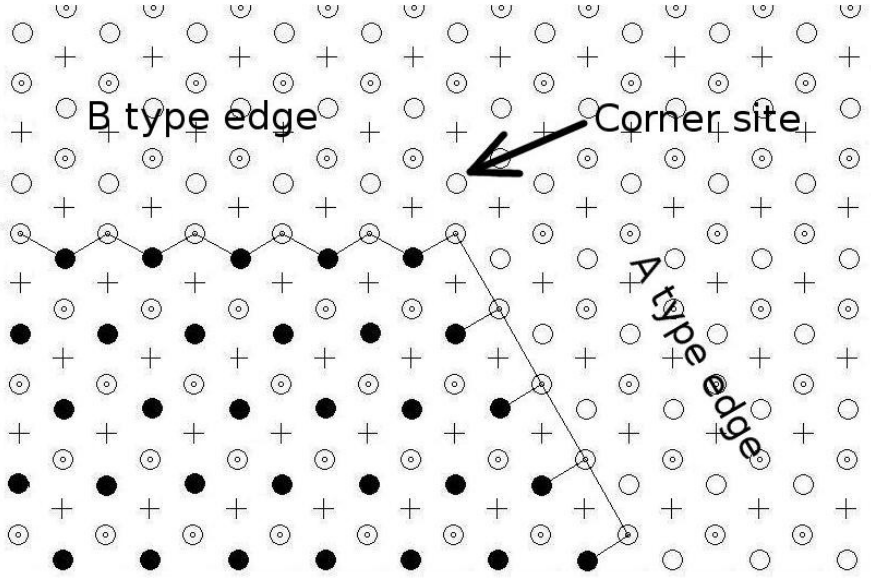

Figure 2.5: *Geometry of the type A and B edges. Dotted circles represent the sites on the substrate, circles and crosses represent the FCC and HCP lattice sites of the growing layer. The filled circles are the FCC sites of the growing layer which are already occupied by the adatoms.*

During the epitaxial deposition of Pt on the Pt(111) surface in a quite broad temperature and deposition flux range, triangular-shaped 2D adatom islands are formed. As a function of the triangle edges, these islands can be of A- or B-type (see Fig. 2.6). Usually at a parameter set only one type of triangular islands can be observed.

Michely et al. [142] reported an interesting inversion of the triangle orientation as the temperature of the sample was changed. The experiments were performed in a special scanning tunneling microscope (STM) apparatus where the temperature could be controlled in a quite broad interval. At low temperatures the nucleated atoms formed islands of fractal or dendritic shape and at higher temperatures the islands became compact. It has been found that by increasing the substrate temperature the compact island can select triangular (bounded by A steps), hexagonal (bounded by A and B steps), inverted triangular (bounded by B steps), and again hexagonal shape. Based on earlier studies for the temperature dependence of the diffusion coefficient on the type A and type B channels [148], the triangular

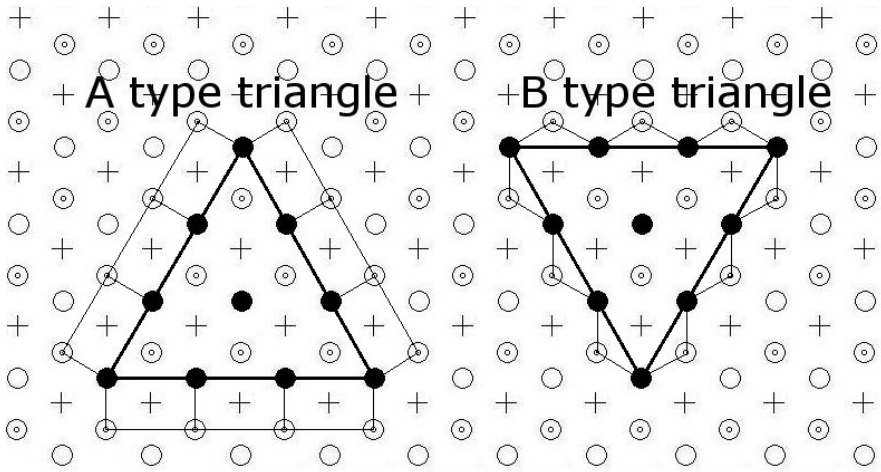

Figure 2.6: *Topology of small A and B type triangular FCC islands, bounded by only A and respectively only B type edges. Dotted circles represent the sites of the substrate, circles and crosses represent the FCC and HCP lattice sites of the growing layer. The filled circles are the occupied FCC sites of the growing layer.*

shape of the islands was attributed to the difference in the diffusion speeds of the adatoms along the A- and B-type steps. It was assumed that the lower the adatom migration speed along a step edge, the higher the probability of a new step nucleation. Therefore, the advancement of this step is faster and as a result of this, the step will disappear more quickly in time.

For lower temperatures, where the triangular shape on type A edges is dominating, Michely et al. concluded that the diffusion coefficient along the A steps (D_A) should be larger than the one along the B steps (D_B). For higher temperatures the opposite should be true and for temperatures where the islands have hexagonal shape, naturally $D_A = D_B$ was assumed. No microscopic mechanism supporting these assumptions was given, however.

The same group who reported the experimental study about the temperature-dependent shape change of the Pt islands published in 1998 an interesting new result [130]. They revealed that the triangle orientation at low temperatures is an effect of carbon monoxide (CO) impurities which are sticking preferentially to A steps. By reducing the amount of CO in the deposition chamber, only islands bounded to B steps are observed at any temperature. Therefore, the inversion of the triangle orientation is not purely a temperature effect, as was assumed earlier. Seemingly, at low temperatures CO passivates the A-step atoms more efficiently than those on the B steps, leading to higher diffusion on A steps, and as a consequence of this a faster advancement and disappearance of B steps. At high temperatures the lifetime of CO bounded to the Pt(111) surface is small, and thus the normal orientation of triangles (bounded to B steps) is observed. The formation of the triangular-shaped islands

bounded by B steps was assumed to be similar to the case of Ir [149], where the responsible phenomenon is the net flux of adatoms from B steps to A steps.

Over the years several theoretical studies were done to explore the atomistic mechanism for the shape selection and orientation of the 2D Pt islands on Pt(111) surfaces. By rescaling the theoretically calculated energy barrier values for different elementary FCC-FCC atomic movements [150], or by choosing the hopping energies in a consistent manner with the field ion microscope (FIM) experimentally measured values [101], kinetic Monte Carlo (kMC) simulations were able to find parameter sets that reproduced the experimentally observed compact island shapes and the transitions between them.

Theoretical explanations were pointing not only to the discussed edge diffusion anisotropy, but considered also the kink-breaking and corner-crossing phenomena. For the dendritic Ag or Pt islands (with a triangular envelope) formed on the Pt(111) surface, Brune [5] and Brune et al. [143] found by effective medium theory (EMT) calculations that the responsible processes are the anisotropic jumps from corners to different types of edges (A or B).

Using parameters obtained by first-principle calculations, a kMC study performed for compact Al islands on the Al(111) surface [144] showed that reversing the edge diffusion anisotropy has no effect on the orientation of the triangular islands. The island orientation changes only when the corner diffusion anisotropy is reversed. The same conclusion was derived also for compact Pt islands by Wu et al. [66]. This group also used kMC simulations to clarify the main mechanisms responsible for the formation of the triangular-shaped islands and the inversion of their orientation. In their study, three elementary atomic processes are discussed: (i) the edge diffusion, characterized by the activation energy $E_{2\to2}$ (the numbers in the notation coming from the number of in-layer first neighbors); (ii) the edge to corner diffusion, with activation energy $E_{2\to1}$; and (iii) the corner to edge diffusion, with activation energy $E_{1\to2}$. Generally, one would expect for a given type of edge the following relation between these energies: $E_{1\to2} < E_{2\to2} < E_{2\to1}$. Using activation energies for Pt strictly from Feibelmans first-principle calculations [85] for a clean Pt epitaxial growth they found islands bounded by B-steps only, independent from of the surface temperature values. They also concluded that the only parameter that could influence the inversion of triangles is the edge to corner energy barrier. By interchanging their values for A- and B-steps, the triangular islands changed their orientation. It was thus assumed that the presence of CO will weaken the binding energy of the Pt at the A-step so much that the difference in the edge to corner diffusion rates for the two steps are reversed in sign. Arguments based on the energetics of the diffusing atoms are also given in the book of Michely and Krug [145] and in the seminal paper of Ewans et. al [92].

Besides kMC simulation methods for investigating this problem, it is worth mentioning an approach based on genetic algorithms for optimizing the shape of 2D adatom islands on (111) surfaces [146] and a dynamical model based on surface interaction potentials and ab-initio calculations [147].

2.2.3 Details of the method

For calculating the potentials experienced by the diffusing atoms, the generalized EAM potential is used (presented in Section 1.1.1). The hopping barrier is determined by the Nudged Elastic Band (NEB) method, presented later on.

Also, in this method single-atom diffusion mechanism is considered, neglecting the concerted and simultaneous moves of several atoms from the cluster. These concerted moves would lead to several complications in applying the NEB method and would strongly increase the necessary computation time. However, as discussed for Cu clusters on $Cu(111)$ surfaces in [151], neglecting the collective motion of atoms might lead to unrealistically small diffusion constant values (and thus unrealistically high diffusion barriers) in the case of small stable cluster configurations like trimers and heptamers. Our results will definitely suffer of this deficiency, however, in case of Pt clusters diffusion on Pt(111) surfaces this effect is expected to be much smaller due to stronger interatomic potentials and much higher effective barrier values. For example, for Cu monomers on Cu(111) surface experiments [151] give $E_m = 37 \pm 5meV$, while for Pt monomers on Pt(111) surface experiments [37] indicate $E_m = 260meV$, a value which is one order of magnitude higher. This huge difference is due to the stronger interatomic potential which decreases the probability of collective motion of the atoms as well.

From experiments it is also known that the energy barrier for a free Pt atom jumping on the sites of the (111) plane of the FCC lattice (sometimes called activation energy or migration energy (E_m)), is around $0.25 - 0.26eV$ [5, 37, 140]. The attempt frequency is taken as $k_0 = 5 \times 10^{12} Hz$, the order of magnitude that is generally assumed for the vibration frequency of atoms. These energy values will give a good first comparison bases for our method.

Geometrical details

For single atom moves all the relevant degrees of freedom for diffusion are taken into account, so we believe that the considered approach is a realistic one. As substrate a triangular lattice ((111) plane of the FCC structure) is used and atoms are considered as spheres, iden-

tical to the first method and visualized in Figure 2.2. In such manner, there are two triangular sub-lattices (empty circles and crosses in Fig. 2.2) on which the adatoms can be deposited and diffuse, forming monolayer lattices of FCC and HCP crystalline phases. Considering a bulk FCC substrate, stacking faults will appear at the interface of the substrate and a growing HCP monolayer island (presented in Fig. 2.3). By this manner, phase boundaries can appear between growing islands of FCC and HCP types.

Because we study Pt systems, we calculate with its geometrical parameters. The edge of the cubes in the Pt FCC structure is $3.92 \times 10^{-10}m$ [152] which yields $2.77 \times 10^{-10}m$ as lattice constant for the considered triangular lattice substrate.

The energy barrier estimation

The Nudged Elastic Band (NEB) method [119, 120] is used for finding the Minimum Energy Path (MEP) of every atomic jump. This method is efficient in determining the saddle points, and therefore the energy barrier for transitions with given initial and final states. The method uses a number of replicas of the moving atom, displaced along a continuous path between the initial and final state of the transition. The replicas are connected with fictitious springs acting only along the path, ensuring its continuity. The external forces are projected, however, orthogonally to this path. The relaxing force acting on the i.-th image writes as

$$\begin{aligned} \vec{F}_i^{\,rel} &= -\nabla V\left(\vec{R}_i\right)|_{\perp} + \left(\vec{F}_i^{spring} \cdot \vec{\tau}_i\right)\vec{\tau}_i \\ &= -\nabla V\left(\vec{R}_i\right) + \left[\nabla V\left(\vec{R}_i\right) \cdot \vec{\tau}_i\right]\vec{\tau}_i \\ &+ \left[k\left(\vec{R}_{i+1} + \vec{R}_{i-1} - 2\vec{R}_i\right) \cdot \vec{\tau}_i\right]\vec{\tau}_i, \end{aligned} \tag{2.4}$$

where k is the spring constant, $\vec{R}_i$ is the coordinate vector of the i.-th image, $V\left(\vec{R}_i\right)$ is the potential, and $\vec{F}_i^{\,spring}$ is the spring force acting on the image. $\vec{\tau}_i$ is the normalized tangent vector at the location of the i.-th image, used to project the desired components of the forces. $\perp$ represents the perpendicular projections of the vectors relative to the tangent vector.

The initial coordinates of the replicas which are forming the band are determined by a simple linear interpolation between the initial and final states of the assumed jump. In order to reach the MEP, the band is optimized using the steepest descent method. The energy barrier of the transition is taken as the sum of the differences between the consecutive potential energy minimums and maximums along the oriented MEP. Usually multiple energy minimums and maximums can appear on the MEP when the path passes in the neighbor-

hood of an intermediate lattice site. Such situation can appear for example in case of an FCC-FCC jump, where the path contains an intermediate minimum due to a neighboring HCP site. Taking into account such jumps (FCC-HCP-FCC or HCP-FCC-HCP) leads to secondary order errors, because jumps to the intermediate site are counted also individually in the cumulative rate function. However, these FCC-FCC direct steps many times are necessary because there are situations when the diffusion from an FCC to a neighboring FCC site is possible via several FCC-HCP and HCP-FCC jumps, which leads to very small FCC-FCC effective (or apparent) diffusion constant. This is the case for example for edge-diffusion along the type B edge (Fig. 2.5), as we will discuss in the next chapter.

For kMC studies using this second method we consider the band discretized with 19 replicas and the used spring-constant is chosen as $k = 0.65$ eV/ Å.

The used interatomic potential

The gEAM potential [46, 54], presented in Section 1.1.1, was used to calculate the interatomic potentials for every iteration step of the used NEB method.

$r_e()$	2.771	$F_{n0}(eV)$	-4.099
$f_e(eV/)$	2.336	$F_{n1}(eV)$	-0.754
$\rho_e(eV/)$	34.108	$F_{n2}(eV)$	1.766
α	7.079	$F_{n3}(eV)$	-1.578
β	3.775	$F_0(eV)$	-4.17
$A(eV)$	0.449	$F_1(eV)$	0
$B(eV)$	0.593	$F_2(eV)$	3.474
κ	0.413	$F_3(eV)$	2.288
λ	0.826	$F_e(eV)$	-4.174
η	1.393		

Table 2.1: *gEAM parameters for Pt*

It is known that gEAM is a less accurate approximation than the ab-initio methods (for a review, see Ref. [18]). However, ab-initio MD simulations need extremely long computational time and therefore the applications of such potentials are restricted for relatively small systems and short simulation times. For simulating a surface phenomenon with a longer time evolution (seconds or minutes), a list of hopping barriers of pre-defined events is used from ab-initio calculations [66, 144]. Another possibility is to use rescaled theoretical [150] or experimental [101] barrier values or to use semi-empirical potentials [54]. Here, in order to maintain a reasonable speed and accuracy, for lattice kMC simulations we use the gEAM

method to calculate the potential. All the parameters used for Pt [120] are listed in Table 2.1. By using this method we also take into account the complete surroundings of the jumping atoms over the paths, leading to more realistic effective potential barrier values. The drawback of our approach is that gEAM is mainly used for bulk systems, and thus its use for surface diffusion processes on Pt(111) surfaces can be debated.

For free diffusion of one Pt atom on Pt(111) surface using this method gives for diffusion pre-factor $D_0 = 4.3 \times 10^{-3} cm^2/s$ and for effective migration barrier energy $E_m = 0.2eV$, which is in agreement with the results from the literature. The values of D_0 and E_m measured from FIM experiments are $2(\times 1.4^{\pm 1}) \cdot 10^{-3}\ cm^2/s$ and $0.26 \pm 0.03\ eV$, respectively [37]. Results of MD simulations using the analitic embedded atom method (AEAM) suggested $D_0 = 2.41 \cdot 10^{-3}\ cm^2/s$ and $E_m = 0.19\ eV$ [47].

Other technical details

The same "modulo" uniform random number generator is used in this kMC method as in the first method, the one written by Tao Pang and published in ref. [135]. Also the same "binary tree" event finding and rate list updating technic was used and the C code was parallelized using OpenMP instructions.

Using the gEAM for calculating interatomic potentials makes the simulations more difficult, since we cannot use a list to store the values of the potential in function of the atomic distances, like in the kMC method A, where we used the LJ pair-potential. To speed up the calculation of this interatomic potential, only its environmental (surrounding of the atom) independent parts can be stored and used from lists, for example the pair-interation part, $\Phi(r_{ij})$ (equation 1.6) and the electron density from the embedding energy part, $f_j(r_{ij})$ (equation 1.9). Because of this, and due to the used NEB method for calculating the hopping barriers, the simulation using this method is slower then the first described method. This is the price of doing more accurate calculations using parameters appropriate to real materials. A cutoff distance of $s = 3$ is taken in the simulations. According to our calculations, the gEAM potential does not change considerably taking higher cutoff values. Using this cutoff distance we have to take 3 layers of substrate into account from the bulk FCC substrate.

For any non-zero deposition flux we consider that the atoms deposited on the top of an existing island are automatically reassigned for a randomly selected site on the edges of the island. This rearrangement does not alter the random site deposition in a sub-monolayer epitaxial growth process and speeds up the simulation by handling elegantly the diffusion of the atoms on the top of the islands and their final jumps to the island edges. Simulations were done with both zero and non-zero deposition fluxes as will be presented in the next chapter.

Chapter 3

Results obtained with the developed kMC methods (kMC methods A and B).

In order to illustrate the applicability of the developed kMC methods we present here some results obtained in classical molecular epitaxy problems. Our results will be discussed in comparison with the experimental and theoretical results available in the literature.

For testing the first kMC method developed in this thesis we studied the qualitative dynamics of one component monolayer formation: island nucleation, growth, coalescence, and phase-boundary movement and annihilation. Here we also consider the formation of impurity decorated island in case of a two component deposition.

With the second, more accurate kMC method (kMC method B) we studied quantitatively the diffusion of Pt atoms and clusters of atoms on Pt(111) surface by analyzing the jump size statistics and cluster shape eccentricity. For this second kMC method we also revealed the microscopic mechanisms responsible for the formation of triangular-shaped islands and their orientation as a function of the experimental conditions.

3.1 Results obtained with the kinetic Monte Carlo method A

We implemented the kMC method A with parameters very similar to the ones used in previous studies by M. Kotrla at al. [88, 89]. We have fixed for all simulations the attempt frequency, $f_0 = 10^{12} Hz$ and the interaction energies at equilibrium distance (1 lattice constant) between the same type of atoms: $E_{AA} = 0.15eV$ and $E_{BB} = 0.0001eV$. These parameter values suggest that aggregation of A particles are favored relative to the aggregation of B

particles, in case of heteroepitaxial deposition.

The method was tested first for homoepitaxial systems (one component epitaxial deposition) then used to study the properties of the impurity decorated islands.

3.1.1 Homoepitaxial island nucleation and growth

As a first study we consider the deposition of only one, type A atom on the triangular substrate formed by the same type of A atoms. This deposition is called homoepitaxial deposition. The only energetic parameter used in this work is E_{AA} (fixed to $0.15eV$, as mentioned above). The value of the deposition flux F was chosen between $0.1 - 10ML/s$ and the temperature T was varied between $400 - 650K$. A system with 512×512 size was considered and we investigated the time-evolution of the system and qualitatively compared it with experimental results.

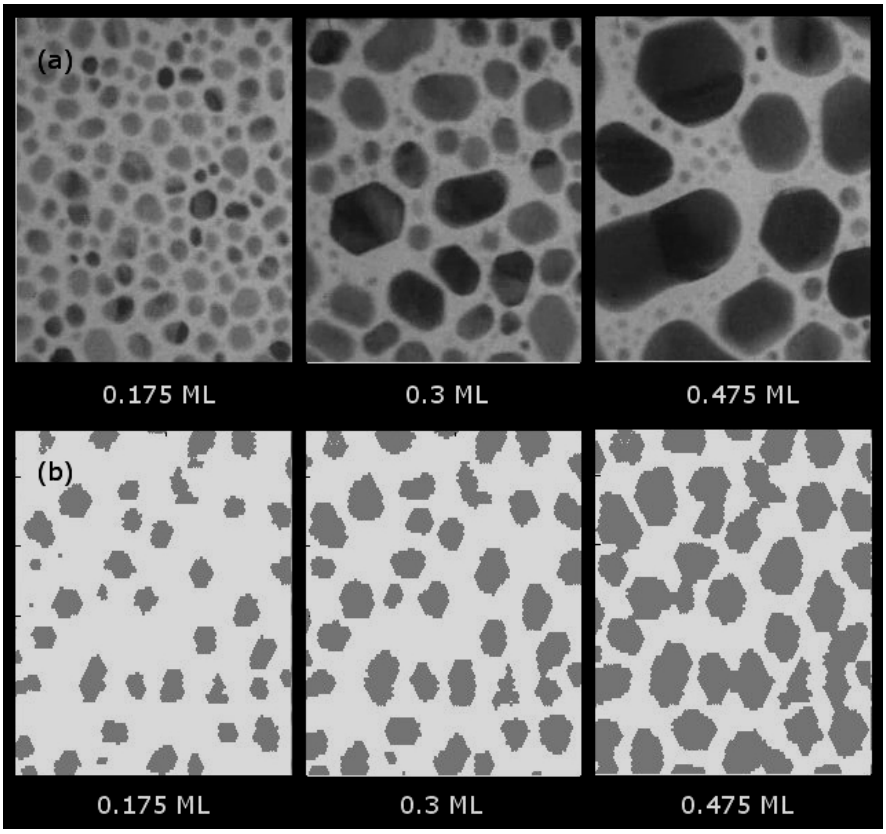

Figure 3.1: *Visual comparison between (a) experimental and (b) simulated island-growth scenario.*

On Fig. 3.1 a visual comparison between the experimental and simulated island growth dynamics is given. Experimental results are from an in-situ transmission electron microscopy

experiment performed for Indium deposition on amorphous Carbon membrane in the MFA-KFKI (Budapest, Hungary) laboratories [129]. One has to be careful while comparing the monolayer growth simulations with this experiment. In the experiment the islands are three-dimensional structures while simulations are for simple monolayers! Islands are growing both perpendicularly on the plane and in the direction of the plane. One can expect thus only qualitative agreement. Simulation shown on Fig. 3.1 was performed for $T = 400K$ with $F = 10ML/s$.

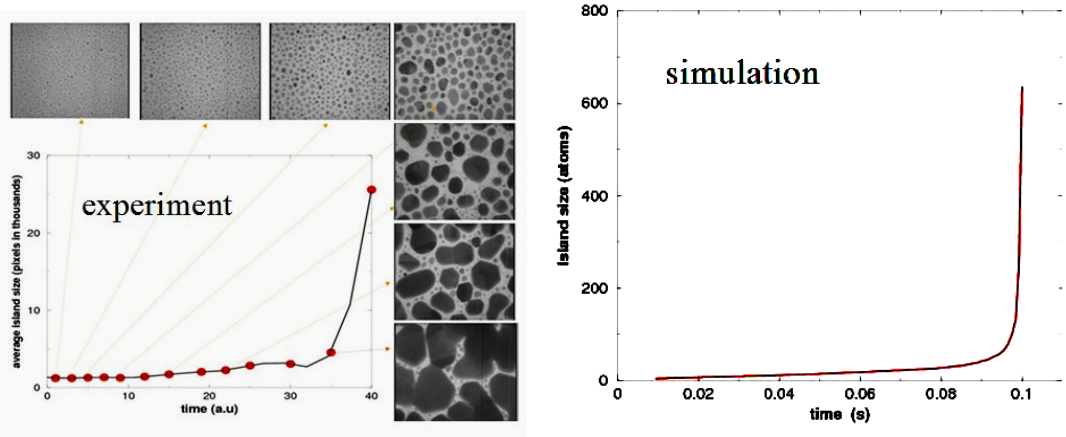

Figure 3.2: *Experimental and simulated trend of the average island size as a function of time during the formation of a continuous covering layer. Simulations are for* $T = 550K$ *and* $F = 10ML/s$ *deposition rate.*

The time-evolution curve of the average island sizes are in qualitative agreement with the experimental one. On Fig. 3.2 the trend for the simulated and experimental data is compared. Experimental data are from the same in-situ TEM experiment as the one presented in Fig. 3.1. Since experiments are for three-dimensional islands, one would expect in such case a less steep curve when the continuous layer forms. As it can be observed in the figure the shape of the curves are quite similar, although the simulated curve is much steeper at the end.

For the same coverage ratio of the monolayer one can follow the average island number in a given surface area as a function of the temperature. As temperature increases, less and less islands create, since the surface-diffusion process is enhanced and island growth is favored. Representing the average island number as a function of the inverse of the temperature, the curve should follow the experimentally proved Arrhenius-type behavior by C.-M.-Zhang et al. in ref. [153], i.e it should be a monotonically increasing function with a constantly decreasing slope. On Fig. 3.3 we present simulation results considering two different filling

(coverage) ratios in the monolayer. The curves have the right, Arrhenius trend and are in qualitative agreement with the experimental results presented in [153].

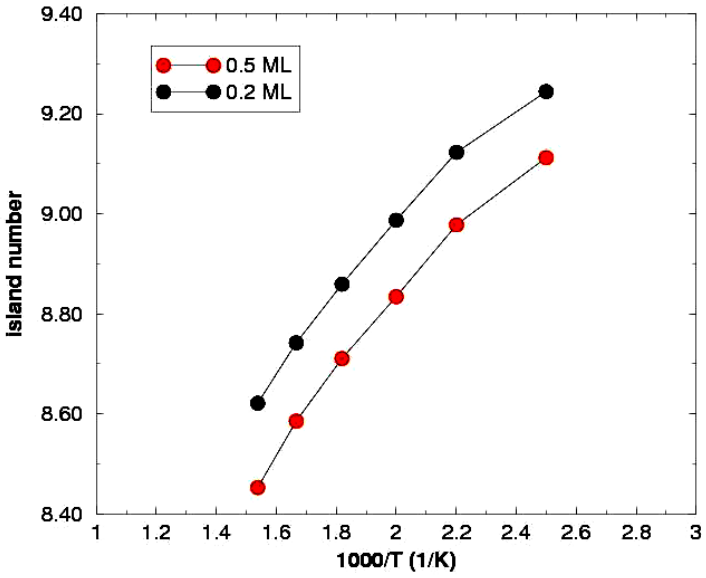

Figure 3.3: *Simulated Arrhenius-like trend for the average number of islands in a given surface area. Simulations were performed with* $F = 10ML/s$.

3.1.2 Evolution and annihilation of stacking-faults related phase-boundaries on an FCC (111) surface for one component system

Considering the case when atoms are deposited with a fixed deposition rate ($F = 10ML/s$) on a planar FCC (111) surface formed by the same type of atoms, similar to the previous case, monolayer domains of the two equivalent orientations but with different, FCC and HCP sequences can nucleate and grow. It is worth mentioning here that although the FCC and HCP sites are geometrically equivalent, using the kMC method A the binding energy is slightly different, the FCC sites being energetically a bit stable. Formation, motion and annihilation of stacking-faults related phase-boundaries appears and can be followed during simulation (Fig. 3.4). Some movies are also given on the home-page dedicated to this study [131].

3.1.3 Island coalescence for a one component system

Coalescence is by definition the process in which islands merge together.

The scenario for island coalescence is also in qualitative agreement with the one observed in experiments. From simulations we observed the realistic formation of necks and the fast

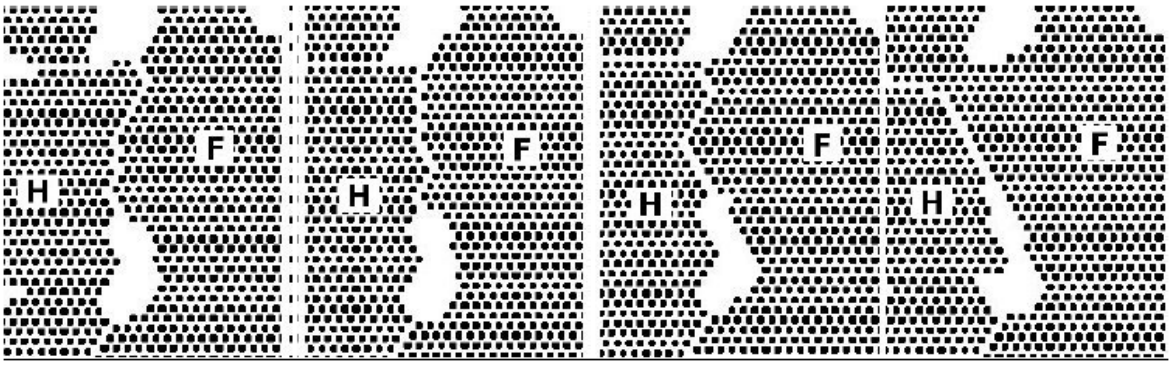

Figure 3.4: *Characteristic time evolution and annihilation of stacking-faults related phase-boundaries for the case when only type A atoms are deposited. The pictures from left to right represent steps in the time-evolution. The F and H islands correspond to FCC and HCP stackings, respectively. Simulation parameters are:* $E_{AA} = 0.15eV$, $T = 650K$, $F = 10ML/s$ *and* $f_0 = 10^{12}Hz$.

rounding of the resulting islands. A simulation sequence in this sense is illustrated in Fig. 3.5. Movies made from simulation results are presented on the home-page dedicated to this study [154].

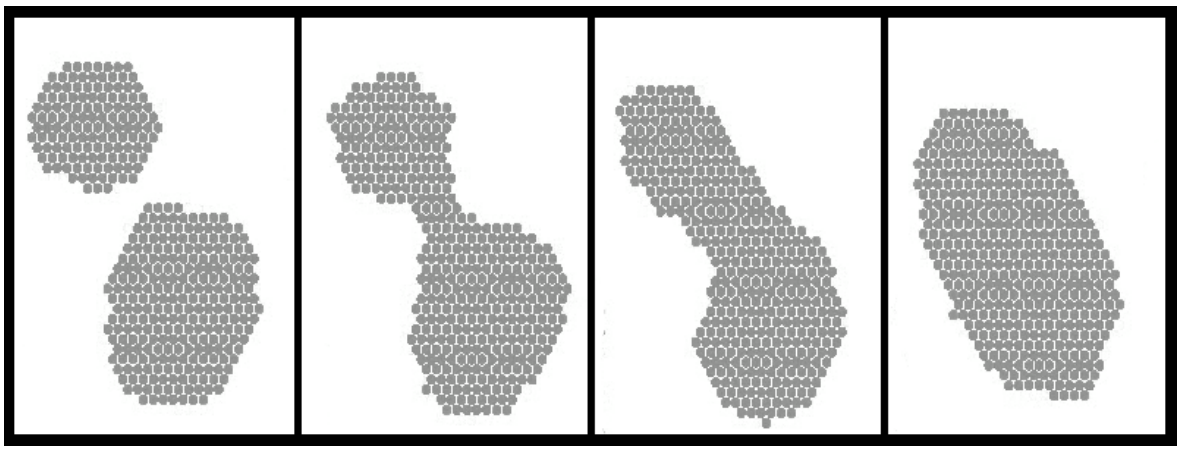

Figure 3.5: *Snapshots from simulated island coalescence. Simulation parameters are:* $T = 450K$ *and* $F = 0.1ML/s$.

3.1.4 Formation of the impurity decorated islands in the case of a two component deposition

Simulations for the co-deposition of the type A and B atoms lead to the expected decorated islands presented in Section 2.1.2. For the fixed parameters $f_0 = 10^{12}Hz$, $E_{AA} = 0.15eV$, $E_{BB} = 0.0001eV$, and as a function of the E_{AB} (varied in the $0.02 - 0.12eV$ interval)

parameter, two main types of structures are observable: (i) island containing intermixed type A and B atoms, and (ii) islands decorated with B impurities.

As expected, for low $E_{AB} < 0.08eV$ values the impurity decorated islands are stable, while for higher $E_{AB} > 0.08eV$ values the islands containing intermixed type A and B atoms are observable as illustrated in Figure 3.6.

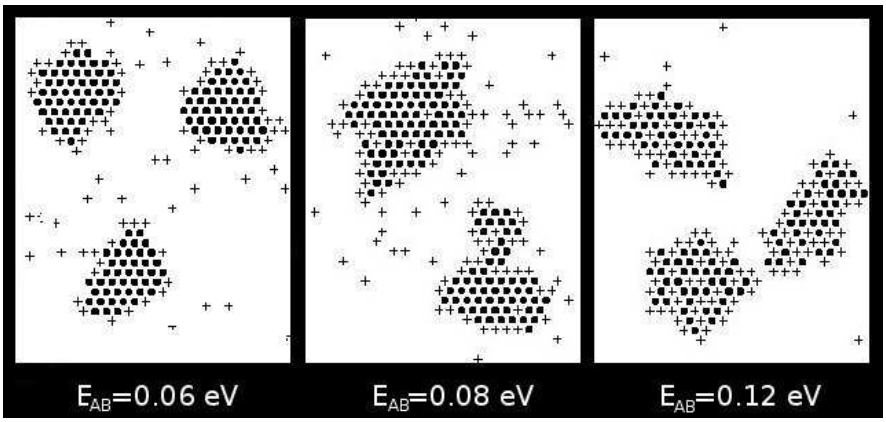

Figure 3.6: *Island structures obtained as a function of the E_{AB} parameter. Simulations done for $E_{AA} = 0.15eV$, $E_{BB} = 0.0001eV$, $T = 650K$, $F_A = F_B = 10ML/s$ and $f_0 = 10^{12}Hz$. The structures from left to right are obtained for $t = 1.25 \times 10^{-2}s$ (60000 MC steps), $t = 2.73 \times 10^{-2}s$ (20000 MC steps) and $t = 1.87 \times 10^{-2}s$ (1500 MC steps) simulation time, respectively. A central part of a much larger simulation area is presented. For $E_{AB} < 0.08eV$ impurity decorated islands are formed.*

Increasing or decreasing the temperature will only shift the boundary between these two types of structures and favor larger or smaller islands of lower or higher number density (nucleation density) respectively, for the same number of deposited atoms. The time evolution of the structures in the case of impurity decorated islands is illustrated in Figure 3.7. Some movies showing a more complete dynamics are available on the home-page [154] dedicated to this study.

We have to emphasize that in our simulations we obtained impurity decorated island without using a phenomenological exchange barrier. As we discussed in Section 2.1.2 this was a must in the previous kMC simulation studies performed by Kotrla et al. 2.1. The exchange mechanism between atoms of different types on neighboring lattice sites appears directly from diffusion, without considering an artificially predefined rate for such a process.

3.1.5 Conclusions

Our aim with the kMC method A was to show that kinetic Monte Carlo methods can easily be improved and made more realistic without loosing its main advantage of simulating large

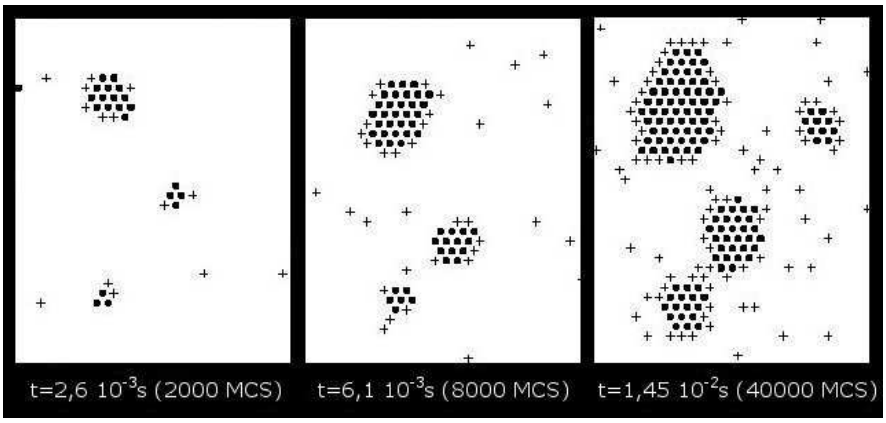

Figure 3.7: *Snapshots from the time evolution of the system. Simulation parameters are* $E_{AA} = 0.15eV$, $E_{BB} = 0.0001eV$, $E_{AB} = 0.06eV$, $T = 650K$, $F_A = F_B = 10ML/s$ *and* $f_0 = 10^{12}Hz$. *A central part of a much larger simulation area is presented.*

systems and reasonably long dynamics time. Systems with lattice sizes up to 512×512 were easily simulated in a few days on normal PC type computers (Pentium4, 3.4 GHz).

The two component co-deposition process was successfully modeled by considering two easy improvements relative to the simple classical method. First, a new hopping barrier formula was used, calculated from the pair interaction potentials of the atoms (assumed to be of Lennard-Jones type in our model). Secondly, more degrees of freedom for the diffusion of particles were allowed by considering a triangular lattice and the growth of a second layer on the top of the simulated one. Interchanges of adatoms between these two layers were made possible. The exchange mechanism between atoms of different types on neighboring lattice sites appears directly from diffusion, without considering an artificially predefined rate for such a process. By this way it is possible to simulate with a reduced number of parameters the special segregation process in which impurities are decorating the growing islands. Vacancies, stacking-faults, phase-boundaries and their dynamics are also successfully reproduced by this improved kinetic Monte Carlo technique. The method can be generalized to computationally study practically important pattern and structure formation problems during the co-deposition of several types of atoms on a given crystalline substrate. The presented method is computationally fast, and systems with tens of thousands of atoms can be simulated within reasonable computational time on PC type computers. The method is, however, limited to the case when the deposited components have similar crystal structures and similar lattice constants. Whenever there is a lattice constant mismatch between the components, the earlier presented off-lattice kinetic Monte Carlo methods have to be used [104, 105, 106, 107, 108, 109, 110].

For specific systems and more accurate simulations, realistic potential or barriers determined

from ab-initio calculations have to be used [71]. These methods will reduce, however, considerably the size of the studied system and the time length of the dynamics that can be investigated with a given computational resource.

kMC method A can be easily generalized for simulating the growth of several layers as well. The obtained results were published in: Communications in Computational Physics [97] and in Journal of Optoelectronics and Advanced Materials [99] .

3.2 Results obtained with the second developed Monte Carlo method (kMC method B)

kMC method B has the advantage relative to kMC method A that it can be used for quantitative studies on specific materials. We used it, first as a verification for the method, to study the statistical properties of the diffusion of Pt atoms and clusters on a Pt(111) surface. The diffusion coefficient is computed for various cluster sizes and system temperatures. From here a simple scaling argument was proposed for the size dependence of the diffusion coefficient's pre-factor. The obtained results are in agreement with the ones taken from the literature, obtained by experimental or theoretical studies. With a detailed statistical analysis of the event-by-event kMC dynamics, we were able to identify mechanisms for the diffusion of the cluster's center of mass. After this check performed on the method we focused on a more delicate topic, the formation of triangular-shaped Pt adatom islands on a Pt(111) surface. The numerical results obtained with our kMC method reveal that the preferential orientation of the triangles cannot be explained solely by the differences in the diffusion coefficients of the atoms along the topologically non-equivalent edges of the islands (edge type A and B visualized in Fig. 2.5) as it was thought before. For a self-consistent explanation of the triangle orientations, we examined the topological and energetic details of the diffusion paths for all the edge diffusion processes, kink-formation or kink-breaking events, and corner to edge jumps.

3.2.1 Diffusion of Pt atoms and clusters on Pt(111) surfaces

In agreement with experimental observations we assume two possible mechanisms for cluster diffusion (shown in Fig. 3.8): a) Diffusion of atoms on the cluster edge (periphery diffusion). b) Dissociation of the cluster in two parts which can diffuse by their own, and recombine in a cluster with the original size.

In order to avoid interaction and mixing between clusters, systems containing initially

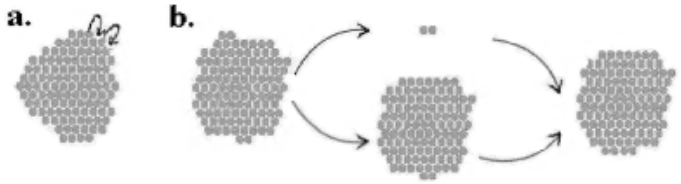

Figure 3.8: *The two leading mechanisms for cluster diffusion: a) edge diffusion of atoms around the cluster and b) dissociation of the cluster into two diffusing clusters that recombine into a cluster with the original size.*

just one cluster are considered. During simulation this cluster might fragment in parts, and the simulation is stopped whenever the biggest component becomes smaller than 90% of the original size. Clusters with sizes $N = 1, 2, 3, 4, 5, 6, 7, 9, 13, 19, 25, 30$, and 37 atoms are studied. For starting configurations, densely packed structures (as close as possible to disc-shape form) are considered. In all our diffusion-related studies no additional deposition of atoms are allowed (deposition flux, $F = 0\ Ml/s$) and various temperatures, ranging from, $300K$ to $900K$, are fixed. The simulated lattice size is 256×256 and periodic boundary conditions are imposed. All the other details of the simulations were presented in the chapter devoted to kMC method B.

For each simulated cluster size and temperature value several runs (of the order of 10) were performed and the obtained results were averaged. The length of one run (the number of atomic jumps) was different for different cluster sizes. While for monomers 20.000 jumps were enough to reach a reasonable distance of the CM relative to the starting position, for larger clusters (for example $N = 37$) around 800.000 individual jumps were necessary. Computational time increased thus very much for large clusters. Calculation of the potentials were parallelized on 6 processors. Simulations were done on a cluster of 88 Xeon Processors, linked by a Myrinet network.

Calculation of the diffusion coefficient and a scaling argument for size dependence of the diffusion coefficient's pre-factor

In general, the diffusion coefficient (D) is derived by following as a function of time the mean-square displacement of the cluster's Center of Mass (CM).

The mathematical definition of D is:

$$D = \frac{\left\langle \left(\Delta\vec{r}(t)\right)^2 \right\rangle}{2d \cdot t}, \tag{3.1}$$

where $\left(\Delta\vec{r}(t)\right)^2$ is the square of the displacement of the CM during a time t, and d is

the dimensionality of the lattice. A simple method to compute D is by plotting $\left\langle (\Delta\vec{r}(t))^2 \right\rangle$ as a function of t and determining the slope of the obtained linear dependence. This was also the method used in the present study. The diffusion coefficient exhibits the well-known Arrhenius-like behavior as a function of temperature [155]:

$$D = D_0 \exp(-\frac{E_m}{k_B T}). \tag{3.2}$$

In (3.2) , D_0 is the pre-factor of the diffusion coefficient, E_m is a phenomenological activation energy (or sometime called migration energy) of the diffusing particle or cluster, k_B is the Boltzmann constant, and T is the thermodynamic temperature of the system. D_0 and E_m can be calculated by studying the diffusion coefficient at different temperatures. One might assume that for clusters of different sizes both D_0 and E_m is dependent as a function of the cluster size, i.e. $D_0 = D_0(N)$ and $E_m = E_m(N)$.

Previously, A. F. Voter [21] considered an MD simulation for studying the diffusion coefficient's dependence as a function of the cluster size. For clusters containing more than 10 atoms they proposed a power-law dependence:

$$D \approx N^{-\gamma} \tag{3.3}$$

Several other theoretical studies reported similar behavior, with largely different scaling exponents, with γ between -0.5 and -1.5, that depends on the considered material, simulation temperature and used model [141, 156, 157, 158]. Many of the previous studies also have a critical view on the scaling behavior, emphasizing that the results are rather ambiguous due to the restricted cluster sizes and due to the oversimplified models.

In our work [52] we proposed a simple theoretical argument for the size dependence of the D_0 pre-factor when periphery diffusion is the dominant mechanism for the cluster diffusion (Fig. 3.8 a.)). Let us assume a cluster of atoms of size N. Assuming that this cluster is usually a compact disk-like structure (configuration close to the minimum energy configuration), its perimeter is proportional with $N^{1/2}$. The number of atoms capable for periphery diffusion, N_{diff} is thus:

$$N_{diff} \sim N^{1/2}. \tag{3.4}$$

For the problem considered in the present study, our simulations proved that the periphery motion of atoms is indeed the leading mechanism for cluster diffusion. This periphery diffusion is a rapid one, atoms performing several thousands of cycles in unit time. Due to the edge diffusion of one periphery atom, the average displacement, $< r_1 >$ of the CM of

the cluster of size N in unit time is proportional with the radius, R_N, of the cluster (average displacement length of one atom) and inversely proportional with the total mass of the cluster (N):

$$\langle r_1 \rangle \sim \frac{R_N}{N} \sim N^{-1/2}. \tag{3.5}$$

The pre-factor of the diffusion coefficient, due to the motion of one single periphery atom, D_{01}, is thus:

$$D_{01} \sim \langle r_1 \rangle^2 \sim N^{-1}. \tag{3.6}$$

The pre-factor D_0 is a result of the edge diffusion of all periphery atoms. One might expect thus:

$$D_0 \sim N_{diff} \cdot D_{01} \sim N^{1/2} \cdot N^{-1} \sim N^{-1/2} \tag{3.7}$$

One of our aims in kMC studies was to prove this simple conjecture.

Arrhenius behavior

Simulations performed at various temperatures prove the validity of the Arrhenius relation (Eq. (3.2)). Results for $ln(D)$ as a function of $1/k_BT$ are plotted on Fig.3.9. Different curves are for different cluster sizes, as illustrated in the legend. The Arrhenius relation holds for all cluster sizes, although for closed shell clusters (for example $N = 7$) the diffusion constant values are lower than expected from the general trend after the cluster sizes.

For single Pt atom diffusion we obtained $D_0 = 4.3 \times 10^{-3} cm^2/s$ and $E_m = 0.2eV$ which are in reasonable agreement with the results from the literature. The experimentally measured values of D_0 and E_m are $2(\times 1.4^{\pm 1}) \cdot 10^{-3}\ cm^2/s$ and $0.26 \pm 0.03\ eV$, respectively [37]. MD simulations using the AEAM potential indicate $D_0 = 2.41 \cdot 10^{-3}\ cm^2/s$ and $E_m = 0.19\ eV$ [140]. Other MD studies using Lennard-Jones potential yield $D_0 = 6.3 \cdot 10^{-4}\ cm^2/s$ and $E_m = 0.19\ eV$ [139].

The above results indicate that the average migration energy, E_m, calculated from the Arrhenius relation (Eq. (3.2)) is somehow smaller than the experimental one. The obtained result is, however, in agreement with the barrier values expected theoretically using the EAM and NEB. In our kMC simulations, the atoms can diffuse on both stackings (FCC and HCP ones). The diffusion barriers for the jumps of one freely moving atom on the same or on different stackings are summarized in Table 3.1.

The average diffusion energy should be thus somewhere between $0.294eV$ and $0.146eV$.

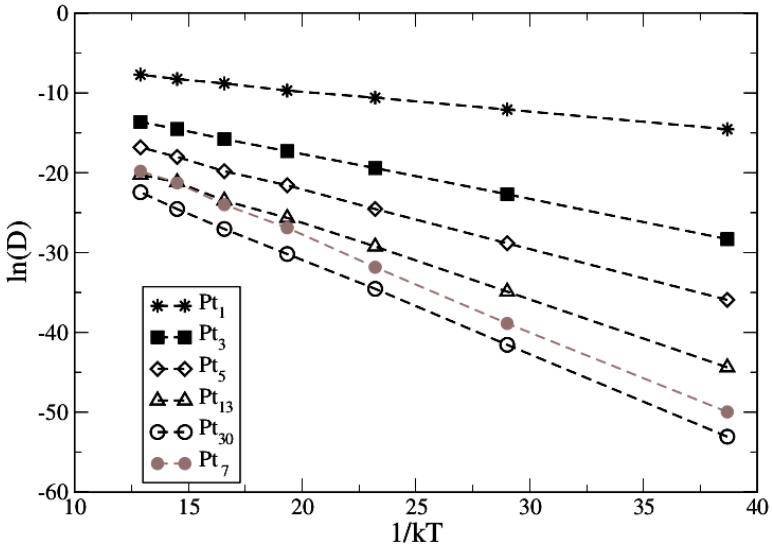

Figure 3.9: *Arrhenius behavior of the diffusion coefficient for several cluster sizes. Note the smaller than expected diffusion constant values for the $N = 7$ closed shell clusters.*

$FCC - FCC$	0.293eV
$HCP - HCP$	0.294eV
$FCC - HCP$	0.148eV
$HCP - FCC$	0.146eV

Table 3.1: *Computed diffusion barriers for a freely moving atom.*

Since the HCP-FCC and FCC-HCP jumps are more frequent, the obtained E_m value should be closer to the lower bonds. The obtained result is in agreement with these requirements.

Now let us turn our attention to the diffusion of the clusters ($N > 1$). As Fig. 3.9 indicates, the Arrhenius behavior is valid in all cases. The migration energy values calculated for clusters of various sizes are summarized in Fig. 3.10. These values can be compared with the values determined from FIM experiments [37] and those calculated by the Effective Medium Theory (EMT) for clusters with sizes up to $N = 7$ atoms [137]. The results are plotted on Fig. 3.11(a). From this figure one concludes a fair agreement of our kMC simulation results with the experimental data. The EMT results have a similar trend, but seemingly their agreement with the experimental results is less impressive. The values of the D_0 prefactors are also in good agreement with the FIM experimental results (Fig. 3.11(b)). A strong difference is obtained for clusters composed by $N = 7$ atoms. In this case the experiments suggest $D_0 = 5.1(\times 3.8 \pm 1)\ 10^{-1} cm^2/s$, while our simulations yield $D_0 = 1.6 \cdot 10^{-2}\ cm^2/s$. The $N = 7$ atom clusters are the smallest closed shell clusters on the FCC lattice. As it was emphasized earlier in Section 2.2.3 for small closed shell clusters, the concerted motion

of atoms becomes important. In the computational approach considered here, these were neglected, so it can be assumed that the difference between experimental results and simulations is a result of our single-atom diffusion approximation. Further closed shell structures are the ones containing $N = 19$ and $N = 37$ atoms. From Fig. 3.10 we conclude that E_m has local maximums in these cases as well. Fig. 3.10 also suggests the saturating trend of the migration energy as the cluster size increases.

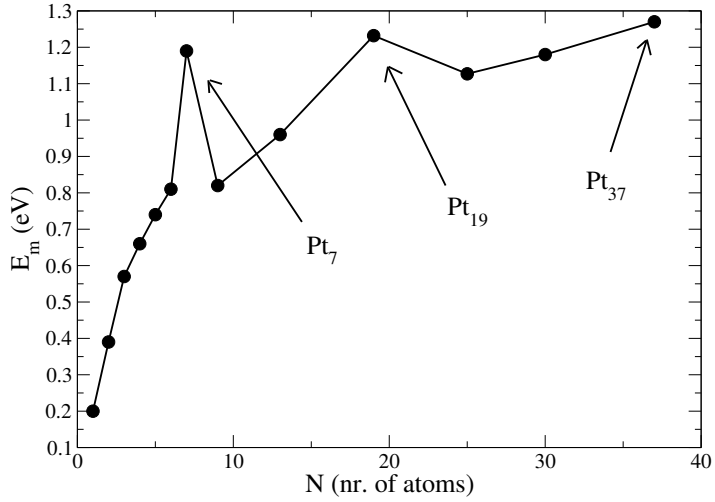

Figure 3.10: *Simulation results for the migration energy, E_m, for clusters of various sizes, N. Please note the local maximum for closed shell clusters.*

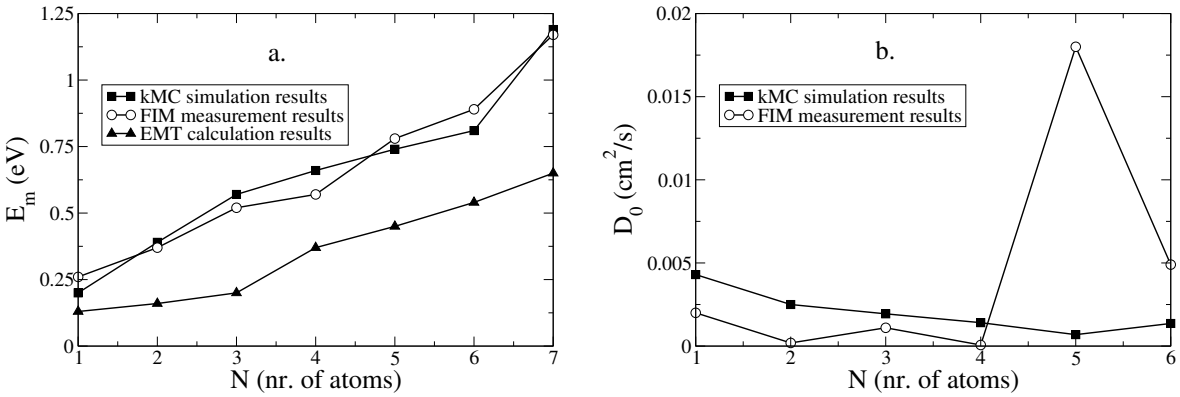

Figure 3.11: *Simulation results for the values of E_m migration energy (a) and for the D_0 pre-factor of the diffusion coefficient (b) as a function of the cluster size, N, for $N \leq 7$.*

Size dependence

We turn our attention now to the size dependence of the diffusion coefficient. As discussed previously, one would expect that both D_0 and E_m depend on the cluster size: $D_0 = D_0(N)$

and $E_m = E_m(N)$. Fig. 3.10 illustrates the trend of the $E_m(N)$ dependence, suggesting a saturating trend for larger clusters. Many earlier numerical studies [21, 141, 156, 157] suggested without any analytical foundation a power-law behavior of $D(N)$ for clusters containing more than 10 atoms. The suggested scaling exponents, as already mentioned, are widely different and depend both on the used model and temperature range.

Plotting the diffusion coefficient versus the cluster size on a log-log plot, one would expect thus lines. For the relatively small clusters ($N \leq 37$) considered in our kMC simulations this conjecture holds relatively well. On Fig. 3.12 (a) we present the $log(D)$ versus $log(N)$ plot for several temperatures. If one would force a power-law fit $D = C \cdot N^{\gamma}$ on these curves the results would yield a γ scaling exponent that is strongly temperature dependent (Fig. 3.12 (b)). However, due to the very restricted cluster sizes, we were able to study with the available computational resources only systems with $N \leq 37$, so the power-law claim is not rigorously sustainable.

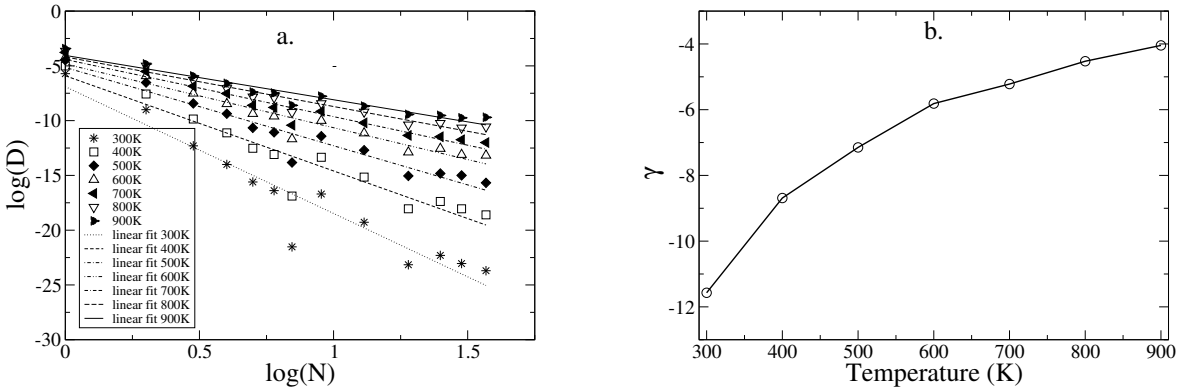

Figure 3.12: *(a) Double logarithmic plot for the diffusion coefficient as a function of N. Results for various temperatures and a $D = C \cdot N^{\gamma}$ power-law fit for the data-points. (b) The dependence of the γ scaling exponent as a function of temperature.*

In Section 3.2.1 we presented a simple argument (Eqs. (3.4) - (3.7)) for the scaling property of the D_0 pre-factor: $D_0 \sim N^{-1/2}$. The D_0 values determined from our kMC simulations support this conjecture. Plotting $log(D_0)$ as a function of $log(N)$ for simulations done at various temperatures leads to almost overlapping curves (Fig. 3.13). The general trends on this log-log plot suggest a scaling with an exponent very close to the predicted -0.5 value. On Fig. 3.13 it is also observable that for the $N = 7$, closed shell configuration, a huge peak is present: the pre-factor increases with almost two orders of magnitudes. As we discussed before, the migration energy has also a clear and understandable maximum for $N = 7$ (Fig. 3.10). This maximum in E_m would decrease the value of the diffusion coefficient. The peak in the pre-factor is, however, much more puzzling, and will balance in

part the effect of E_m. Several previous experimental and simulation studies [35, 36, 37, 38, 138] noticed this peak in D_0, both for the Pt_7 and Ir_7 clusters. Presently there is no final and conclusive explanation for its occurrence. Our feeling is that this peak is also an artifact due to the single-atom diffusion approximation considered in our kMC simulations.

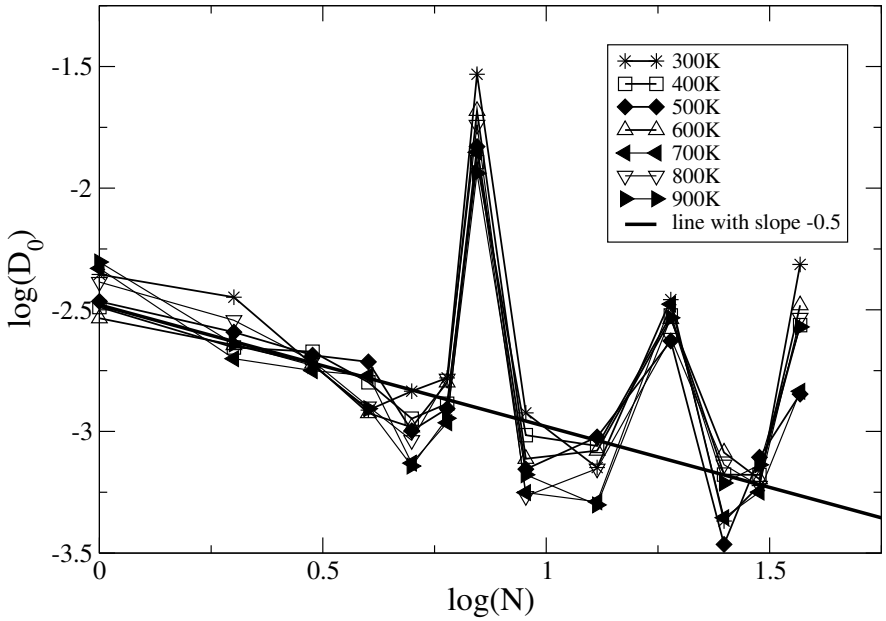

Figure 3.13: *Size dependence of the D_0 pre-factor of the diffusion coefficient.*

Jump-size statistics

Up to now the surface diffusion of the clusters was described by means of an ensemble averaged phenomenological quantity: the diffusion coefficient. However, computer simulations allow much more! The surface diffusion of the clusters can be approached on an event-by-event level, analyzing the individual displacements in the clusters CM as well. After each kMC event, one can compute this absolute displacement and their statistics could yield additional information on the diffusion process. Our studies will focus on an open shell cluster: Pt_{13}. In the following we will simply use the term "jump" for the displacement of the CM in one simulation step. The size of these jumps will be measured in lattice constant units.

On Fig. 3.14(a) and Fig. 3.14(b) results for simulations performed at $T = 900K$ are given, plotting the size of the jumps as a function of time. Fig. 3.14(b) is a magnification of a small part of Fig. 3.14(a), illustrating the quantized nature of these jumps and the fact that in the kMC simulation time evolves in non-uniform steps.

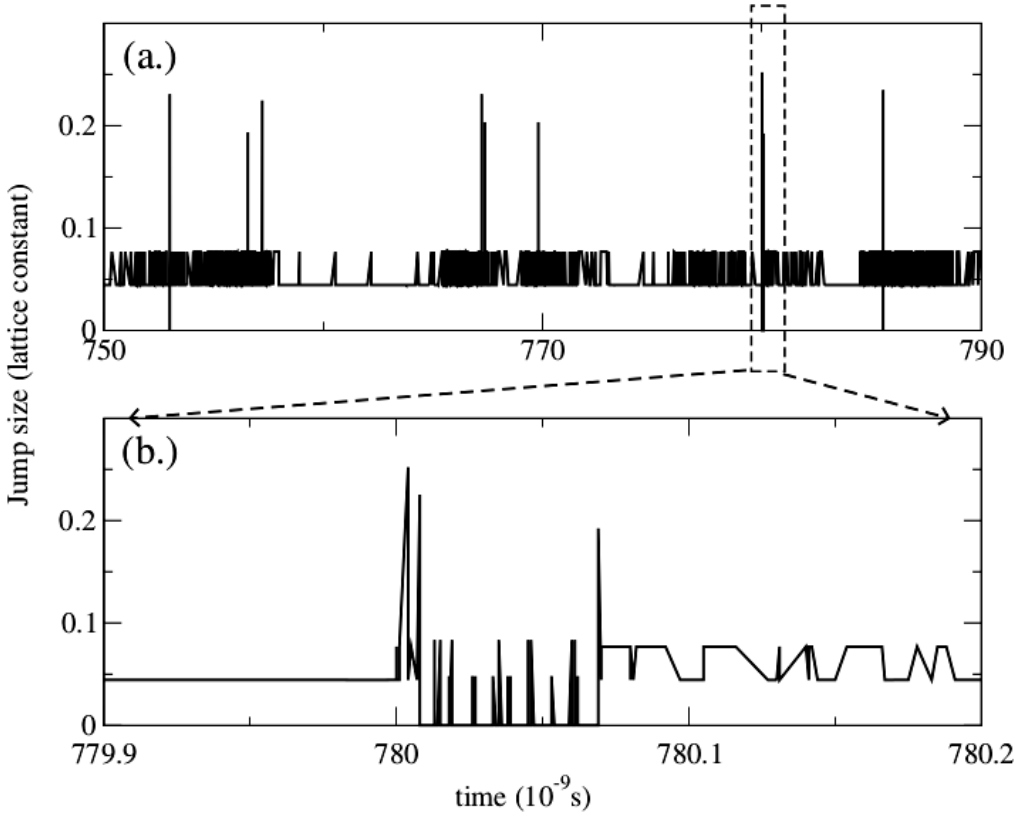

Figure 3.14: *Jumps of the clusters CM as a function of time. (b) is a magnification of the windows shown in (a).*

Jumps of sizes 0 occur when a freely moving atom (an atom which escaped from the cluster) makes a diffusion step. In this case the CM of the cluster remains immobile for this time period. Jumps smaller than 0.12 lattice constants are characteristic for edge diffusion. This threshold value can be obtained by simple geometrical considerations, following what happens with the position of the CM when an atom on the edge of a cluster with $N = 13$ moves to a neighboring empty site.

In our model two different types of edge diffusion mechanisms are competing as it was shown in Fig. 3.8. The first one is when an atom from the cluster's edge moves between an FCC and HCP site. The second one is when the moving atom remains on the FCC or HCP sub-lattice. In the first case we observe jump sizes smaller than 0.07 lattice constant, while in the second case we get jump sizes between 0.07 and 0.12 lattice constant. Whenever an atom leaves a cluster or re-attaches to the cluster, the displacement of the clusters CM changes more drastically than in the case of the diffusion of atoms on the edge of the cluster. The jump sizes are bigger than 0.12 lattice constant in such cases.

It is instructive now to follow the jump size statistics of non-zero jumps at different

temperatures. Simulations at $300K$, $500K$, $700K$, and $900K$ temperature were performed. The jump size statistics are presented as simple histograms in Figs. 3.15. For all studied temperatures the majority of the CM's jumps are around 0.05 lattice constant. In order to visualize the frequency of much less abundant jumps, we use a logarithmic scale. These histograms illustrate nicely the effect of temperature on the relative frequency of the main diffusion mechanisms in the model. At lower temperatures ($T = 300K$) the edge diffusion mechanism is the leading one, since the jump sizes are mostly below 0.12 lattice constants. As one would naturally expect, for higher temperatures ($T = 700K$ and $T = 900K$) the cluster fragmentation probability becomes higher, leading to jumps bigger than 0.12 lattice constants.

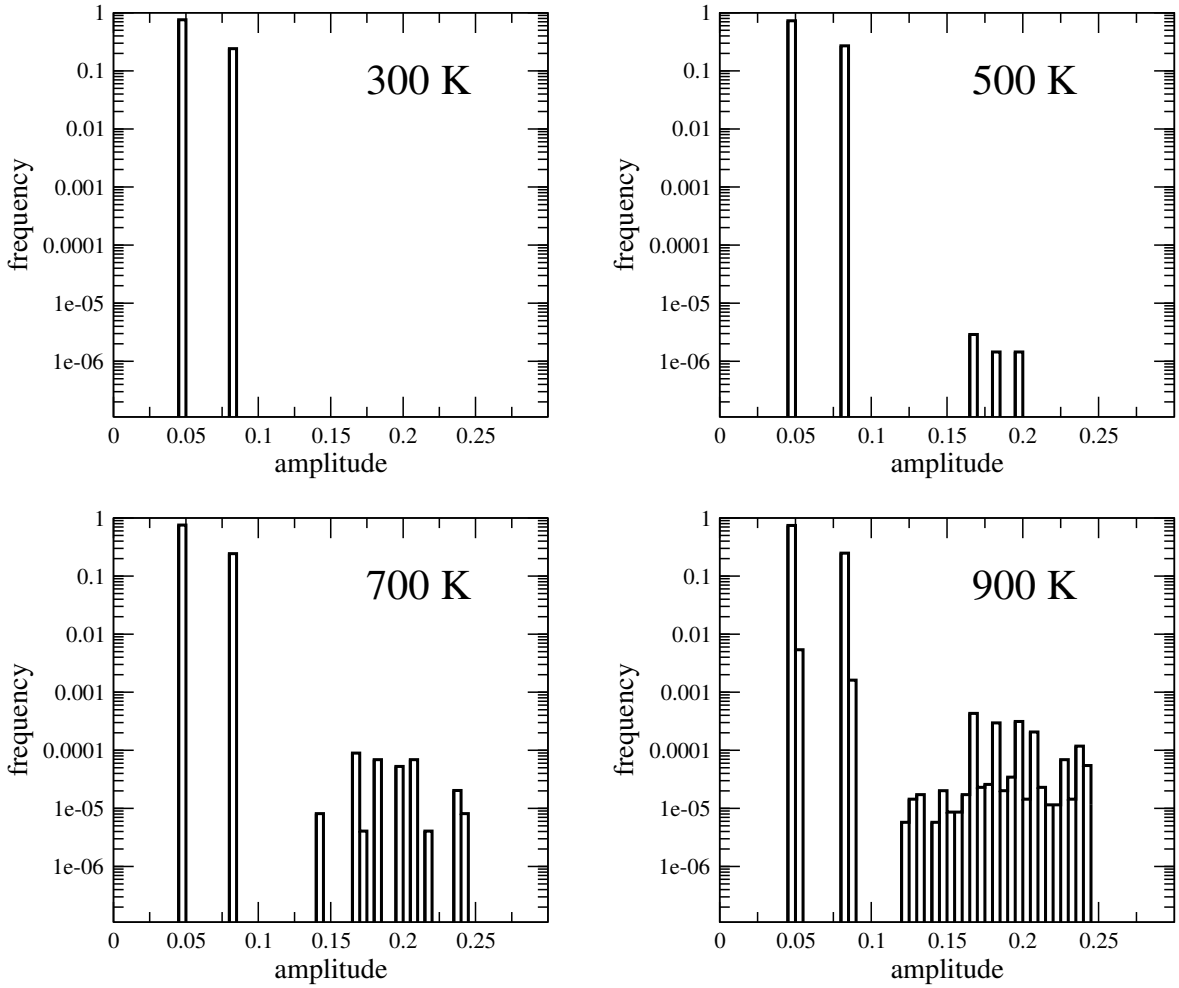

Figure 3.15: *Jump size statistics (histograms) for different temperatures. Please note the logarithmic vertical scale.*

Analyzing the statistics of the jump sizes we got the same conclusion as from the analysis of the diffusion coefficient as a function of the cluster size. At high temperatures the

dissociation-recombination (or evaporation-condensation) mechanism becomes more and more important.

Cluster eccentricity

From the event-by-event analysis of the cluster configuration, one can also study the temperature dependence of the average cluster shape. This is quantified by the cluster's average eccentricity (ϵ), characterizing the asymmetric nature of the average cluster configuration. The eccentricity of a cluster configuration is calculated from the coordinates of the component atoms. Our main mathematical tool is the 2×2 eccentricity matrix, E

$$E = \begin{pmatrix} E_{xx} & E_{xy} \\ E_{yx} & E_{yy} \end{pmatrix} \tag{3.8}$$

with elements

$$E_{xx} = \sum_i \left(X_{MC} - X_i\right)\left(X_{MC} - X_i\right), E_{xy} = \sum_i \left(X_{MC} - X_i\right)\left(Y_{MC} - Y_i\right),$$

$$E_{yx} = \sum_i \left(Y_{MC} - Y_i\right)\left(X_{MC} - X_i\right), E_{yy} = \sum_i \left(Y_{MC} - Y_i\right)\left(Y_{MC} - Y_i\right).$$

where X_{CM} and Y_{CM} denotes the X, respectively Y coordinates of the clusters CM; X_i and Y_i are the coordinates of i^{th} atom of the cluster. The eccentricity, ϵ, of a configuration is a scalar, computed from the eigenvalues, λ_1 and λ_1, of matrix E:

$$\varepsilon = \frac{|\lambda_1 - \lambda_2|}{\max\{\lambda_1, \lambda_2\}}. \tag{3.9}$$

The eccentricity defined in equation (3.9) takes values between 0 and 1. For a disc shaped cluster $\varepsilon = 0$ and for a linear cluster $\varepsilon = 1$.

During the kMC simulations the time-averaged eccentricity of the Pt clusters containing $7, 9, 13, 19, 30$, and 37 atoms were studied in a temperature range between $T = 300K$ and $T = 900K$. The results are plotted in Fig. 3.16. As one would naturally expect, the average eccentricity is always monotonically increasing with the temperature. The increased thermal fluctuations will distort the minimum energy disc-like configurations in increasing manner.

Fig. 3.16 also indicates that the considered clusters can be classified into two groups after their $\varepsilon(T)$ trend. The first group contains clusters with eccentricities varying almost linearly as a function of temperature ($N = 9,\ 13$, and 30). The second group contains clusters with

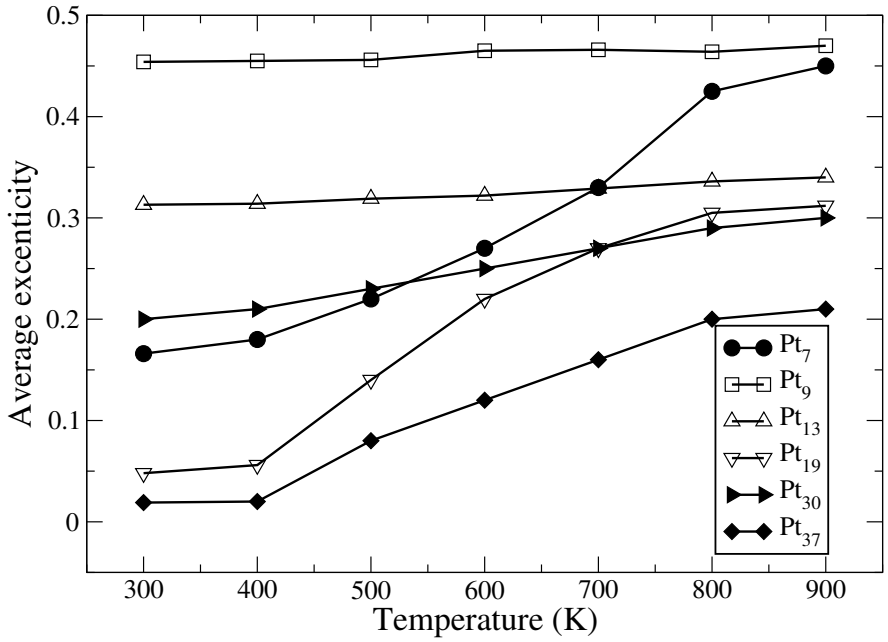

Figure 3.16: *Average eccentricity of the Pt_7, Pt_{13}, Pt_{19}, Pt_{25}, Pt_{30} and Pt_{37} clusters as a function of the system temperature.*

eccentricity values much smaller at low temperatures and with a non-linear (saturation-like) variation of the eccentricities as a function of temperature ($N = 7,\ 19$, and 37). This second group contains the clusters with closed shell structures.

The eccentricity of the smaller closed shell clusters is higher than the eccentricity of the bigger closed shell configurations. The reasoning is simple: the movement of an atom (a basic event in simulation) will influence in a larger manner the value of the eccentricity for smaller clusters than for the bigger ones. As an example let us consider the case of Pt_7 and Pt_{19} closed shell clusters. In their basic compact configurations the eccentricities are $\varepsilon = 0$ for both of them. Starting from this configuration, if an edge atom makes an FCC-HCP diffusion jump, the cluster remains the closest possible to disk shape. A simple calculation shows that the new eccentricity values will become $\varepsilon(Pt_7) = 0.32$ and $\varepsilon(Pt_{19}) = 0.09$. For the FCC-FCC jump of an edge atom, the eccentricity will change to $\varepsilon(Pt_7) = 0.49$ and $\varepsilon(Pt_{19}) = 0.13$. In both cases the eccentricity of the $N = 7$ cluster is larger.

Conclusions

Earlier studies [21, 94, 141] already proved the applicability of kMC methods for studying several thin-film growth related phenomena. Using the kMC method B to study the statistics of the diffusion of Pt clusters on a Pt(111) surface, the results obtained for the value of the

diffusion coefficient of clusters up to $N = 37$ atoms and the temperature and size dependence of the diffusion coefficient are all in reasonable agreement with previous experimental and theoretical studies for this system. The simulation data also confirm the validity of the Arrhenius equation regarding the temperature dependence of D and the simple $D_0 \sim N^{-1/2}$ scaling assumption for the pre-factor.

Visualization of the dynamics and interpretation of the statistical data revealed two different mechanisms for the diffusion in the considered model: (i) diffusion of atoms around and on the periphery of the cluster; (ii) dissociation of the cluster in two or more smaller parts, which can diffuse on the surface and recombine to the original cluster size. The jump size statistics of the cluster's CM and the eccentricity of the cluster's shape, both as a function of temperature and cluster size, offered additional and valuable insights in the diffusion process. A clear picture emerges for the dominant diffusion mechanism. At low temperatures (below $T = 400K$) the periphery diffusion is the leading mechanism, while at high temperatures (above $T = 800K$) the contribution of dissociation-recombination mechanism becomes more and more important.

kMC method B using the gEAM potential and the NEB method for determining the energy barrier for diffusion proved to be a fair approximation for studying diffusion of Pt clusters on Pt(111) surfaces. Results were published in: Communications in Computational Physics [52] .

3.2.2 The formation, dynamics, and stability of triangular-shaped Pt islands on Pt(111) surfaces

In Section 2.2.2 we briefly discussed the formation and inversion of the triangular shaped Pt islands grown on Pt(111) surface. Concerning this phenomenon, here the results obtained with the kMC method B will be presented and critically discussed.

Growth and stability of triangular islands

As a first simulation step, the fast deposition of Pt atoms was simulated, by starting from a compact seed containing seven atoms. We have chosen the starting configuration with seven atoms due to the fact that these islands are already quite immovable (as pointed out by Müller et al. [159]). Even for such high deposition fluxes as $1000\ ml/s$, the kinetic shapes of the simulated islands are compact and triangle-like, as can be seen in Fig. 3.17.

The islands drawn with crosses are formed on HCP sites and the ones plotted with disks are formed on FCC sites. Formation of the stable HCP stacking islands is due to the high

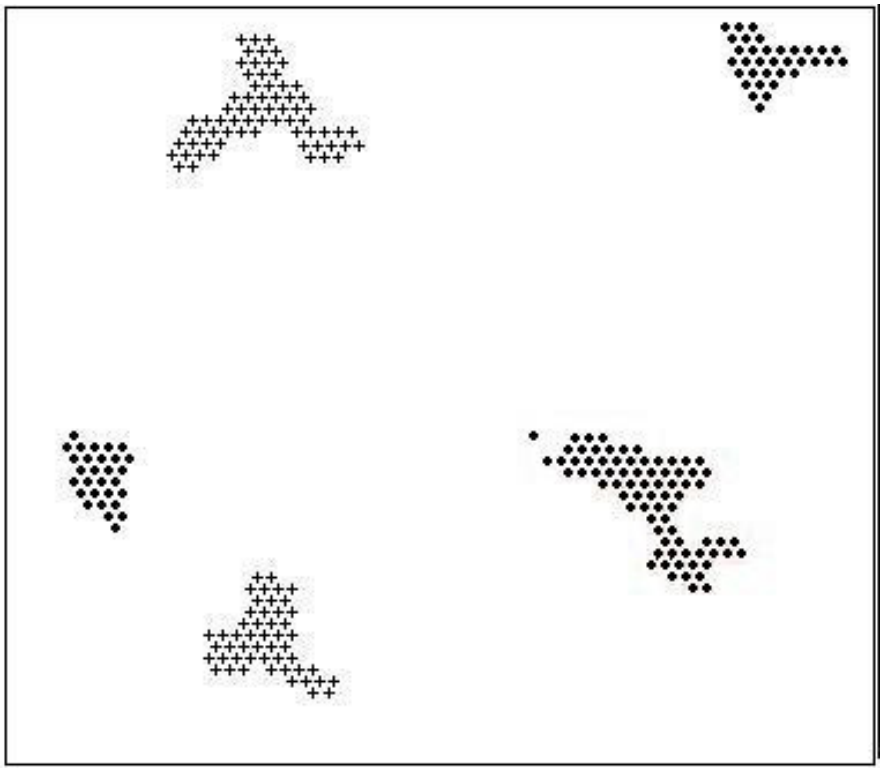

Figure 3.17: *kMC simulation results for* $1000\ ml/s$ *adatom deposition flux at* $300K$ *after* 227 *kMC steps (corresponding to a real time of* 4.3×10^{-5} *s). The simulated system size is* $64 \times 64 \times 4$*, disks and crosses represent the atoms in the growing layer occupying FCC and HCP lattice sites, respectively.*

deposition flux ($1000\ ml/s$) and low temperature ($300K$). Under such conditions the islands created with more than five atoms on the HCP sites are stable in time, in spite of the well-known fact that FCC stacking islands are energetically more favorable than the HCP ones for Pt. The triangular-shaped FCC and HCP stacking islands are both B-type islands. Due to the topological differences for the two different stackings, the direction of the HCP triangles is just the opposite of the FCC triangles.

As a second study in this topic, in order to illustrate the stability of islands of different types, A- and B-type FCC triangular islands formed by 21 atoms are evolved at different temperatures, without depositing new atoms (deposition flux is zero). As can be seen in Fig. 3.18, for all the simulated temperatures ($300K$, $400K$, $500K$, and $600K$) the B-type triangular islands will keep their orientation or become truncated B-type triangles. This clearly does not hold for the A-type islands. The islands which are initially A type ones, are distorted at lower temperatures and even inverted to B-type triangles at higher temperatures.

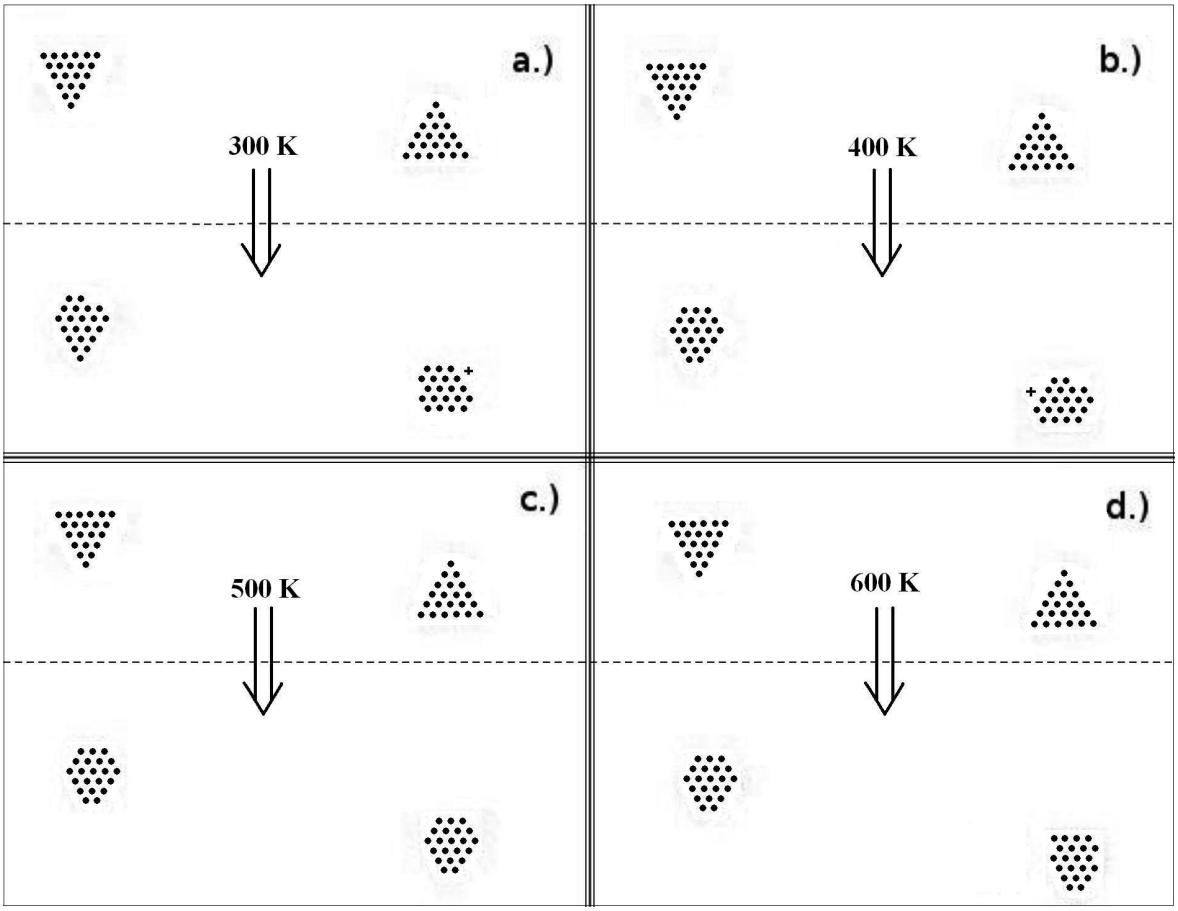

Figure 3.18: *Time evolution of A (right) and B (left) type triangles without an external deposition flux. Each box indicates the initial (upper) and final (lower) configurations at different temperatures: (a) after* 488 *Monte Carlo steps corresponding to simulated time* 7.6×10^{-2} *s, at* 300 *K, (b) after* 490 *Monte Carlo steps* 6.9×10^{-3} *s, at* 400 *K, (c) after* 149 *Monte Carlo steps,* 1.4×10^{-3} *s, at* 500 *K, and (d) after* 151 *Monte Carlo steps,* 1.1×10^{-4} *s, at* 600 *K.*

Energetic considerations for the hopping barrier

For a better understanding of both the triangular-shaped island formation phenomenon and the higher stability of the B-type triangular islands, in the following we present the calculations for the characteristic energy barriers of the relevant microscopical events.

First, the diffusion of Pt atoms on A- and B-type edges is studied. The energy barriers (or activation energies) for the jumps along the edges can be computed also from the statistics of the atom diffusion on these edges. On the top of a bulk FCC substrate a compact monolayer strip (or band) with three atomic rows is considered (Fig. 3.19). The diffusion of single Pt atoms on the two sides of this band can now be studied by simulations. The bottom and top sides correspond to A- and B-type edges, respectively. The three atomic rows' width of the

band is wide enough, and is equivalent in our approach with an infinite-width step because the cutoff distance of the potential calculation is set to three lattice constants, as discussed earlier. We recall here that the same cutoff distance was also imposed for the calculation of the potential and interaction with the substrate.

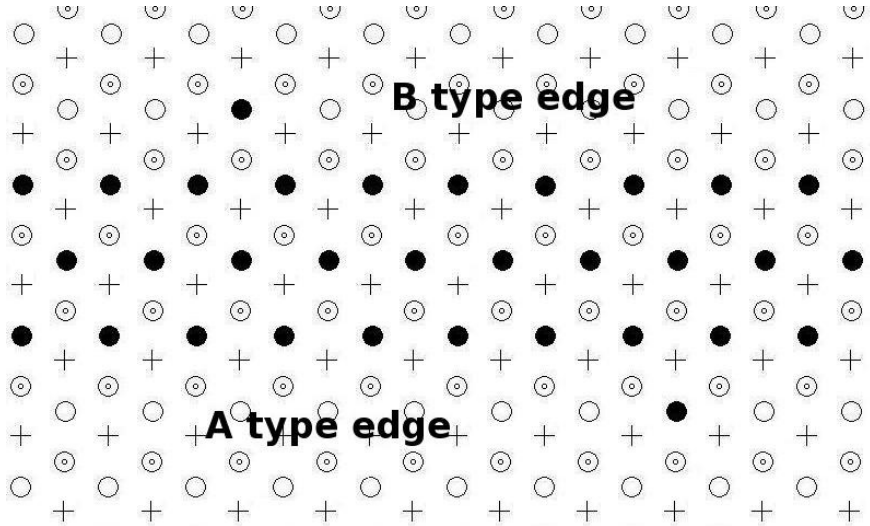

Figure 3.19: *Diffusion of single atoms along A- and B-type edges of a 2D strip (band). Dotted circles represent the sites of the substrate, circles and crosses represent the FCC and HCP lattice sites of the growing layer, respectively. Filled circles are the FCC sites of the growing layer which are already occupied by the adatoms.*

The diffusion coefficient (D) is calculated from the mean-square displacement of the atoms as a function of time. The common definition, equation (3.1) of D is used. In our case the dimensionality of the motion is $d = 1$, the motions being restricted along the edges. The diffusion coefficient is expected to exhibit the well-known Arrhenius-like behavior given in equation (3.2).

Results for single-atom diffusion on both the A- and B-type edges are presented in Fig. 3.20. These results prove the validity of the Arrhenius relation in this case too and indicate for the A-type edge $E_m = 0.36eV$ and $D_0 = 5.14 \times 10^{-3}\ cm^2/s$ and for the B-type edge $E_m = 0.6\ eV$ and $D_0 = 4.38 \times 10^{-3}\ cm^2/s$.

These activation energies are, of course, effective values, taking into account all possible types of jumps, namely FCC-FCC, FCC-HCP, HCP-FCC, and HCP-HCP jumps. The results indicate a considerable difference for the single-atom diffusion coefficient on the two types of edges. They are contradicting the earlier explanations [142], based solely on the differences in the diffusion coefficient values. Our results show that the atoms can diffuse more easily on the A-type edges; however, the stable island shape is the B-type triangle for all temperatures.

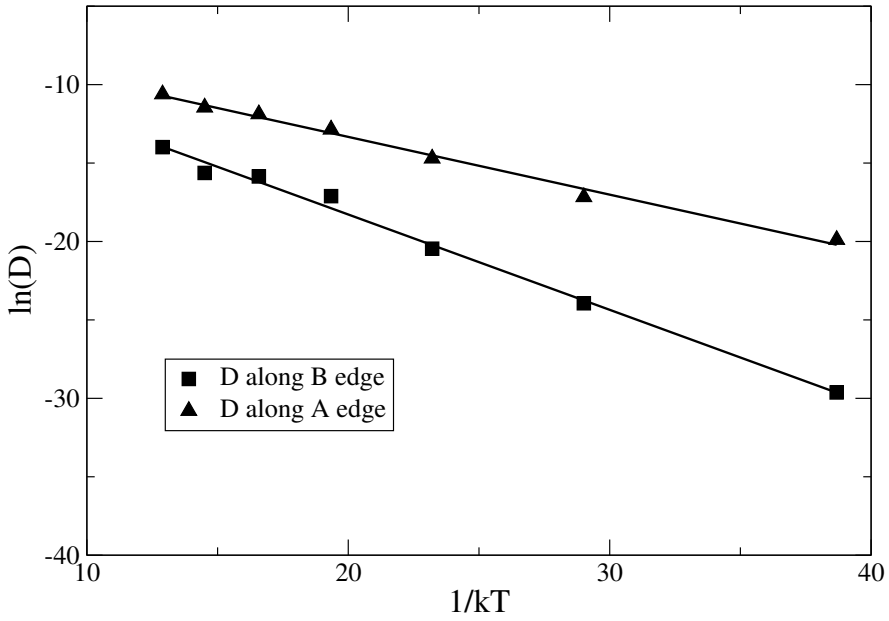

Figure 3.20: *Arrhenius behavior for the diffusion coefficient of a single atom along A- and B-type edges.*

Due to the fact that in our kMC approach the atoms can diffuse on both stacking, there are many topologically non-equivalent diffusion steps allowed. Going into more details and studying these diffusion steps separately on both types of edges will help to better understand the differences obtained for the diffusion coefficients. As an example, one can take the FCC-FCC type jumps along both edges and study the MEP (Minimum Energy Path) of the individual diffusion steps on A- and B-type edges using the presented NEB (Nudged Elastic Band) method. We have chosen to discuss only the FCC-FCC jumps, due to the fact that in all previously reported calculations only these diffusion jumps are considered and therefore this gives us a good ground for comparison.

For an FCC-FCC jump of an atom on the A-type edge, the MEP contains an intermediate HCP site and gives an energy barrier $E_{A_{2\to 2}} = 0.372eV$. In contrast with this, for an FCC-FCC jump on the B-type edge the MEP does not contain an intermediate site; therefore, the energy barrier is different: $E_{B_{2\to 2}} = 0.589eV$. The topological differences for these FCC-FCC steps are clearly visible in Fig. 2.5. The anisotropy of edge diffusion for Al on Al(111) was also attributed to the topological (geometrical) differences of the A and B edges [160]. An explanation for the FCC-FCC jumps using HCP sites as intermediate sites for A-type edges was made by Brune [5], studying dendritic islands with triangular envelope.

With the NEB method it is also possible to calculate the energy barriers for edge to corner and corner to edge jumps, denoted in the following as $E_{A_{1\to 2}}$, $E_{A_{2\to 1}}$ and $E_{B_{1\to 2}}$, $E_{A_{2\to 1}}$

	GGA	NEB 19	NEB 19z	NEB 4	NEB 4z
$E_{A_{1\to2}}(eV)$	0.44	0.143	0.370	0.161	0.323
$E_{A_{2\to2}}(eV)$	0.71	0.372	0.589	0.373	0.469
$E_{A_{2\to1}}(eV)$	0.84	0.541	0.768	0.557	0.720
$E_{B_{1\to2}}(eV)$	0.38	0.370	0.370	0.335	0.323
$E_{B_{2\to2}}(eV)$	0.77	0.589	0.589	0.484	0.467
$E_{B_{2\to1}}(eV)$	0.76	0.767	0.768	0.729	0.721

Table 3.2: *Energy barrier results for FCC-FCC jumps. Column 1 (GGA) summarizes the results of Feibelman [85]. Column 2 (NEB 19) presents our results with an unrestricted NEB and 19 replicas. Column 3 (NEB 19z) presents the results obtained with a NEB restricted perpendicularly on the surface and with 19 replicas. Column 4 (NEB 4) presents the results obtained by an unrestricted NEB with 4 replicas, and column 5 (NEB 4z) shows the results obtained with a NEB restricted perpendicularly on the surfaces and using 4 replicas.*

respectively, the numbers represent the number of nearest neighbors as discussed already in Section 2.2.2. These results (second column of Table 3.2) follow the expected trend for both A and B edges, $E_{1\to2} < E_{2\to2} < E_{2\to1}$, as was previously discussed by Wu et al. [66] who used Feibelman's generalized gradient approximation (GGA) calculations [85]. The results of GGA calculations are listed in the first column of Table 3.2. Our calculations with 19 NEB nodes show that for all three cases ($1 \to 2$, $2 \to 2$, and $2 \to 1$), the energies on the A-type edge are smaller than the corresponding energies for the B-type edge (second column of Table 3.2). We have to remember here that all calculated energy values are for FCC-FCC jumps; therefore, the energies of $2 \to 2$ jumps will differ slightly from the effective energies calculated from the diffusion along the edges.

From the results presented in Table 3.2, one can conclude that atoms on A-type edges will diffuse more easily than atoms on B-type edges and this holds not only along the edges, but also for jumps to and from the corners.

The energy barriers calculated by Feibelman [85] differ (sometimes considerably) from those calculated by us. In almost all cases our calculations underestimate the GGA results. This is somehow expected for a semi-empirical approach next to an ab-initio calculation, which ought to be much more precise. The differences might also come from the fact that the gEAM potentials are more appropriate for bulk atoms than surface ones. This can also be seen in our results for the free diffusion of a Pt atom on a Pt(111) surface, where an error of order 20% is obtained for the energy barrier value calculated with gEAM and NEB relative to the value obtained in experiments. The larger deviations observable for jumps on A-type edges might also be a consequence of the differences between the performed NEB

calculations.

In our kMC method we have used 19 replicas (NEB nodes) of the system, while in the GGA calculations only 4 replicas were used. In order to investigate whether the large differences in Table 3.2 are due to the implementation of the NEB method, we have made some further studies.

First, the NEB band was relaxed using as interatomic potential the gEAM potential with 19 replicas of the system, but the band is restricted to relax only in a perpendicular direction to the surface. Under such restrictions the energies are already closer to the GGA calculations (third column of Table 3.2). In this restricted case the MEP for FCC-FCC jumps on A-type edges will not contain intermediate HCP sites, because the band will not flare out sideways and as a result of this the energy barriers are the same for jumps along A- and B-type edges. We suspect thus that in the work of Feibelman [85] such restrictions were also imposed.

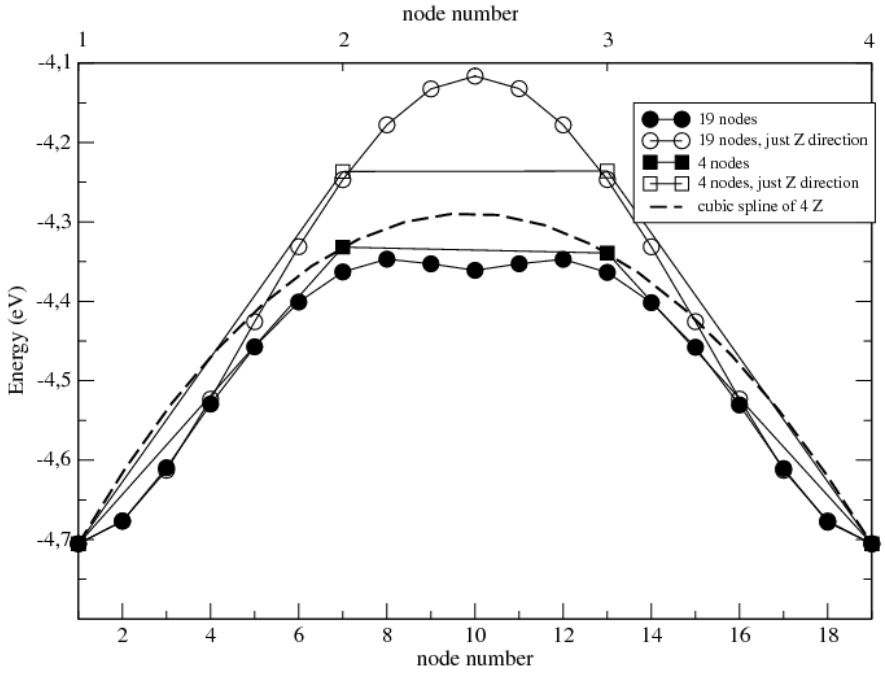

Figure 3.21: *NEB node energies for bands containing* 19 *and* 4 *nodes, for both unrestricted and perpendicularly restricted (z direction) relaxations of* $A_{2\to 2}$ *FCC-FCC jumps.*

Secondly, if the calculations are taken with only 4 NEB nodes, the energy barriers calculated from a spline fit (this is the method used by Feibelman in [85]) can be quite far from the real values. This is illustrated in Fig. 3.21 for $A_{2\to 2}$ FCC-FCC jumps. For the sake of comparison we also show that by using 19 nodes, the energy plot of the nodes is much more smooth. The local minimum for the unrestrictedly relaxed band indicates the presence of the intermediate HCP site. One can also observe that the results obtained by us with only 4

NEB nodes are now much closer to the GGA results. Taking into account the difference in how the NEB method was implemented in the present study and in the study of Feibelman [85], we suspect that the larger deviations in the obtained energy barriers are not due to the interatomic potential values used, but to the NEB calculations.

The kink-formation and kink-breaking phenomenon (Fig. 3.22) is another elementary process in step advancement and therefore can be an important process in triangle-shape formation. The energy barriers calculated for kink-formation and kink-breaking events are listed in Table 3.3.

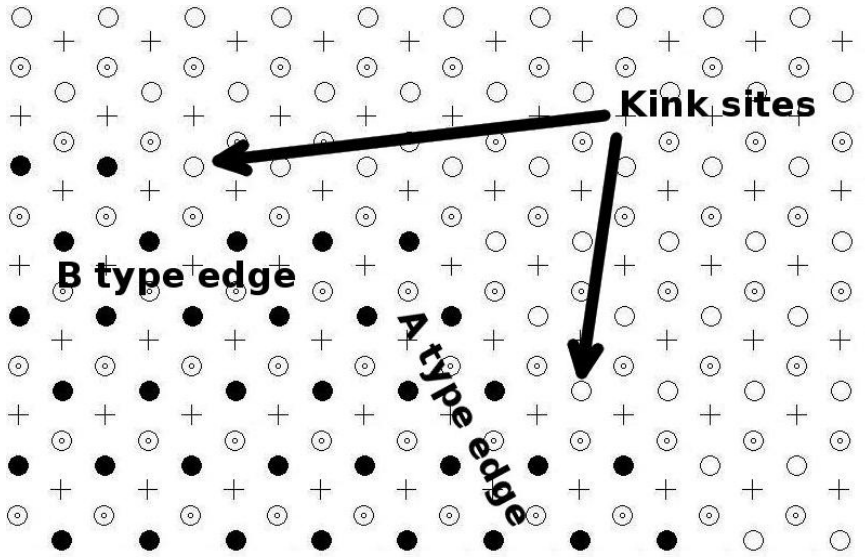

Figure 3.22: *Kink sites on A and B type edges.*

	kink-formation energy	kink-breaking energy
on A edge	$0.281\ eV$	$0.624\ eV$
on B edge	$0.469\ eV$	$0.830\ eV$

Table 3.3: *Calculation results*

Summarizing now the above-discussed energetic aspects, one can list the following statements that could help in explaining the creation of the B-type triangular islands:

1. The diffusion of atoms on A type edges is easier than on B type edges.
2. The kink-formation is easier on A type edges than on the B type ones.
3. On A type edges the kink-breaking energy is high enough - relative to the kink-formation energy - to allow the step advancement on these edges.

4. The $E_{A_{1\to 2}} < E_{B_{1\to 2}}$ condition is favorable for A step advancement, because the probability for a corner atom to choose the A edge is higher than the probability for choosing the B type edge.

Items 1 and 4 alone do not suggest the growth of B-type triangles. These effects would favor a more rapid growth of the B-type edges and ultimately the formation of A-type triangles. The facts summarized under items 3 and 4 are, however, responsible for the quicker advancement of the A-type edges leading to the formation of B-type triangular compact islands. Seemingly these latter effects are the stronger ones, and will favor the growth of B-type triangles.

3.2.3 Conclusions

One of the aims for using kMC method B was to reconsider the formation of B-type triangular-shaped Pt adatom islands on a Pt(111) surface. This method has proven its applicability in studying the adatom island diffusion.

By studying the diffusion of Pt atoms along the island edges, a more complete picture about the formation of triangular islands and their stability in time was drawn. The obtained results indicate a higher diffusion speed of atoms along A-type island edges. Also, the jump rates from edge to corner and corner to edge are higher for A-type edges compared to B-type ones. These results alone do not explain the better stability of the B-type islands, but on the contrary, taking into account the earlier explanations [142, 130, 66, 144, 101], these results suggest a more stable A-type triangular island.

Studying the energies necessary for kink-formation and kink-breaking reveals, however, that the atoms will assemble with a higher probability on A-type edges, leading to a higher advancement speed of the A-type steps. The higher jump probability from the corner sites to A-type edges leads also to a quicker advancement of A-type edges and ultimately to the formation of B-type triangular-shaped islands. The obtained results were published in:
[53] Physica Status Solidi B, vol. 249, pp. 1709-1716, 2012.

Final conclusions

The aims of the present thesis were to study some thin film related questions and problems by using two original kinetic Monte Carlo methods developed by us (kMC method A and kMC method B).

The kMC method A improves the classical method by using a new hopping barrier formula and more degrees of freedom for the diffusion of particles. The latter is achieved by considering a triangular lattice topology. A Lennard-Jones type pair-potential was used for calculating the interactions between the particles. With this kMC method the two component co-deposition process was successfully modeled. Impurity decorated islands were formed without using a predefined rate for exchange of the neighboring particles. With this kMC method, for the one component system the island growth, the coalescence, the appearance of stacking-faults related phase-boundaries and their motions were all successfully reproduced.

The kMC method B performs a more accurate calculation of hopping barriers by using the Nudged Elastic Band method (NEB). The interaction of the particles are calculated with the generalized Embedded Atom Method (gEAM). By using gEAM we had the possibility to study material-related problems and quantitatively compare the results with those from experiments and from ab-initio calculations. Using this method we studied the statistics of the diffusion of Pt atom clusters on a Pt(111) surface. The results obtained for the diffusion coefficient of different cluster sizes (up to $N = 37$) are in good agreement with those from the literature. By studying the jump-size statistics of the clusters center of mass and the eccentricity of the clusters as a function of the temperature and cluster size, we found the leading microscopic mechanisms of the cluster diffusion process.
At low temperatures ($T \leq 400K$) the cluster diffusion occurs by periphery diffusion of the atoms, while for higher temperatures ($T \geq 800K$) the dissociation-recombination mechanism becomes more and more important.

Our study shed light also on the debated problem concerning the origin, formation, and stability of the oriented triangular Pt islands on Pt(111) surface. The results indicate a higher diffusion speed of atoms along A-type island edges. In the mean-time the rates of edge

to corner and corner to edge jumps are higher for A-type edges, compared to the B-type ones. Taking into account these results and in agreement with the literature a more stable A-type triangular island is expected. Studying, however, the kink formation and kink breaking energies we revealed the origin of the formation and stability of the B-type triangular islands. Our conclusion was that the atoms will populate the A-type edges with a higher probability, but the atoms will also assemble with a higher probability on these types of edges. These conditions lead to the quicker advancement and disappearance of the A-type edges, finally resulting in stable B-type triangular islands.

Bibliography

[1] P. M. Martin, *Handbook of Deposition Technologies for Films and Coatings (Third Edition): Science, Applications and Technology*. Elsevier Inc., 2010.

[2] A. Cho, "Film Deposition by Molecular Beam Techniques," *Journal of Vacuum Science & Technology*, vol. 8, pp. S31–S38, 1971.

[3] A. Cho and J. Arthur, "Molecular Beam Epitaxy," *Solid-State Chemistry*, vol. 10, pp. 157–192, 1975.

[4] P. Barna and M. Adamik, "Fundamental structure forming phenomena of polycrystalline films and the structure zone models," *Thin Solid Films*, vol. 317, pp. 27–33, 1998.

[5] H. Brune, "Microscopic view of epitaxial metal growth: nucleation and aggregation," *Surface Science Reports*, vol. 31, p. 121, 1998.

[6] G. Cao, *Nanostructures and Nanomaterials, Synthesis, Properties and Applications*. London: Imperial College Press, 2004.

[7] D. Kandel and E. Kaxiras, "The surfactant effect in semiconductor thin film growth," *Solid State Physics*, vol. 54, p. 219, 2000.

[8] D. Kashchiev, *Nucleation: Basic Theory with Applications*. Oxford: Oxford: Division of Reed Educational and Professional Publishing Ltd, 2000.

[9] J. Meyer, H. van der Vegt, J. Vrijmoeth, E. Vlieg, and R. Behm, "Reversible place-exchange during film growth: a mechanism for surfactant transport," *Surface Science Letters*, vol. 388, pp. 375–380, 1996.

[10] J. F. Pócza, A. Barna, P. B. Barna, I. Pozsgai, and G. Radnoczi, "In Situ Electron Microscopy of Thin Film Growth," *Jpn. J. Appl. Phys. Suppl.*, vol. 2, p. 525, 1974.

[11] G. Rosenfeld, R. Servaty, C. Teichert, B. Poelsema, and G. Comsa, "Layer-by-layer growth of Ag on Ag(111) induced by enhanced nucleation: A model Study for Surfactant-Mediated Growth," *Physical Review Letters*, vol. 71, p. 895, 1993.

[12] H. A. van der Vegt, H. M. van Pinxteren, M. Lohmeier, E. Vlieg, and J. M. C. Thornton, "Surfactant-Induced Layer-By-Layer Growth of Ag on Ag(111)," *Physical Review Letters*, vol. 68, pp. 3335–3338, 1992.

[13] M. Wanner, R. Werner, and D. Gerthsen, "Dynamics of gold clusters on amorphous carbon films induced by annealing in a transmission electron microscope," *Surface Science*, vol. 600, pp. 632–640, 2006.

[14] W. Burton, N. Cabrera, and F. Frank, "The Growth of Crystals and the Equilibrium Structure of their Surfaces," *Philos. Trans. R. Soc. London A*, vol. 243, pp. 299–358, 1951.

[15] J. A. Venables, P. A. Bennett, H. Brune, J. Drucker, and J. H. Harding, "Selective nucleation and controlled growth: quantum dots on metal, insulator and semiconductor surfaces," *Phil. Trans. R. Soc. Lond. A*, vol. 361, pp. 311–329, 2003.

[16] M. F. Gyure, C. Ratsch, B. Merriman, R. Caflisch, S. Osher, J. Zinck, and D.D.Vvedensky, "Level-set methods for the simulation of epitaxial phenomena," *Phys. Rev. E*, vol. 58, p. R6927, 1998.

[17] D. C. Rapaport, *The Art of Molecular Dynamics Simulation*. Cambridge: Cambridge University Press, 1995.

[18] D. Marx and J. Hutter, *in Modern Methods and Algorithms of Quantum Chemistry, Proceedings, Second Edition, J. Grotendorst (Ed.), NIC series, Vol. 3,*. Julich: John von Neumann Institute for Computing, 2000.

[19] A. B. Bortz, M. H. Kalos, and J. L. Lebowitz, "A new algorithm for Monte Carlo simulation of Ising spin systems," *J. Comput Phys,*, vol. 17, pp. 10–18, 1975.

[20] P. Rikvold, "Simulations of a stochastic model for cluster growth on a square lattice," *Phys. Rev. A*, vol. 26, pp. 647–650, 1982.

[21] A. Voter, "Classically exact overlayer dynamics: Diffusion of Rhodium clusters on Rh(100)," *Phys. Rev. B*, vol. 34, pp. 6819–6829, 1986.

[22] F. M. Bulnes, V. D. Pereyra, and J. L. Riccardo, "Collective surface diffusion: n-fold way kinetic Monte Carlo simulation," *Phys. Rev. E*, vol. 58, p. 86, 1998.

[23] P. Ruggerone, C. Ratsch, and M. S. Scheffer, *Growth and Properties of Ultrathin Epitaxial Layers, Eds. D.A. King, D.P. Woodruff., The Chemical Physics of Solid Surfaces, vol. 8.* Amsterdam: Elsevier, 1997.

[24] A. F. Voter, *Radiation Effects in Solids, Ed. K. E. Sickafus and E. A. Kotomin*. Dordrecht, The Netherlands: Springer, NATO Publishing Unit,, 2005.

[25] P. Politi, G. Grenet, A. Marty, A. Ponchet, and J. Villain, "Instabilities in crysta growth by atomic or molecular beams," *Physics Reports*, vol. 324, p. 271, 2000.

[26] V. A. Shchukin and D. Bimberg, "Spontaneous ordering of nanostructure on crystal surfaces," *Rev. Mod. Phys.*, vol. 71, p. 1125, 1999.

[27] D. A. Case, T. A. Darden, T. E. C. III, C. L. Simmerling, J. Wang, R. E. Duke, R. Luo, R. C. Walker, W. Zhang, K. M. Merz, B. Roberts, S. Hayik, A. Roitberg, G. Seabra, J. Swails, A. W. Goetz, I. Kolossvary, K. F. Wong, F. Paesani, J. Vanicek, R. M. Wolf, J. Liu, X. Wu, S. R. Brozell, T. Steinbrecher, H. Gohlke, Q. Cai, X. Ye, J. Wang, M. J. Hsieh, G. Cui, D. R. Roe, D. H. Mathews, M. G. Seetin, R. Salomon-Ferrer, C. Sagui, V. Babin, T. Luchko, S. Gusarov, A. Kovalenko, and P. A. Kollman, "Amber12." http://ambermd.org/, 2012.

[28] J. C. Phillips, R. Braun, W. Wang, J. Gumbart, E. Tajkhorshid, E. Villa, C. Chipot, R. D. Skeel, L. Kale, and K. Schulten, "Scalable molecular dynamics with NAMD," *Journal of Computational Chemistry*, vol. 26, pp. 1781–1802, 2005.

[29] W. Smith, C. W. Yong, and P. M. Rodger, "DL_POLY: Application to molecular simulation," *Molecular Simulation*, vol. 28, p. 385, 2002.

[30] D. H. Gay and A. L. Rohl, "MARVIN: a new computer code for studying surfaces and interfaces and its application to calculating the crystal morphologies of corundum and zircon," *Journal of the Chemical Society, Faraday Transactions*, vol. 91, pp. 925–936, 1995.

[31] S. R. Niketic and K. Rasmussen, *The Consistent Force Field: A Documentation Lecture Notes in Chemistry 3*. Springer-Verlag, 1977.

[32] G. Binnig, H. Rohrer, C. Gerber, and E. Weibel, "A microscopic model of the stock market: cycles, booms, and crashes," *Phys. Rev. Lett.*, vol. 49, p. 57, 1982.

[33] J. M. Wen, J. W. Evans, M. C. Bartelt, J. W. Burnett, and P. A. Thiel, "Coarsening mechanisms in a metal film: from cluster diffusion to vacancy ripening," *Physical Review Letter*, vol. 76, pp. 652–655, 1996.

[34] J. J. D. Miguela, A. Sancheza, A. Cebolladaa, J. M. Gallegoa, J. Ferrona, and S. Ferrera, "The surface morphology of a growing crystal studied by thermal energy atom scattering(TEAS)," *Surface Science*, vol. 189-190, pp. 1062–1068, 1987.

[35] M. Marinica, C. Barreteau, D. Spanjaard, and M. Desjonqueres, "Influence of short-range adatom-adatom interactions on the surface diffusion of Cu on Cu(111)," *Phys. Rev. B.*, vol. 72, p. 115402, 2005.

[36] S. C. Wang and G. Ehrlich, "Diffusion of large surface clusters: direct observations on Ir(111)," *Phys. Rev. Lett.*, vol. 79, pp. 4234–4237, 1997.

[37] K. Kyuno and G. Ehrlich, "Diffusion and dissociation of platinum clusters on Pt(111)," *Surface Science*, vol. 437, pp. 29–37, 1999.

[38] S. C. Wang, U. Krpick, and G. Ehrlich, "Surface diffusion of compact and other clusters: Irx on Ir(lll)," *Physical Review Letters*, vol. 81, pp. 4923–4926, 1998.

[39] P. Batlone, W. Andreoni, R. Car, , and M. Parrinello, "Equilibrium Structures and Finite Temperature Properties of Silicon Microclusters from ab initio Molecular-Dynamics Calculations," *Physical Review Letters*, vol. 60, p. 271, 1988.

[40] W. Kohn and L. J. Sham, "Self-Consistent Equations Including Exchange and Correlation Effects," *Physical Review*, vol. 140, p. A1133, 1965.

[41] P. Perdew, *Electronic Structure of Solids '91 edited by P. Ziesche and H. Eschrig*. Berlin: Akademie Verlag, 1991.

[42] M. S. Daw, S. M. Foiles, and M. I. Baskes, "The embedded-atom method: a review of theory and applications," *Materials Science Reports*, vol. 9, pp. 7–8, 1993.

[43] J. E. Lennard-Jones, "Cohesion," *Proceedings of the Physical Society*, vol. 43, pp. 461–482, 1931.

[44] J. Tersoff, "New empirical approach for the structure and energy of covalent systems," *Physical Review B*, vol. 37, p. 6991, 1988.

[45] M. S. Daw and M. I. Baskes, "Semiempirical, Quantum Mechanical Calculation of Hydrogen Embrittlement in Metals," *Physical Review Letters*, vol. 50, p. 1285, 1983.

[46] H. N. G. Wadley, X. Zhou, R. A. Johnson, and M. Neurock, "Mechanism, models and methods of vapor deposition," *Proggress in Materials Science*, vol. 46, p. 329, 2001.

[47] J. Yang, W. Hub, and M. Xu, "Comparative study of compact hexagonal cluster self-diffusion on Cu(111) and Pt(111)," *Applied Surface Science*, vol. 255, pp. 1736–1740, 2008.

[48] A. Carlsson, "Beyond Pair Potentials in Elemental Transition Metals and Semiconductors," *Solid State Physics*, vol. 43, p. 1, 1990.

[49] F. Ercolessi, M. Parrinello, and E. Tosatti, "Simulation of gold in the glue model," *Philosophical Magazine A*, vol. 58, p. 213, 1988.

[50] M. W. Finnis and J. E. Sinclair, "A simple empirical N-body potential for transition metals," *Philos. Mag. A 50*, vol. 50, p. 45, 1984.

[51] F. Stillinger and T. A. Weber, "Computer simulation of local order in condensed phases of silicon," *Physical Review B*, vol. 31, p. 5262, 1985.

[52] R. Deák, Z. Néda, and P. B. Barna, "A kinetic Monte Carlo approach for self-diffusion of Pt atom clusters on a Pt(111) surface," *Communications in Computational Physics*, vol. 10, pp. 920–939, 2011.

[53] R. Deák and Z. Néda, "Kinetic monte carlo approach for triangular-shaped pt islands on pt(111) surfaces," *Physica Status Solidi B*, vol. 249, pp. 1709–1716, 2012.

[54] X. W. Zhou, H. N. G. Wadley, R. A. Johnson, D. J. Larson, N. Tabat, A. Cerezo, A. K. Petford-Long, G. D. W. Smith, P. H. Clifton, R. L. Martens, and T. F. Kelly, "Atomic scale structure of sputtered metal," *Acta Materialia*, vol. 49, p. 4005, 2001.

[55] P. H. Huang, T. H. Fang, and C. S. Chou, "The coupled effects of size, shape, and location of vacancy clusters on the structural deformation and mechanical strength of defective nanowires," *Current Applied Physics*, vol. 11, p. 878, 2011.

[56] L. Verlet, "Computer Experiments on Classical Fluids. I. Thermodynamical Properties of Lennard-Jones Molecules," *Physical Review*, vol. 159, p. 98, 1967.

[57] L. Verlet, "Computer Experiments on Classical Fluids. II. Equilibrium Correlation Functions," *Physical Review*, vol. 165, p. 201, 1967.

[58] A. Rahman, "Correlations in the Motion of Atoms in Liquid Argon," *Phys. Rev.*, vol. 136, p. A405, 1964.

[59] R. Feynman, R. B. Leighton, and M. Sands, *The Feynman Lectures on Physics*. 1963.

[60] M. P. Allen and D. J. Tildesley, *Computer Simulation of Liquids*. New York: Oxford University Press, 1987.

[61] R. Car and M. Parrinello, "Unified Approach for Molecular Dynamics and Density-Functional Theory," *Physical Review Letters*, vol. 55, p. 2471, 1985.

[62] Y. Imamura, N. Matsui, Y. Morikawa, M. Hada, T. Kubo, M. Nishijima, and H. Nakatsuji, "First-principles molecular dynamics study of Co adsorption on the Si(001) surface," *Chememical Physics Letters*, vol. 287, p. 131, 1998.

[63] I. Stich, "First-principles finite-temperature simulation of surface dynamics: Si(111)-(7 x 7)," *Surface Science*, vol. 368, p. 152, 1996.

[64] A. Alavi, P. Hu, T. Deutsch, P. L. Silvestrelli, and J. Hutter, "Co oxidation on Pt(111): An Ab Initio Density Functional Theory Study," *Physical Review Letters*, vol. 80, p. 3650, 1998.

[65] C. J. Zhang, P. J. Hu, and A. Alavi, "A General Mechanism for Co Oxidation on Close-Packed Transition Metal Surfaces," *Journal of the American Chemical Society*, vol. 121, p. 7931, 1999.

[66] J. Wu, E. G. Wang, K. Varga, B. G. Liu, S. T. Pantelides, and Z. Zhang, "Island Shape Selection in Pt(111) Submonolayer Homoepitaxy with or without Co as an Adsorbate," *Physical Review Letters*, vol. 89, pp. 146103–1, 2002.

[67] P. J. Feibelman, "Interlayer Self-Diffusion on Stepped Pt(111)," *Physical Review Letters*, vol. 81, p. 168, 1998.

[68] S. Esch, M. Hohage, T. Michely, and G. Comsa, "Origin of oxygen induced layer-by-layer growth in homoepitaxy on Pt(111)," *Physical Review Letters*, vol. 72, p. 518, 1994.

[69] P. J. Fiebelman, "Scaling of hopping self-divusion barriers on fcc(100) surfaces with bulk bond energies," *Surface Science*, vol. 423, pp. 169–174, 1999.

[70] P. Ehrenfest, "Bemerkung uber die angen aherte Gultigkeit der klassischen Mechanik innerhalb der Quantenmechanik," *Zeitschrift fur Physik*, vol. 45, p. 455, 1927.

[71] R. N. Barnett, U. Landman, A. Nitzan, and G. Rajagopal, "Born Oppenheimer dynamics using density-functional theory: Equilibrium and fragmentation of small sodium clusters," *Journal of Chememical Physics*, vol. 94, p. 608, 1991.

[72] M. C. Payne, M. P. Teter, D. C. Allan, T. A. Arias, and J. D. Joannopoulos, "Iterative minimization techniques for ab initio total-energy calculations: molecular dynamics and conjugate gradients," *Review of Moderd Physics*, vol. 64, p. 1045, 1992.

[73] R. N. Barnett and U. Landman, "Born-oppenheimer molecular-dynamics simulations of finite systems: Structure and dynamics of (h2o)2," *Physical Review B*, vol. 48, p. 2081, 1993.

[74] C. Leforestier, "Classical trajectories using the full ab-initio potential energy surface $H^- + CH4 \longrightarrow CH4 + H^-$," *J. Chem. Phys*, vol. 68, p. 4406, 1978.

[75] J. C. Greer, R. Ahlrichs, and I. V. Hertel *Zeitschrift fur Physik D*, vol. 18, p. 413, 1991.

[76] M. J. Field, "Constrained optimization of ab initio and semiempirical hartree-fock wave functions using direct minimization or simulated annealing," *Journal of Physical Chemistry*, vol. 95, p. 5104, 1991.

[77] B. Hartke and E. A. Carter, "Ab initio molecular dynamics simulated annealing at the generalized valence bond level. application to a small nickel cluster," *Chemical Physics Letters*, vol. 216, p. 324, 1993.

[78] D. A. Gibson and E. A. Carter, "Generalized valence bond molecular dynamics at constant temperature," *Molecular Physics*, vol. 89, p. 1265, 1996.

[79] A. J. R. da Silva, J. W. Pang, E. A. Carter, and D. Neuhauser, "Anharmonic Vibrations via Filter Diagonalization of ab Initio Dynamics Trajectories," *Journal of Physical Chemistry A*, vol. 102, p. 881, 1998.

[80] A. Warshel and M. Karplus, "Semiclassical trajectory approach to photoisomerization," *Chemical Physics Letters*, vol. 32, p. 11, 1975.

[81] J. Broughton and F. Kahn, "Accuracy of time-dependent properties in electronic-structure calculations using a fictitious Lagrangian," *Physical Review B*, vol. 40, p. 12098, 1989.

[82] G. Kresse and J. Furthmuller, "Vienna ab initio simulation package." `http://www.vasp.at/`, 2001.

[83] K. Chiho, K. Sang-Pil, K. Yoon-Suk, K. Hanchul, and C. Yong-Chae, "Ab initio Investigation of the Early Stage of Nano-scale Thin Film Growth: Al and Co Adatoms on Co(111) surface," *Japanese Journal of Applied Physics*, vol. 43, pp. 3815–3817, 2004.

[84] D. Vanderbilt, "Soft self-consistent pseudopotentials in a generalized eigenvalue formalism," *Physical Review B*, vol. 41, p. 7892, 7990.

[85] P. Feibelman, "Self-diffusion along step bottoms on Pt.111.," *Physical Review B*, vol. 60, p. 4972, 1999.

[86] J. D. Weeks and G. H. Gilmer, "Dynamics of Crystal Growth," *Advances in Chemical Physics*, vol. 40, p. 157, 1979.

[87] C. Levi and M. Kotrla, "Theory and simulation of crystal growth," *Journal of Physics: Condensed Matter*, vol. 9, p. 299, 1997.

[88] M. Kotrla, J. Krug, and P. Smilauer, "Submonolayer epitaxy with impurities: Kinetic Monte Carlo simulations and rate-equation analysis," *Physical Review B*, vol. 62, p. 2889, 2000.

[89] M. Kotrla, J. Krug, and P. Smilauer, "Submonolayer growth with decorated island edges," *Surface Science*, vol. 454-456, pp. 681–685, 2000.

[90] A. Voter and J. Doll, "Transition state theory description of surface self-diffusion: Comparison with classical trajectory results," *Journal of Chemical Physics*, vol. 80, p. 5832, 1984.

[91] G. Henkelman, B. Uberuaga, and H. Jhonsson, "A climbing image nudged elastic band method for finding saddle points and minimum energy paths," *Journal of Chemical Physics*, vol. 113, p. 9901, 2000.

[92] J. W. Evans, P. A. Thiel, and M. C. Bartelt, "Formation of 2D and 3D island mounds," *Surface Science Reports*, vol. 61, p. 1, 2006.

[93] X. P. Wang, F. Xie, Q. W. Shi, and T. X. Zhao, "Effect of atomic diagonal motion on cluster diffusion coefficient and its scaling behavior," *Surface Science*, vol. 561, pp. 25–32, 2004.

[94] P. M. Agrawal, B. M. Rice, and D. L. Thompson, "Predicting trends in rate parameters for self-diffusion on FCC metal surfaces," *Surface Science*, vol. 515, pp. 21–35, 2002.

[95] W. D. Callister and Jr., *Materials Science and Engineering: An Introduction, Sixth edition*. John Wiley and Sons, New York, 1985.

[96] R. A. Johnson, "Analytic nearest-neighbor model for fcc metals," *Physical Review B*, vol. 37, p. 3924, 1988.

[97] R. Deák, Z. Néda, and P. B. Barna, "A Simple Kinetic Monte Carlo Spproach for Epitaxial Submonolayer Growth," *Communications in Computational Physics*, vol. 3, pp. 822–833, 2008.

[98] P. M. Lam, D. Bayayoko, and X.-Y. Hu, "Monte Carlo simulation of coarsening in a model of submonolayer epitaxial growth," *Surface Science*, vol. 429, p. 161, 1999.

[99] R. Deák, Z. Néda, and P. B. Barna, "A novel kinetic Monte Carlo method for epitaxial growth," *Journal of Optoelectronics and Advanced Materials*, vol. 10, pp. 2445–2450, 2008.

[100] S. Liu, Z. Zhang, G. Comsa, and H. Metiu, "Kinetic Mechanism for Island Shape Variations Caused by Changes in the Growth," *Physical Review Letters*, vol. 71, p. 2967, 1993.

[101] J. Jacobsen, K. W. Jacobsen, and J. K. Norskov, "Island shapes in homoepitaxial growth of Pt(111)," *Surface Science*, vol. 359, p. 37, 1996.

[102] F. Tavazza, L. Nurminen, D. P. Landau, A. Kuronen, and K. Kaski, "Hybrid Monte Carlo molecular dynamics algorithm for the study of islands and step edges on semiconductor surfaces: Application to Si/Si(001)," *Physical Review E*, vol. 70, p. 036701, 2004.

[103] V. Shchukin and D. Bimberg, "Spontaneous ordering of nanostructures on crystal surfaces," *Reviews of Modern Physics*, vol. 71, p. 1125, 1999.

[104] H. Spjut and D. A. Faux, "Computer simulation of strain-induced diffusion enhancement of Si adatoms on the Si(001) surface," *Surface Science*, vol. 306, p. 233, 1994.

[105] W. M. Plotz, K. Hingerl, and H. Sitter, "Monte Carlo simulation of epitaxial growth," *Physical Review B*, vol. 45, p. 12122, 1992.

[106] A. Schindler, *Theoretical Aspects of Growth on One and Two Dimensional Strained Crystal Surfaces*. Dissertation, Duisburg, 1999.

[107] S. Russo, "Computation of strained epitaxial growth in three dimensions by kinetic monte carlo." http://arxiv.org/pdf/cond-mat/0501651.pdf, 2008.

[108] M. Biehl, M. Ahr, W. Kinzel, and F. Much, "Kinetic Monte Carlo simulations of heteroepitaxial growth," *Thin Solid Films*, vol. 428, pp. 52–55, 2003.

[109] F. Much and M. Biehl, "Simulation of wetting-layer and island formation in heteroepitaxial growth," *Europhysics Letters*, vol. 63, pp. 14–20, 2003.

[110] C. H. Lam, C. K. Lee, and L. M. Sander, "Competing roughening mechanisms in strained heteroepitaxy: a fast kinetic Monte Carlo study," *Physical Review Letters*, vol. 89, pp. 216102–1, 2002.

[111] W. H. Press, S. A. Teukolsky, W. T. Vetterling, and B. P. Flannery, "Numerical recipes in c." http://www.nr.com/com/storefront.html, 1992.

[112] N. W. Ashcroft and N. D. Mermin, *Solid State Physics*. Cornell University, NY: Saunders College Publishing, 1976.

[113] K. J. Strandburg, "Two-dimensional melting," *Rev. Mod. Phys*, vol. 60, p. 161, 1988.

[114] J. P. Hirth and J. Lothe, *Theory of Dislocations*. NY: McGraw-Hill Book Company, 1968.

[115] G. Cohen-Solal, F. Bailly, and M. Barbe, "Critical thickness in heteroepitaxial growth of zinc-blende semiconductor compounds," *Journal of Crystal Growth*, vol. 138, p. 68, 1994.

[116] T. Volkmann, F. Much, M. Biehl, and M. Kotrla, "Interplay of strain relaxation and chemically induced diffusion barriers: Nanostructure formation in 2D alloys," *Surface Science*, vol. 586, pp. 157–173, 2005.

[117] R. Q. Hwang, "Chemically Induced Step Edge Diffusion Barriers: Dendritic Growth in 2D Alloys," *Physical Review Letters*, vol. 76, p. 4757, 1996.

[118] P. Kratzer, *Monte Carlo and Kinetic Monte Carlo Methods - A Tutorial - in Multiscale Simulation Methods in Molecular Sciences, J. Grotendorst, N. Attig, S. Bluger, D. Marx (Eds.)*.

[119] G. Mills and H. Jonsson, "Quantum and thermal effect in H2 dissociative adsorption: Evaluation of free energy barriers in multidimensional quantum systems," *Physical Review Letters*.

[120] G. Henkelman and H. Jonsson, "Improved tangent estimate in the nudged elastic band method for finding minimum energy paths and saddle points," *Journal of Chemical Physics*, vol. 113, p. 9978, 2000.

[121] T. P. Nolam, R. Sinclair, R. Rajan, and T. Yamashita, "Transmission electron microscopic analysis of microstructural features in magnetic recording media," *IEEE Transitions on Magnetics*, vol. 29, pp. 292–299, 1993.

[122] S. Veprek, "Electronic and mechanical properties of nanocrystalline composites when approaching molecular size," *Thin Solid Films*, vol. 297, p. 145, 1997.

[123] P. B. Barna, M. Adamik, J. L. Labar, L. Kover, J. Toth, A. Devenyi, and R. Manaila, "Formation of polycrystalline and microcrystalline composite thin films by codeposition and surface chemical reaction," *Surface and Coatings Technology*, vol. 125, pp. 147–150, 2000.

[124] J. Patscheidera, T. Zehndera, and M. Diserens, "Structure performance relations in nanocomposite coatings," *Surface and Coatings Technology*, vol. 145-147, pp. 201–208, 2001.

[125] I. Petrov, P. B. Barna, L. Hultman, and J. E. Greene, "Microstructural evolution during film growth," *Jornal of Vacuum Science and Technology A*, vol. 21, pp. 117–128, 2003.

[126] M. Copel, M. C. Reuter, E. Kaxiras, and R. M. Tromp, "Surfactants in epitaxial growth," *Physical Review Letters*, vol. 63, pp. 632–635, 1989.

[127] J. E. Prieto, C. Rath, S. Muller, L. Hammer, K. Heinz, and R. Miranda, "Surfactant action in heteroepitaxy: Growth of Co on (4x4) Pb/Cu(111) studied by LEED and STM," *Physical Review B*, vol. 62, pp. 5144–5149, 2000.

[128] E. Bauer and H. Poppa, "Recent advances in epitaxy," *This Solid Films*, vol. 12, p. 167, 1972.

[129] P. B. Barna, *Proc. 9th International Vacuum Congress, J. de Segovia (Ed.)*. 1983.

[130] M. Kalff, G. Comsa, and T. Michely, "How Sensitive is Epitaxial Growth to Adsorbates?," *Physical Review Letters*, vol. 81, p. 1255, 1998.

[131] M. Kalff, P.Smilauer, G. Comsa, and T. Michely, "No coarsening in Pt(111) homoepitaxy," *Surface Science Letters*, vol. 426, pp. 447–453, 1999.

[132] N. Cabrera and D. A. Vermiyea, *R. H. Doremus and B. W. Roberts and D. Turnbull (Eds.), Growth and Perfection of Crystals,*.

[133] A. Barna, P. B. Barna, G. Radnoczi, F. M. Reicha, and L. Toth, "Formation of Aluminium Thin Films in the Presence of Oxygen and Nickel," *Physica Status Solidi A*, vol. 55, p. 42, 1979.

[134] R. Deák, Z. Néda, and P. B. Barna, "A realistic kinetic monte carlo approach for two-component deposition processes,." 48th IUVSTA workshop on Influence of Impurities on Nucleation and Growth of Thin Films., 2006, August 26-31.

[135] T. Pang, *An Introduction to Computational Physics*. Cambridge: Cambridge University Press, 1997.

[136] "Openmp application program interface." `http://www.openmp.org`.

[137] S. Liu, Z. Zhang, J. Nerskov, and H. Metiu, "The mobility of Pt atoms and small Pt clusters on Pt(111) and its implications for the early stages of epitaxial growth," *Surface Science*, vol. 321, pp. 161–171, 1994.

[138] U. Kurpick, B. Fricke, and G. Ehrlich, "Diffusion mechanisms of compact surface clusters: Ir7 on Ir(111)," *Surface Science Letters*, vol. 470, pp. 45–51, 2000.

[139] C. Liu, J. Cohen, J. Adams, and A. Voter, "EAM study of surface self-diffusion of single adatoms of fcc metals Ni, Cu, Al, Ag, Au, Pd, and Pt," *Surface Science*, vol. 253, pp. 334–344, 1991.

[140] J. Yang, W. Hu, and M. Xu, "Comparative study of compact hexagonal cluster self-diffusion on Cu(111) and Pt(111)," *Applied Surface Science*, vol. 255, pp. 1736–1740, 2008.

[141] S. Stanescu, C. Boeglin, A. Barbier, and J.-P. Deville, "Epitaxial growth of ultra-thin NiO films on Cu(111)," *Surface Science*, vol. 549, pp. 172–182, 2004.

[142] T. Michely, M. Hohage, M. Bott, and G. Comsa, "Inversion of growth speed anisotropy in two dimensions," *Physical Review Letters*, vol. 70, pp. 3943–3946, 1993.

[143] H. Brune, G. S. Bales, J. Jacobsen, C. Boragno, and K. Kern, "Measuring surface diffusion from nucleation island densities," *Physical Review B*, vol. 60, pp. 5991–6006, 1999.

[144] S. Ovesson, A. Bogicevic, and B. I. Lundqvist, "Origin of Compact Triangular Islands in Metal-on-Metal Growth," *Physical Review Letters*, vol. 83, pp. 2608–2611, 1999.

[145] T. Michely and J. Krug, *Islands, Mounds and Atoms*. Berlin: Springer, 2004.

[146] P. Zhang, Y. Xie, X. Ning, and J. Zhuang, "Equilibrium structures and shapes of clusters on metal fcc(111) surfaces," *Nanotechnology*, vol. 19, pp. 255704–255714, 2008.

[147] C. Yin, X.-J. Ning, J. Zhuang, Y.-Q. Xie, X.-F. Gong, X.-X. Ye, C. Ming, and Y.-F. Jin, "Shape prediction of two-dimensional adatom islands on crystal surfaces during homoepitaxial growth," *Applied Physics Letters*, vol. 94, p. 183107, 2009.

[148] Q. W. Bassett and P. R. Webber, "Diffusion of single adatoms of Platinum, Iridium and Gold on Platinum surfaces," *Surface Science*, vol. 70, pp. 520–531, 1978.

[149] T.-Y. Fu, Y.-R. Tzeng, and T. T. Tsong, "Self-diffusion and dynamic behavior of atoms at step edges of iridium surfaces," *Physical Review B*, vol. 54, pp. 5932–5939, 1996.

[150] K. Thornton, J. Agren, and P. Voorhees, "Modelling the evolution of phase boundaries in solids at the meso- and nano-scales," *Acta Materialia*, vol. 51, pp. 5675–5710, 2003.

[151] A. Karim, A. N. A.-R. ans Abdelkader Kara, and T. S. Rahman, "Diffusion of small two-dimensional Cu islands on Cu(111) studied with a kinetic Monte Carlo method," *Physical Review B*, vol. 73, p. 165411, 2006.

[152] M. J. Mehl and D. A. Papaconstantopoulos, "Applications of a tight-binding total-energy method for transition and noble metals: Elastic constants, vacancies, and surfaces of monatomic metals," *Physical Review B*, vol. 54, p. 4519, 1996.

[153] C. M. Zhang, M. C. Bartelt, J. M. Wen, C. J. Jenks, J. W. Evans, and P. A. Thiel, "Submonolayer island formation and the onset of multilayer growth during Ag/Ag(100) homoepitaxy," *Surface Science*, vol. 406, pp. 178–193, 1998.

[154] R. Deák, Z. Néda, and P. B. Barna. http://phys.ubbcluj.ro/~zneda/kmc.htm.

[155] D. Turnbull, "The supercooling of aggregates of small metal particles," *Transactions of the American Institute of Mining and Metallurgical Engineers*, vol. 188, pp. 1144–1148, 1950.

[156] A. Bogicevic, S. Liu, J. Jacobsen, B. Lundqvist, and H. Metiu, "Island migration caused by the motion of the atoms at the border: size and temperature dependence of the diffusion coefficient," *Physical Review B.*, vol. 57, pp. R9459–R9462, 1998.

[157] W. W. Pai, A. K. Swan, Z. Zhang, and J. F. Wendelken, "Island diffusion and coarsening on metal (100) surfaces," *Physical Review Letters*, vol. 79, pp. 3210–3213, 1997.

[158] G. Rosenfeld, K. Morgenstern, I. Beckmann, W. Wulfhekel, E. Laegsgaard, F. Besenbacher, and G. Comsa, "Stability of two-dimensional clusters on crystal surfaces: from ostwald ripening to single-cluster decay," *Surface Science*, vol. 401, pp. 402–404, 1998.

[159] M. Muller, K. Albe, C. Busse, A. Thoma, and T. Michely, "Island shapes, island densities, and stacking-fault formation on Ir(111): Kinetic Monte Carlo simulations and experiments," *Physical Review B.*, vol. 71, pp. 075407–1, 2005.

[160] A. Bogicevic, J. Stromquist, and B. I. Lundqvist, "Low-Symmetry Diffusion Barriers in Homoepitaxial Growth of Al(111)," *Physical Review Letters*, vol. 81, pp. 637–640, 1998.

Original contributions related to the thesis

ISI papers

1. **R. Deák**, Z. Néda, B. P. Barna, A simple kinetic Monte Carlo approach for eptaxial submonolayer growth, *Communications in Computational Physics*, **3**, 822–833 (2008).

2. **R. Deák**, Z. Néda, B. P. Barna, A novel kinetic Monte Carlo method for epitaxial growth, *Journal of Optoelectronics and Advanced Materials*, **10**, 2445–2450 (2008).

3. **R. Deák**, Z. Néda, B. P. Barna, A kinetic Monte Carlo approach for self-diffusion of Pt atom clusters on a Pt(111) surface, *Communications in Computational Physics*, **10**, 920–939 (2011)

4. **R. Deák**, Z. Néda, Kinetic Monte Carlo approach for triangular-shaped Pt islands on Pt(111) surfaces, *Physica status solidi B*, **249**, 1709–1716 (2012)

Conferences and Workshops

1. **R. Deák**, Z. Néda, "48th IUVSTA workshop on Influence of Impurities on Nucleation and Growth of Thin Films", 26-31 August 2006, Budapest, Hungary

2. **R. Deák**, Z. Néda, "International Conference on Computational Methods in Modern Physics", 2-4 November 2006, Cluj-Napoca, Romania

3. **R. Deák**, Z. Néda, "International Conference on Advanced Materials", 9-10 November 2007, Oradea, Romania

4. **R. Deák**, Z. Néda, "International Workshop on Stochastic Phenomena", 26-31 May 2008, CLuj-Napoca, Romania